

NASA

CR-54479

LINEAR SOLAR MODULE

Refinement, Measurement, and Evaluation of Optics

by

J. ROBERT GETTEL

GARY F. COMISKEY

RICHARD A. KARLIN

FACILITY FORM 802

N66 35205
(ACCESSION NUMBER)

226
(PAGES)

CR-54479
(NASA CR OR TMX OR AD NUMBER)

(THRU)

1
(CODE)

23
(CATEGORY)

Prepared under Contract No. NAS3-2794 by
LINEAR, INC.
Evanston, Ill.

GPO PRICE \$ _____

CFSTI PRICE(S) \$ _____

Hard copy (HC) 3.75

Microfiche (MF) 1.25

for

Lewis Research Center

National Aeronautics and Space Administration

653 July 65

TABLE OF CONTENTS

- 1 Summary
- 2 Introduction
 - 2.1 Problem of Large-Volume Solar Simulation
 - 2.2 Objectives of the Current Program
 - 2.3 Scope of the Current Program
- 3 Optical Design Adaptation
 - 3.1 Linear Solar Module #0430
 - 3.1.1 Choice of Source
 - 3.1.2 Optical System
 - 3.1.3 Optical Configuration of #0430
 - 3.1.4 Summary of #0430
 - 3.2 Westinghouse SAHX-2500F Mercury-Xenon, Short-Arc Lamp
 - 3.3 Optical Concepts
 - 3.3.1 Definitions and Symbols
 - 3.3.2 Characterization of a Radiation Field
 - 3.3.3 Power
 - 3.3.4 Uniformity in the Test Volume
 - 3.3.5 The Angular Distribution of Flux
 - 3.3.6 Source Representation
 - 3.3.7 Integration over the Arc Disc
 - 3.3.8 Integration over a defining Surface
 - 3.3.9 Flux Collection
 - 3.3.10 Beam Determination
 - 3.3.11 Beam Modification

3.4 Design Adaptation

3.4.1 Collection

3.4.2 Beam Modification

3.4.3 Removal of radiation at undesirable angles

3.5 Prediction of Module Performance

3.5.1 Function $q_1(\theta)$ - radiance weighting as a function of θ

3.5.2 Function $q_2(r)$ - differential radiance as a function of arc disc radius

3.5.3 Function $q_3(\lambda)$ - weighting function over wave length

3.5.4 Function q_4 - reflectivity

3.5.5 Module total flux output

3.5.6 Angular distribution of flux output

3.5.7 Prediction of module efficiency

3.5.8 Beam irradiance crosssection

4 Measurement Program

4.1 Parameters to Be Measured

4.2 Measurement Facility and Instrumentation

4.2.1 Module housing and mounting

4.2.2 Measurement area

4.2.3 Module supports

4.2.4 Radiometer

4.2.5 Radiometer cart

4.2.6 Control Console

- 4.3 Measurement Technique
 - 4.3.1 Individual reflector measurements
 - 4.3.2 Module Alignment
 - 4.3.3 Wide angle energy
- 4.4 Data Processing and Reduction
 - 4.4.1 Scale factor
 - 4.4.2 Total power computation
 - 4.4.3 Filter factors
 - 4.4.4 Automatic data reduction
- 4.5 Estimate of Data Accuracy
- 4.6 Measurement Data
- 5 Module Performance
 - 5.1 Reflectors Only Configuration
 - 5.1.1 Total output
 - 5.1.2 Angular distribution
 - 5.1.3 Beam irradiance crosssection
 - 5.1.4 Uniformity of intensity
 - 5.1.5 Spectral uniformity
 - 5.2 Two Lens Plate Configuration
 - 5.2.1 Total output
 - 5.2.2 Angular distribution
 - 5.2.3 Beam irradiance crosssection
 - 5.2.4 Uniformity of intensity
 - 5.2.5 Spectral uniformity
 - 5.3 One Lens Plate Configuration
 - 5.3.1 Total output
 - 5.3.2 Angular distribution

5.3.3 Beam irradiance crosssection

5.3.4 Uniformity of intensity

5.3.5 Spectral uniformity

6 Solar Module Future

6.1 Summary of Program Results

6.2 Specification of Simulator Parameters

6.2.1 Total output - Efficiency

6.2.2 Angular distribution

6.2.3 Representative Module Adaptations

6.2.4 Beam pattern and uniformity of irradiation

6.2.5 Spectral uniformity

6.2.6 Other factors

6.3 Complete Engineering Prototype

6.3.1 Source selection

6.3.2 Reflector adaptation

6.3.3 Lenticular plate adaptation and molding

6.3.4 Module seals

6.3.5 Housing and cooling provision

6.3.6 Array edge modification

6.3.7 Power and control provision

6.4 Conclusions

LIST OF FIGURES

- 3- 1 Schematic of the optical configuration of #0430
- 3- 2 Outline drawing of the SAHX-2500F
- 3- 3 Polar Radiation Diagram of the SAHX-2500X
- 3- 4 150-Brightness contour lines for the SAHX-2500F
- 3- 5 Beam irradiance profile
- 3- 6 Effect of misalignment with hard and soft profiles
- 3- 7 Flux at angle β
- 3- 8 Angular distribution of flux for three hypothetical modules
- 3- 9 Angle of divergence
- 3-10 Arc as seen from a point of view 'p'
- 3-11 Vector T from dA_R thru entire arc volume
- 3-12 Radiation in $d\omega$ from dA_s to dA_R
- 3-13 Module coordinate system
- 3-14 Source defining disc coordinate system
- 3-15 Integration over parabolic reflector
- 3-16 Angularly displaced ellipsoid
- 3-17 Tipped paraboloid
- 3-18 Lenticular plate
- 3-19 Sharp angular section
- 3-20 Baffle Tube
- 3-21 Bending of rays striking lense
- 3-22 Prototype optical schematic
- 3-23 Power curve over cencentric arc disc
- 3-24 % total flux within V_i
- 3-25 Front surface aluminum mirror #747 - $q_+(\lambda)$
- 3-26 Predicted angular distribution - reflectors only
- 3-27 Predicted beam irradiance crossection - reflectors only, 60 feet.

List of Figures (Continued)

- 4-1 Module Support bars
- 4-2 Radiometer Calibration certificate
- 4-3 Radiometer Calibration curves
- 4-4 X and Y Axes
- 4-5 Radiometer Mounted on Cart
- 4-6 Schematic of Motor Control System
- 4-7 Control Console and X - Y Plotter
- 4-8 Schematic of Control Console Circuits
- 4-9 Operation of Console During Beam Measurement
- 4-10 Irradiance and Power Curves
- 4-11 Data Sheet
- 5-1 Prototype Module - Reflectors Only
- 5-2 Angular Distribution Measured vs. Predicted
- 5-3 Offset focus
- 5-4 Beam Irradiance Crosssection - Reflectors Only
- 5-5 Beam Irradiance Crosssection - Measured vs. Predicted
- 5-6 Spectral Beam Pattern and Deviation - Reflectors Only
- 5-7 Prototype Module - Two Lens Plates
- 5-8 Beam Pattern at 60 Feet with Two Lens Plates
- 5-9 Beam Irradiance Crosssection - Two Lens Plates
- 5-10 Beam Pattern for Two Lens Plates Focused at 15 Feet
- 5-11 Beam Pattern at 60 Feet for Two Lens Plates Focused at 15 Feet
- 5-12 Spectral Beam Pattern and Deviation - Two Lens Plates
- 5-13 Beam Irradiance Crosssection - One Lens Plate
- 5-14 Spectral Beam Pattern and Deviation - One Lens Plate

LIST OF TABLES

- 3-1 SAHX-2500F Technical Data
- 3-2 $\cos^2 \theta$ As a Function of R and
- 3-3 Prototype Reflector Elements
- 4-1 Instruments
- 4-2 List of Filters
- 4-3 List of Filters
- 4-4 Components Used in Estimate of Error
- 5-1 Beam Intensity Pattern - Reflectors only
- 5-2 Beam Intensity Pattern - Two Lens Plates
- 5-3 Beam Intensity Pattern - One Lens Plate
- 6-1 Approximate Characteristics of Representative Module Adaptations

1 SUMMARY

The optical portion of a Linear Solar Module has been refined, adapted, prototyped, and evaluated. The ultimate objective is a modular-type solar simulator capable of operation within a space environment facility.

The module uses a mercury-xenon or xenon short-arc source in an on-axis system consisting of segmented reflectors, one or two lenticular plates, and baffles.

This program has confirmed the design concepts and mathematical models used by Linear, Inc., and the performance of the prototype optical system clearly indicates that efficiencies of 25 to 30 per cent can be achieved within a 15 inch module diameter using a 2500 watt source.

The advisability of a wider angular distribution specification has been indicated. The ability to meet a much tighter uniformity specification has been shown. Excellent spectral uniformity, due to an almost complete absence of chromatic aberration plus spectral integration by the lenticular plates has been demonstrated.

Revised specifications have been discussed. The requirements for a complete engineering prototype have been mentioned and a brief outline of a program to produce it, given.

2 INTRODUCTION

2.1 Problem of large-volume Solar Simulation

Solar Radiation is one of the most important factors in space environment. Space systems are designed both to utilize solar radiation and to avoid its harmful effects. Accurate simulation of solar radiation is essential to accurate testing of a space system. The problems of providing solar simulation capability have grown more severe than in any other area of space-environment simulation. As space equipment has become larger, the volume to be covered by the simulator has increased. Running time requirement has increased, because of longer anticipated space missions. The larger zones of radiation required and the low efficiencies that have been achieved have made interruptions in the vacuum walls for relay of radiation from outside the chamber less and less feasible, particularly in view of large guard vacuum spaces between double walls. Because of low efficiencies, initial equipment costs, and to an even greater extent, operating costs have increased to prohibitive levels.

Simulation results have been far short of the effect of actual phenomena in spite of major expenditures. Exact duplication of solar radiation would require:

1. Radiation intensity variable from 50 to 275 watts/sq. ft. for the portion of space

between the orbits of Venus and Mars.
(130 watts/sq. ft. at Earth outside the
atmosphere.)

2. Radiation intensity uniform both across the test area and in depth throughout the test volume. Such uniformity applies not only to total energy but likewise to the energy in each spectral zone.
3. Energy with the same spectral distribution as zero air mass solar radiation.
4. Collimation of the energy to within a 0.4° half-angle for the high intensity and within 0.2° half-angle for the lower intensity.
5. Provision for the prevention of stray radiation and for the prevention of the re-reflection of flux reflected from the test object.

Each of these factors is achievable individually, but the combination of them all is not attainable to any high degree of accuracy, because of economic and technological limitations.

In specifying a large solar simulation system in the near future, the greatest skill will be required in the balancing of:

1. Degree of accuracy or deficiency in the simulation of each factor,
2. Initial cost and operating costs, and
3. Test requirements.

None of these should take precedence. In the best balancing they must interact.

2.2 Objectives of the Current Program

The ultimate objective of the work performed under this contract is a modular-type solar simulator that is capable of operation within a space environment and is complete with power supply, control, housing, and cooling. An array of these modules would simulate solar radiation throughout the test volume.

This program was restricted to the refinement, design adaptation, prototyping and evaluation of the optical component of the Linear, Inc. "High Energy^{Solar} Simulator."

This Linear Solar Module was based on the use of a xenon short-arc source in an on-axis system utilizing lenticular lenses for direct beam irradiation of the test area. This module was designed to achieve the following goals:

1. Efficiency essentially twice that of the best efficiency previously attained.
2. Uniformity of spectral distribution.
3. Covering dark areas caused by lamp failure by means of reserve modules.
4. Extending running time capability by means of reserve modules.
5. Two or three times the basic array intensity by means of multiple array operation.
6. Reduced equipment and operating costs.
7. Prevention of stray radiation and re-reflection.

2.3 Scope of the Current Program

The program was strictly limited to design adaptation, prototyping, and evaluation of the optical portion of the module.

Source. - A 2,500-watt mercury-xenon short-arc lamp (anode-down operation) was specified. The most basic limitation in present solar simulation is found in the flux source. The only source with any degree of demonstrated capability for continuous-duty application is the short-arc lamp. It is true that the various available short-arc lamps have certain deficiencies, yet it must be accepted that any major space simulation facility, scheduled to become operational in the next two to five years, is essentially committed to the short-arc lamp for solar simulation.

While information on this and similar sources has more recently improved, the available information in directional, total, and spectral flux measurements on these sources was inadequate early in the program, and especially during the design-adaptation phase. Although further measurement was considered, design adjustments were completed without it. No other brands or types of lamps were evaluated since, without lengthy tests, comparisons of life and spectral characteristics quickly appeared to be tenuous.

Detailed spectral distribution measurements and evaluation also were outside the scope of this program. Spectral regions were important in evaluating spectral uniformity and quite helpful in evaluating some other operating characteristics, but careful evaluation of spectral distribution is a

significant effort in itself. Information included on spectral distribution, as such, was derived only incidentally from these other efforts.

Target Parameters. - Target parameters for a primary array were stated as follows:

1. Collimation and uniformity of intensity are to be maintained within a range of 20 to 60 feet from the module.
2. Half Angle of collimation shall be two degrees for ninety (90) percent of the energy.
3. Intensity in the target zone shall be 1.2 earth solar constants at rated power after twenty (20) hours of running time on lamp.
4. Uniformity of intensity shall be ± 5 percent when measured with a one (1)-foot-square sensor in an infinitely large array, and ± 50 percent when measured with a one (1)-inch-diameter sensing area.

It should be emphasized that the foregoing were, exactly as labeled, "targets" and that they were open to discussion and balancing throughout the program, when and if necessary.

Evaluation. - Evaluation of the prototype, under the program as originally established, called for the measurement and evaluation of the prototype module operation with a total radiation detector for:

1. Flux Intensity,
2. Uniformity of Intensity, and
3. Collimation.

Program. - The optical evaluation and design adaptation was conducted in conjunction with John R. Miles Corp., as subcontractor. Fabrication of optical elements was subcontracted. Measurement and evaluation were performed at the facilities of Linear, Inc.

3 OPTICAL DESIGN ADAPTATION

3.1 Linear Solar Module #0430

The Linear Solar Module #0430 was designed to provide a solar simulator module of greater efficiency, greater uniformity, and lower cost than had been achieved in previous designs. The design also provided for stacking up to three arrays and for continuous operation inside an evacuated and cycled aerospace environment chamber.

The complete module consists of a sealed housing with provisions for cooling, a regulated power supply and ignition system, a lamp and optical system, and provision for remote monitoring and control.

The problem of designing the optical portion of the solar simulator module can be summarized very briefly. First a source must be chosen on the basis of radiating efficiency, spectral distribution, life, physical geometry, and radiative geometry. Next, an optical system must be designed to deliver the maximum possible flux into the target volume within the acceptable limits of angular distribution and uniformity of flux intensity. The design of the optical system must balance total flux collected against losses due to absorption, unwanted reflection, and vignetting of energy magnified to excessive angle. Finally, provision must be made to remove unwanted flux.

3.1.1 Choice of Source. - The short-arc lamp was chosen as the source for the Linear Solar module #0430 because of superior life, radiating efficiency, and differential radiance.

Specifically, an anode-up, xenon, short-arc lamp was chosen.

3.1.2 Optical System. - Every reflector surface and lens surface and every millimeter of lens path in an optical system causes loss due to absorption or unwanted reflection. Thus from an efficiency standpoint, we can state as a truism: 'All other factors being equal, the number of surfaces and the millimeters of lens path should be minimized.' In more useful form, the statement becomes a design criteria to use the fewest surfaces and the shortest lens path possible. Any increase in surfaces or lens path must more than offset the loss introduced, by permitting added collection within the acceptable angle and uniformity.

3.1.3 Optical Configuration of #0430. - Figure 3-1 is a schematic of the optical configuration of #0430. A reflector segmented into three pieces collects flux from the anode-up, short-arc lamp, and directs this flux toward an annular focus. The reflector is an angularly displaced ellipsoid. The flux is intercepted by a lenticular plate prior to focus. Each lenslet on this plate forms an image of the arc. The target volume is irradiated by an integration of these separate images. A second lenticular plate may be used at the focus of the first lenticular plate where a relatively square beam-intensity profile is desirable .

3.1.4 Summary of #0430. - Module #0430 achieves collection over a wide angle using only one reflective surface and requires only a single lens element to direct the flux into the target volume. This basic design provides mechanisms for achieving

excellent uniformity of irradiance (including uniformity by spectral zones) and a wide choice of beam intensity patterns. The efficiency of this design is high and it can be manufactured at a relatively low cost.

In arriving at this design, Linear, Inc. considered a wide variety of possible configurations including multiple reflectors and complex condensing lense systems. While this theoretical work preceeded the current program, some of these considerations are discussed later in this chapter.

3.2 Westinghouse SAHX-2500F, Mercury-Xenon Short-Arc Lamp

The Westinghouse SAHX-2500C anode-down, mercury-xenon, short-arc lamp was specified for this program. Early in the program, Westinghouse advised that this lamp was no longer in regular production. They advised that they had modified this design to reduce arc wander and shadowing and improve maintenance of output. The revised lamp, SAHX-2500F, was therefore used in this program. Figure 3-2 is an outline drawing of the SAHX-2500F. Table 3-1 is the manufacturer's technical data. Figure 3-3 presents the polar radiation diagram. Figure 3-4 is a plot of iso-brightness contour lines for the SAHX-2500F. (2)

3.3.1 Definitions and Symbols. - (8) (9) (7)

W - Energy. - Energy is used as in classical physics. (5) (6)

It is conserved. (7) Energy is a scalar quantity. Typical unit is the joule.

P - Power. - Power is change in energy per unit time. Because energy is conserved power must always refer to the flow of energy from one volume to another or to the conversion of energy from one form to another. Power is a scalar. Typical unit is the watt.

F - Flux. - A line of flux is a power flow vector. A flux field is a vector field describing the flow of power thru a volume (or through a surface.) Flux can also be used as a scalar to indicate the magnitude of power flow. Typical unit of magnitude is the watt.

E - Intensity.* - Intensity is flux density. It is the amount of flux passing thru a unit area normal to the flux. Intensity is a vector quantity and has the same direction as the flux. Typical unit of magnitude is the watt.

*In some references intensity is defined as the flux per unit solid angle. The symbol is then usually I. We caution that as used in this report intensity is always the classical field intensity - i.e. flux density on an area basis, and the symbol is E.

H - Irradiance. - Irradiance is the projection of the intensity

vector upon the unit area vector. Thus

$$H = E \cdot \hat{a} = E \cos \beta \quad (3-1)$$

Since H is the inner product of two vectors it is a scalar. Dimensionally H is the normal component of the intensity, thus typically watts per cm^2 .

I - Radiance. - Radiance is the flux emitted per unit solid angle. If the radiance is known the total flux in solid angle ω is

$$F = \int I_{\omega} d\omega \quad (3-2)$$

where I_{ω} is I as a function of angle. If intensity is required

$$E = \frac{\omega}{R^2} \quad (3-3)$$

where R is distance from the source.

The concept of radiance is most useful when applied at a distance large enough so the source can be considered a point source. When the source must be treated as finite, a small portion of the source area dA will be assumed to have an incremental radiance dI . An integration over the entire source will then produce the radiance I. Radiance is a vector. Typical units are watts per steradian.

Collimation. - Bringing rays of light parallel with each other, or parallel with an axis or normal.

Collimation Angle. - (Common usage) The angle between a ray of light and the system normal.

Collimation Angle. - The arc subtended by the field as viewed from the source.

3.3.2 Characterization of a Radiation Field. - A magnetic field can be described by assigning one vector to each point in space. The length of the vector is proportional to the magnitude of the magnetic field at that point, and the direction of the vector is the direction of the magnetic field at that point. Regardless of the number of sources, only one vector is required at each point in space, because the fields sum and a resultant field is formed. Thus, two equal and opposite fields cancel. Two fields at 90° to each other produce a new field at an intermediate angle. (10)

Incoherent electro-magnetic fields in free space are non-interacting. The fields from several sources will not sum. A complete description of the electro-magnetic radiation in a volume of space requires a vector from each point in every direction. These vectors cannot be summed to find a resultant. Therefore, the description of an electromagnetic field is much more complex than the description of an electric or magnetic field. This type of description is extremely cumbersome and would be almost impossible to work with and certainly uneconomical.

One method of simplifying this problem is to assume that the source is small enough to be characterized as a point. A single point source will produce only one vector at each point in space. Unfortunately, in the practical design of a solar simulator, the point source assumption leads to gross error between theory and practice.

Let us examine two examples to see why the point source

assumption causes unacceptably large errors. The SAHX-2500F source has an arc radius of at least 6 millimeters based on the manufacturer's data. (2) The focal length of reflector element number three of the prototype produced in this program is approximately 25 millimeters. Since the arc radius is at least 25% of the focal length, the requirement that arc radius be a negligible fraction of focal length has clearly not been met, and the point source assumption must not be used.

The use of an element of so short a focal length is justified by the results produced, as later chapters will show.

The top edge of reflector element number one of the prototype produced in this program is 42 millimeters from the arc center. At this point on the reflector a 6 millimeter arc subtends a half-angle of 8.1° . Since this half-angle is far in excess of the desired field-angle the point source assumption will clearly cause erroneous results.

The worst facet of making the point source assumption is the distortion created in the conception of the problem. Excellent solutions are erroneously rejected and poorer solutions are retained.

Since the use of the point source assumption is unacceptable, this assumption has never been used in this program. The source is always treated as a finite radiator.

The problem of characterizing the radiation field remains as difficult as before. Fortunately, there is a far better solution. In any medium of homogeneous index of refraction, with respect to both space and wavelength, light travels in straight lines. Further, at any reflective surface, the light changes direction to a new straight line in accordance with the law of reflection, and at any boundary between media of different indexes of refraction, the light assumes a new straight line according to the law of refraction. (11)

Since light flux travels in straight lines, the laws of euclidean geometry can be applied to predict the radiation field at one surface from a knowledge of the field at another surface. The requirement is that the complete radiation field be defined on a continuous surface enclosing all of the sources.*

*This requirement can be relaxed when the radiation field is to be defined for a limited part of space.

The field may now be defined on any surface outside the first surface. It must be recalled however, that to define the radiation field on the first surface, one must define the intensity field in every direction for every point on the surface. Alternatively, the radiance can be defined as a function of direction for every point on the defining surface.

3.3.3 Power. - The electrical power input to the source will be referred to as P_t . Since energy is conserved, on a thermal steady-state basis, the entire input power must appear as some form of output power. (7) A large part of this power

appears as radiant energy. Some of the input power is removed by heat conduction thru the electrodes to the clamp and leads. Some of the input power is removed by convection from the bulb and leads. Power lost thru conduction and convection is not useful in a solar simulator. Further, not all of the radiated power is useful. Power radiated by the bulb, the stems, and most of the electrodes originates too far from the arc to be usefully accepted by the optics. If such power does get thru the optical system, it will probably exit at an undesirable angle and may have to be removed by stops or baffles.

However, it is not correct to separate radiant energy into arc and electrode radiation and count the former and discount the latter. Radiation from the hot cathode tip may originate well within the arc volume and may be quite useful. On the other hand, some of the arc radiation may originate from an area which the optics cannot accept.

There is another limit on useful radiant power. Some of the power radiated may lie at wavelengths shorter or longer than the optical system pass-band. The loss that results could be considered a reflection (or transmission) loss, but it often simplifies the analysis to remove radiant energy which is well outside the pass-band from consideration at the onset.

Now the return to the consideration of a source with input power P_t . Within some defined optical band (λ_1 to λ_2), and originating from some defined arc volume V_a , the source

radiates a power P_r . The radiant efficiency of the source is now defined by

$$\text{Radiant efficiency} = \frac{P_r}{P_t} \quad (3-4)$$

It should be clear from the foregoing that radiated power (and thus radiant efficiency) is a function of optical pass-band and arc volume. When radiated power is measured, then optical pass-band is set by the pass-band of the radiometer and arc volume is set by the acceptance angle of the radiometer. In view of this, it is remarkable to note that the optical pass-band and acceptance angle are almost universally omitted from published data on radiant efficiency. Such omission severely limits the usefulness of the data.

All power not usefully radiated will ultimately appear as unwanted heat, and will have to be removed from the chamber. The necessity of removing this power places an extra bonus on high efficiency.

Consider a given source of input power P_t and usefully radiated power P_r and assume that an infinite array of modules is to produce an irradiance in the target volume of at least H_s . If the optical efficiency of the module is η , then module output, P_o is given by

$$P_o = \eta P_r \quad (3-5)$$

The area which one module can cover is now derived:

$$A_m \leq \frac{P_o}{H_s} = \frac{\eta P_r}{H_s} \quad (3-6)$$

In hexagonal array, the projected area covered by each module is

$$A_h = 3.4644 R_u^2 \quad (3-7)$$

where R_u is one-half the center-to-center distance between modules.

Returning to equation 3-6, and equating A_h from equation 3-7 and A_m we find

$$3.4644R_u^2 \leq \frac{\eta P_r}{H_s} \text{ and therefore,} \quad (3-8)$$

$$R_u \leq \left(\frac{\eta P_r}{H_s} \frac{1}{3.4644} \right)^{1/2} \quad (3-9)$$

Thus we have established the maximum allowable effective module radius (R_u) for a required irradiance (H_s), a given useful radiated power from source (P_r), and an overall module efficiency. (η).

At this point, it is important to realize that in a general sense both η and P_r are functions of module radius, and both will tend to decrease as module radius decreases. This will be further developed later, but at this point we can note that R_u will be described by an equation of second or higher order.

3.3.4 Uniformity in the test volume. - A primary requirement for the simulated solar radiation in any chamber is that it be uniform. By uniformity, we mean that a test area held perpendicular to the normal of the simulator, will receive the same irradiance regardless of where it is placed in the working volume.

For a modular simulator, it is necessary to derive the restrictions applicable to the module in order to achieve uniformity in the test volume. Consider an infinite array of similar modules mounted on a ceiling or wall of the test volume. A first look on a very elementary level suggests that perhaps the module itself should be uniform. Suppose the module projected a perfectly collimated beam with a

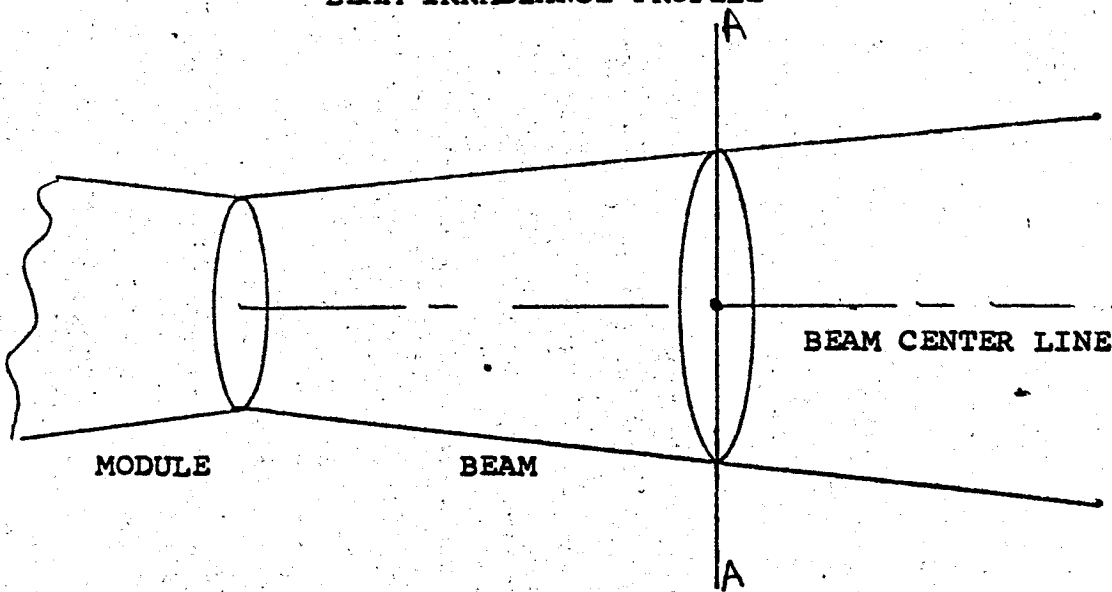
diameter -
square beam irradiance profile. As used here, beam profile is the irradiance measured along a line passing thru beam center cutting across the beam. (See figure 3-5.) The diameter of such a beam would be equal to the module exit pupil and would remain constant to infinity. Clearly to avoid holes exit pupils would have to cover the entire wall (or ceiling) without interruption by additional optical elements or supports. Moreover, consider the effect when a module is imperfectly aligned. Its beam will skew leaving a dark hole on one side and creating a factor-of-two hot spot on the other side. Clearly, the perfectly collimated module makes uniform irradiance difficult if not impossible. In fact even with a less than perfectly collimated module, experience has shown these matching difficulties to be far from academic.

Nor does a rounded beam irradiance profile help a collimated module. Since each module covers its own volume, a soft profile would cause unacceptable intensity variation.

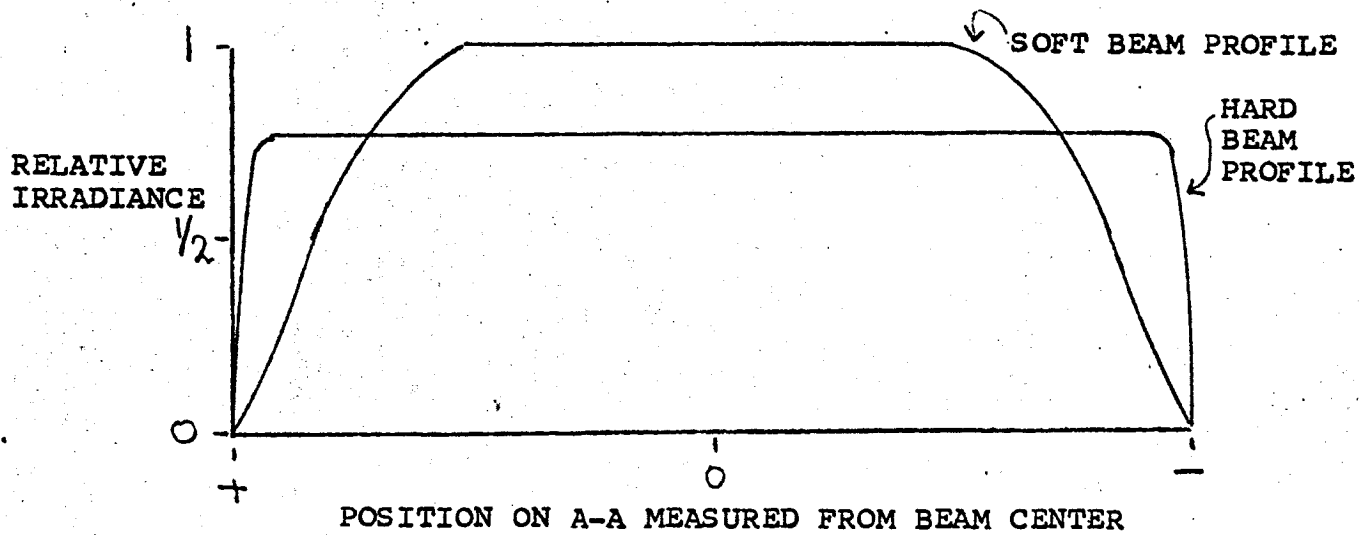
We must accept the fact that arcs are not perfectly symmetrical, sources vary somewhat from one to another, and optics can never be perfectly aligned. We require a solution to uniformity from an array of modules which tolerates the imperfectness of real-world modules as contrasted with the perfection of those which have been too highly refined on paper. In short, this becomes a problem of fitting irradiance patterns together without excessive holes or hot-spots, even though the patterns are not perfect in symmetry or alignment.

It becomes intuitively obvious that the solution requires a beam with a soft irradiance profile. The soft edges of two

FIGURE 3-5
BEAM IRRADIANCE PROFILE



The irradiance is measured along the line A-A.



When the irradiance drops from maximum to zero very rapidly, then the profile is termed hard, and when the irradiance slopes more gently to zero, then the profile is termed soft.

patterns merge gradually and slight misalignments no longer cause drastic peaks and valleys. The actual beam irradiance profile required depends on the size and shape of the module exit pupil, the geometry of the array, and the center-to-center distance between adjacent modules. Figure 3-6 shows the effect of misalignment with a perfectly collimated and therefore absolutely hard profile and with a soft profile.

There are a wide range of beam irradiance profiles which can produce an acceptable uniformity pattern. The requirement is to find one acceptable profile.

The beam irradiance profile is a complex function of the angular distribution of power from each point on the module exit pupil.

The statement that beam divergence or collimation is related to uniformity versus depth in the test volume is sometimes seen in the literature. The statement is true for a single module. For an infinite array or for positions away from the skirt of a finite array, the statement is completely incorrect. At any position for which the array can be considered infinite, if a surface is placed parallel to the simulator normal, then based only on symmetry we can assert that equal flux cuts the surface on both sides. This will be true for any such surface. If we erect a cylindrical surface, we can demonstrate that the amount of flux carried into the volume by divergence is equal to the amount carried out by divergence. Thus for a large array, small collimation angle is not a requirement for uniformity. In fact, we have seen that a very small collimation angle requires a hard profile in order to avoid excessive

peaks and valleys but that this hard profile creates severe alignment problems.

3.3.5 The Angular Distribution of Flux. - In section 3.3.1, flux and intensity were defined as vector quantities. Flux and intensity have a defined direction in space. Let us call the angle between a flux or intensity vector and the simulator normal β . Note that a flux vector can have angle β and still assume an infinite number of positions by rotating around the normal. In other words, β defines all the flux vectors contained on the surface of a cone of apex half-angle β . This is illustrated in figure 3-7.

β is of prime importance, because it is the angle at which the flux will strike a surface which is perpendicular to the normal. β is also the angle at which a flux vector diverges from a normal dropped from the vector source end.

It is extremely important to appreciate the significance of the angle β . Therefore, we examine step-by-step all of the implications of β .

Flux at angle β to a surface normal irradiates the surface according to the formula 3-1,

$$H = E \cdot \cos \beta$$

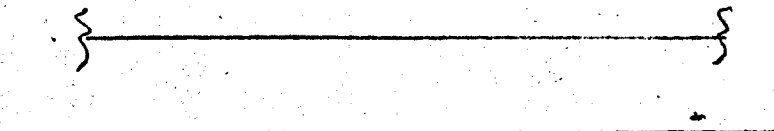
Thus, for a given intensity E , at angle β , the irradiance H is proportional to $\cos \beta$. Note however, that the cosine of 5° is .99619 and the cosine of 8° is .99027. Since most of the flux will be well within these angles, we are justified in ignoring the $\cos \beta$ term and equating intensity and irradiance for the normal surface.

FIGURE 3-6

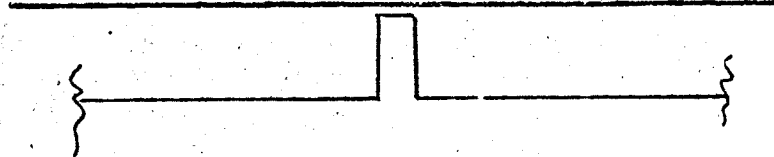
EFFECT OF MISALIGNMENT WITH HARD AND SOFT PROFILES



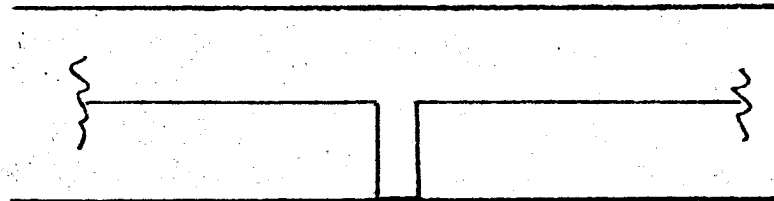
Hard profiles from two perfectly collimated modules.



Perfect alignment produces even irradiance.



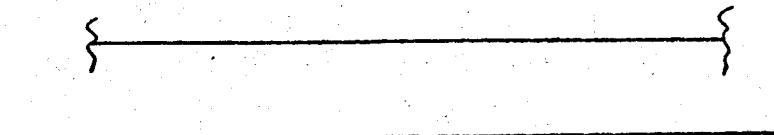
Two-times spike due to overlap misalignment.



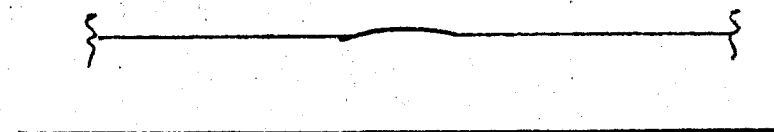
Complete hole due to gap misalignment.



Soft profiles from two modules with reasonable collimation



Perfect alignment produces even irradiance.

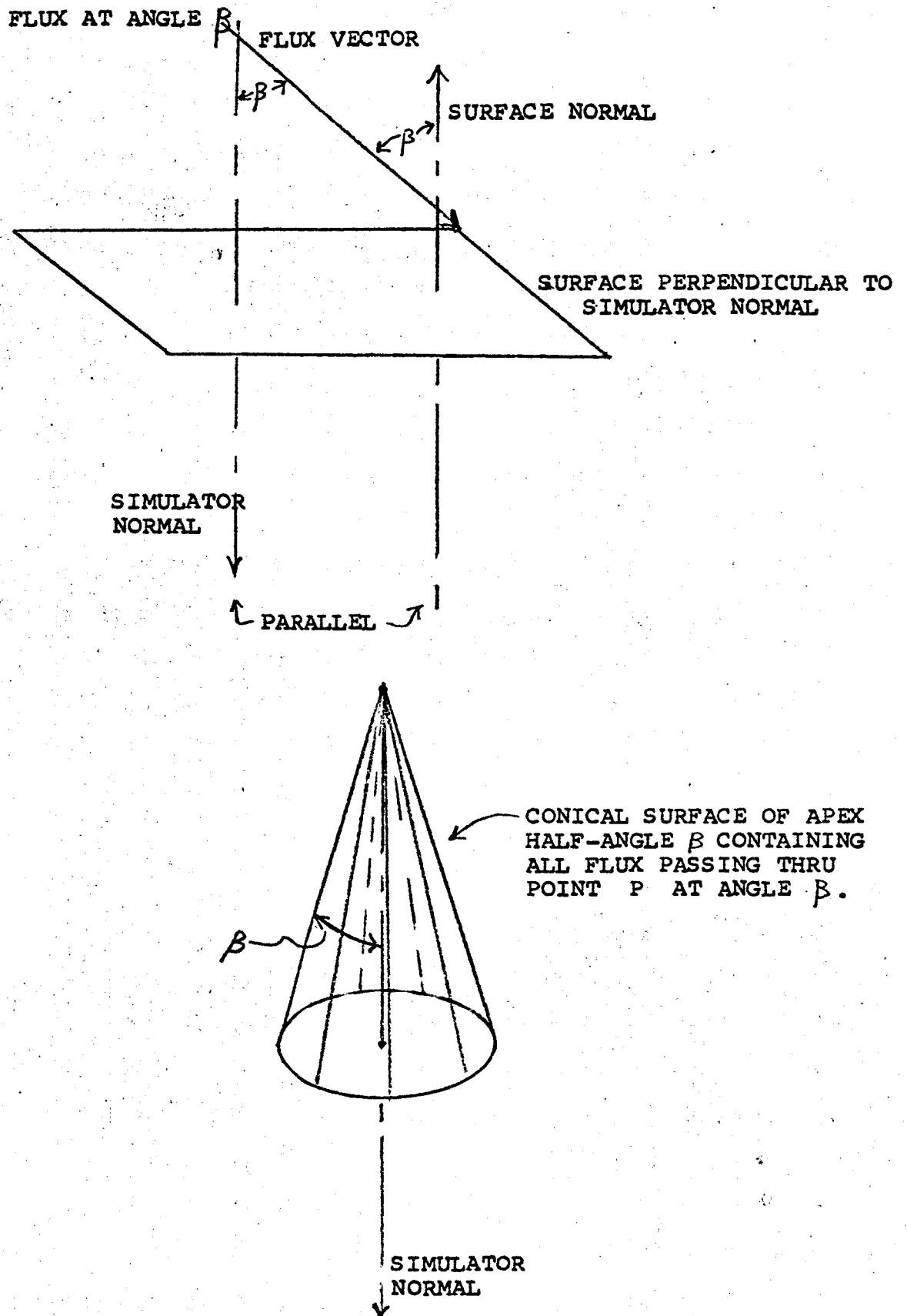


Overlap only produces a slight bump.



Gap produces a slight dip.

FIGURE 3-7



Assume a surface in the test volume parallel to the normal. If all flux was at $\beta = 0$, the surface would receive zero irradiation since all flux would be parallel to the surface. When some flux has angle β then the surface irradiation is non-zero. This effects the computation of the radiation being received by the object. Another way of stating this is that shadowing is a function of the distribution of flux by angle β . Note however that if the distribution of flux by angle β is known, shadowing can be computed for any angle and charted for rapid use. On the other hand, if the complete distribution of flux as a function of β is not known, then shadowing cannot be computed. Thus, knowledge of the complete distribution is essential.

It is tempting to define the distribution of flux as a function of β with some simple number, such as collimation angle, or field angle, or beam divergence. These expressions are all limiting expressions. They define various maximum angles, but they tell nothing at all about the actual power distribution within these angles. Knowing the point at which a function goes to zero is of little value when the function itself is unknown. Especially since it is the bulk of the power we are interested in and wish to account for. If the bulk of the power behaves properly, the question of whether the last few per cent exit at $\beta = 5^\circ$ or $\beta = 25^\circ$ is trivial, for this residual is the easiest to remove with stops or baffles.

The distribution of flux as a function of β is a function of the source and the optical system. It can be controlled within certain limits in the optical design.

To appreciate the inadequacy of collimation, field angle, and divergence, refer to figure 3-8. The distribution of flux as a function of β is charted for three hypothetical modules with identical exit pupils, collimation angles, field angles, and beam divergences. Yet the distribution is completely different for these three modules.

The concepts of collimation angle, field angle, and beam divergence are too weak for the proper description of a solar simulator and we shall use the more complex but far more accurate concept of the distribution of flux by angle.

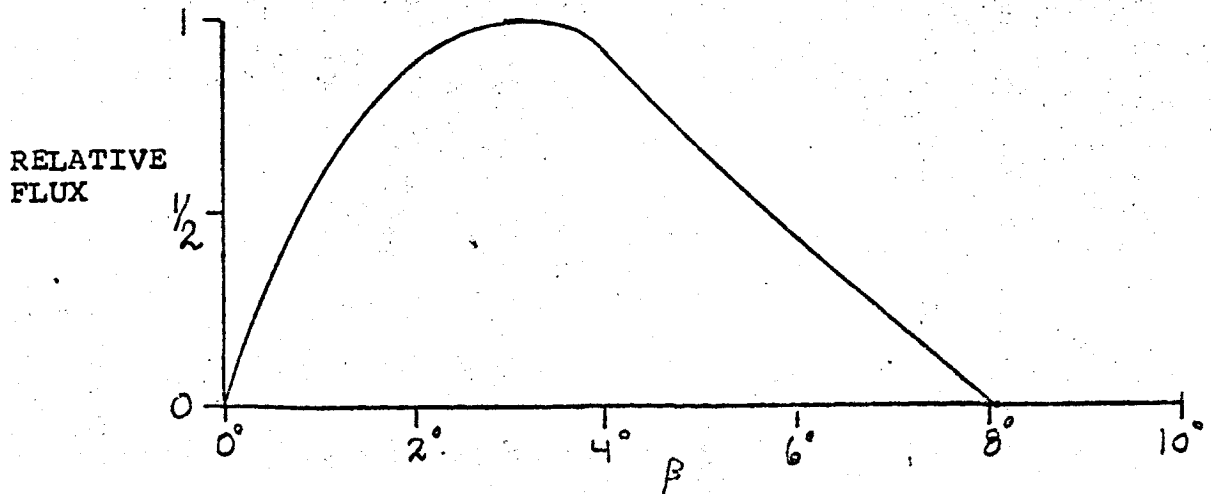
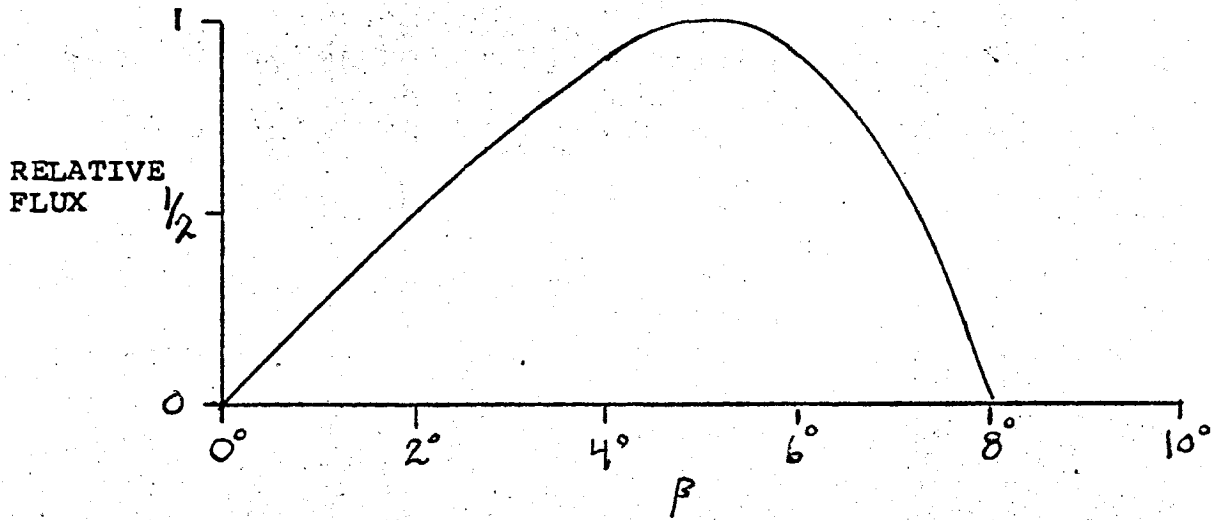
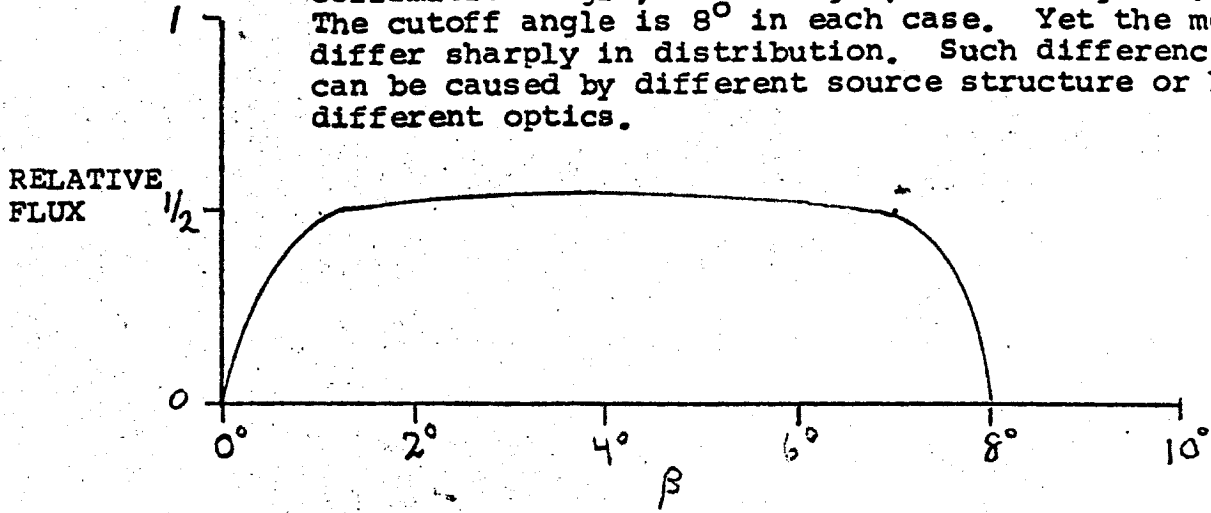
A point source radiates in all directions. By means of an optical system (for example a spherical reflector and a parabola) the flux from a point source can be brought perfectly parallel. Such a source has been perfectly collimated.

The statement is sometimes made that a parabola is not a collimator. This statement can be examined from the point of view of the formal definition of collimation angle: 'The angle subtended by the field as viewed from the source.' For the classical parabola of infinite length, the angle subtended by the field is zero and the classic, infinite, parabola is a collimator. For the finite parabola, for a view from the source toward the mouth, the angle subtended by the field is non-zero, thus the finite parabola is not a collimator. However, if the view toward the mouth is stopped or if the spherical-reflector is properly placed, then the collimation angle again goes to zero and the parabola-stop or parabola-spheric is again a perfect collimator.

FIGURE 3-8

ANGULAR DISTRIBUTION OF FLUX FOR THREE HYPOTHETICAL MODULES

These three modules have the same exit pupil, collimation angle, field angle, and divergence. The cutoff angle is 8° in each case. Yet the modules differ sharply in distribution. Such differences can be caused by different source structure or by different optics.



A finite source radiates in all directions, but the radiation does not all come from a single point. A finite source can never be perfectly collimated (lasers excepted.) The proof of this is quite simple. If a finite source could be perfectly collimated, then the perfectly collimated beam could be intercepted by a parabolic reflector and would be brought to focus at a true point at the center of the parabola. The irradiance at this point would be infinite. This would violate the second law of thermodynamics. Therefore, perfect collimation of a finite source is not possible. (7) (10) (11) (12)

The angle of divergence is set by the source size and the distance to the first optical element. This is illustrated by figure 3-9. It is seen that

$$\tan \alpha = \frac{r}{R} \quad \text{and thus,} \quad (3-10)$$

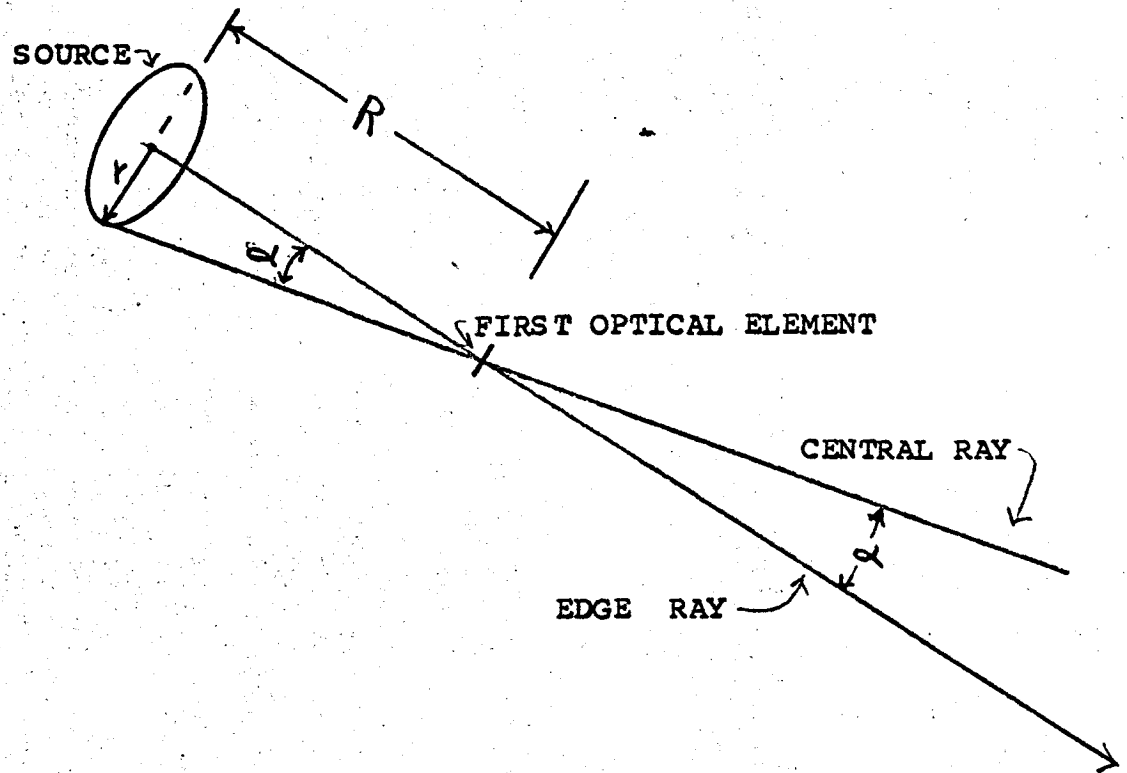
$$\alpha = \arctan \frac{r}{R} \quad (3-11)$$

The angle α may always be degraded by subsequent optics, and the distribution of energy versus α may be altered, but it is impossible to improve the mean energy distribution by α regardless of what subsequent optics may be used. If this could be done it would lead to a violation of the second law of thermodynamics, and one could build a perpetual motion machine of the second kind. (7) (12)

It was shown that the half-angle α was determined by source radius and distance to optics. In general, the source radius may be a function of angle of view and except for a spherical element, the distance to optics will differ with angle. Thus α must be determined by a summation of all views and all portions of the optics.

FIGURE 3-9

ANGLE OF DIVERGENCE



Angle α is found from $\tan \alpha = \frac{r}{R}$. Thus $\alpha = \arctan \frac{r}{R}$

FIGURE 3-10

ARC AS SEEN FROM A POINT OF VIEW P

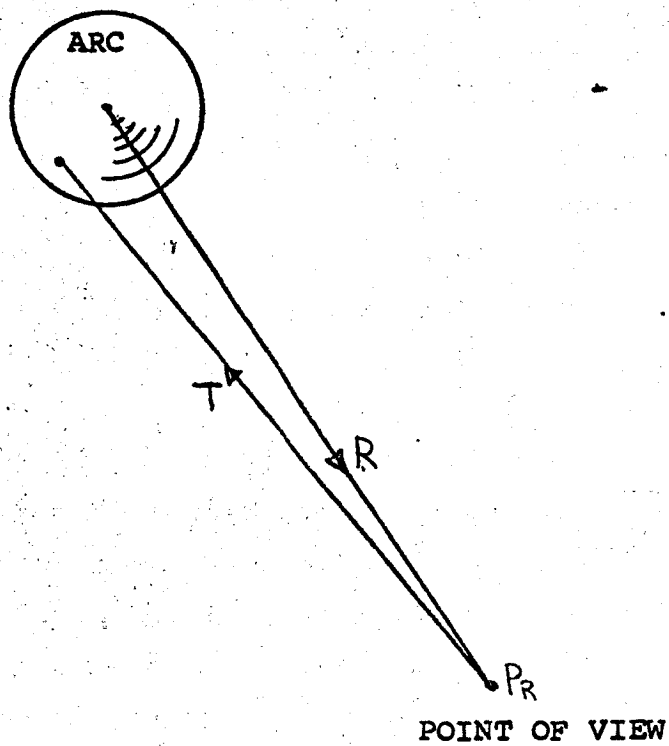
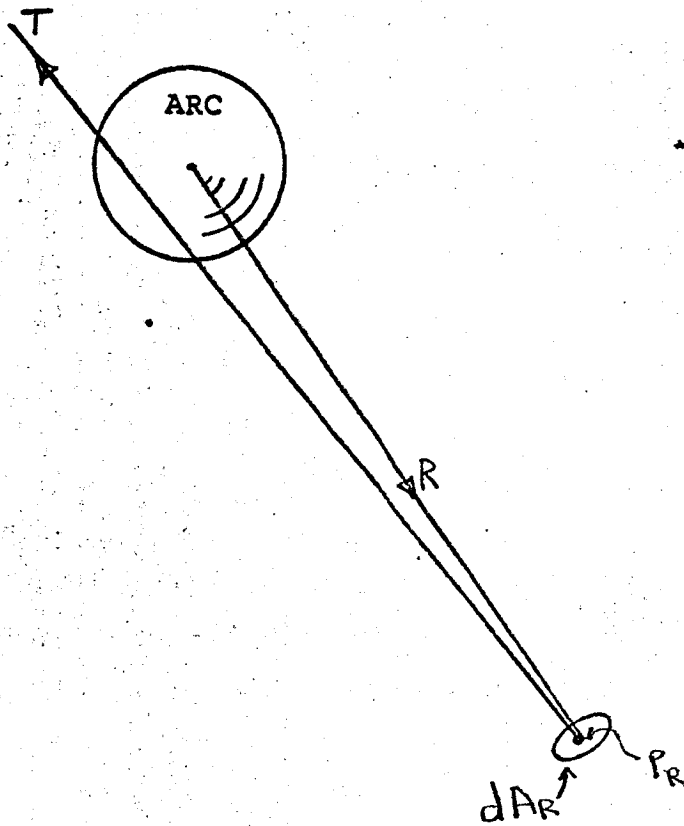


FIGURE 3-11

VECTOR T FROM da_R THROUGH THE ENTIRE ARC VOLUME



3.3.6 Source Representation. - The source is an arc occupying some volume in the general region of the electrodes. Throughout the arc volume, ionization and recombination with the attendant release of radiation takes place. However, some of the radiation traveling thru the arc volume will be absorbed and re-radiated. This phenomenon raises the percentage of radiation which appears to originate from near the surface and can be looked upon visually as opacity.

The arc is neither a true surface radiator nor a true transparent volume radiator, but rather it is somewhere in between. Figure 3-10 depicts an arc occupying a volume in space being viewed from a point P_r . The figure is drawn with the point of view and the arc center both in the plane of the paper. R is the distance from arc center to P_r . Imagine some portion of the arc radiating in all directions. Point of view ' P_r ' can only receive the radiation directed toward it. Now let us assume that the point of view P_r is the center of a small area dA_r . This incremental area subtends some incremental solid angle $d\omega$ from each point on the arc. Let us consider the vector T from the center of dA_r to a given point in the arc volume $U_{x,y,z}$. (U is a point in the three-dimensional space which the arc occupies, thus U_{xyz} .) At first it would seem that we must compute the radiation from every U in the arc volume. However, this is not required. Let a vector T from the point P_r pierce the entire arc volume. (Figure 3-11). There are many points along this vector T . For radiation from any of them to reach the area dA_r , such radiation must travel along T . Thus, all radiation can be described by

stating the flux along each vector T . (10) (13)

Let us erect a plane perpendicular to the radius vector R , and containing the arc center. There is a one-to-one correspondence between the set of all vectors thru the arc $[T]$ and the set of all points on the plane. We shall call this plane the 'arc defining plane.' Figure 3-12 shows a vector T from a point P_s on the arc defining plane to P_r at the center of dA_r . Now let us construct the solid angle $d\omega$ centered on T . The angle $d\omega$ is the angle subtended by dA_r . Finally, we shall allow the point P_s to become the very small area dA_s .

We wish to write an equation for the flux going from dA_s to dA_r . Another way of saying this is that we want the flux radiated in solid angle $d\omega$ from area element (of the defining disc) dA_s . Thus we need to know the amount of flux per unit area per unit ^{solid} angle coming from P_s in direction T . Let us call this the differential of radiance with respect to area and assign the symbol I' . Then

$$I'_s = \frac{\partial^2 F_s}{\partial \omega \partial A_s} \quad (3-12)$$

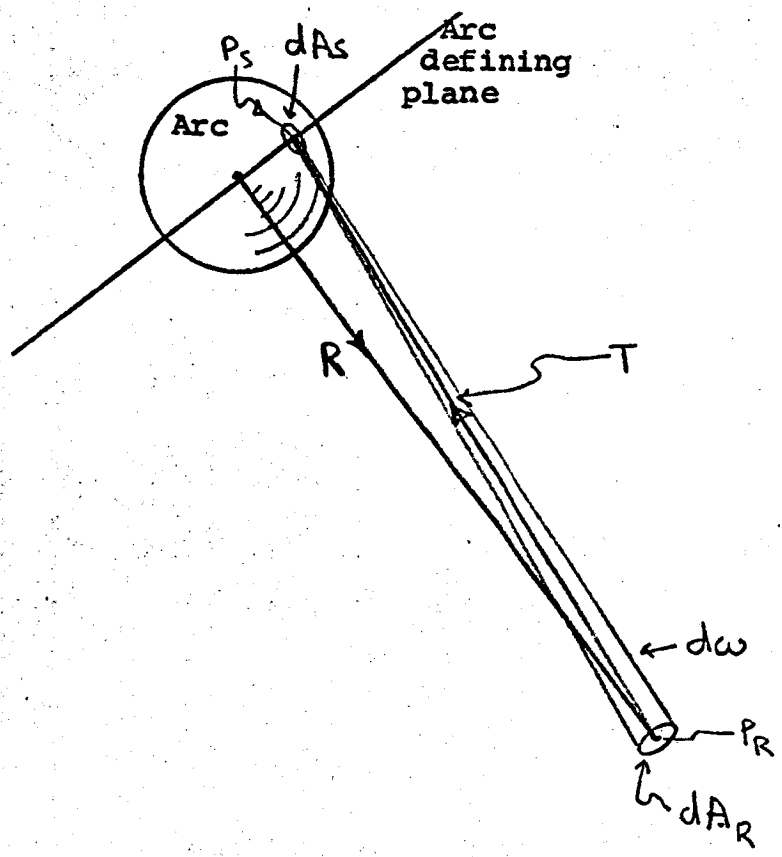
The subscript S is placed after I' and F to indicate that these quantities will have to be defined over the entire arc, which as we have seen, means over the arc defining disc.

We can now state that the increment of flux in angle $d\omega$ from area A_s is

$$d^2F = I'_s d\omega dA_s = \frac{\partial^2 F_s}{\partial \omega \partial A_s} d\omega dA_s \quad (3-13)$$

The next step will be to integrate dF over the source disc to find dF , the incremental flux arriving at A_r due to the entire source. However, before we do this, we shall develop a coordinate system to describe the position of P_r with respect to

FIGURE 3-12
RADIATION IN $d\omega$ FROM dA_s TO dA_R



the source, and a coordinate system to describe the position P_s on the source defining disc.

Figure 3-13 shows the source viewed from the side (stems up and down.) Any of several coordinate systems might be chosen, but due to the rotational symmetry of the source, the polar system is most useful. (In array computations the cartesian system may be preferred, however it is still far easier to work in polar in the module and transform for array computations.) The radius vector from the source center to any point in space is denoted by R . The magnitude of R is the distance from source center to the point, and the angles ϕ and θ describe the vector direction. The direction of the bulb stem which points toward the exit pupil is taken as $\phi = 0^\circ$. The angle ϕ is thus measured from optical axis or module normal. The angle θ describes position around the source. θ is the symmetry angle. Thus a change in θ usually produces no change in the various parameters. We must take note of two important points.

1. Source (arc) center is an arbitrary point and it will have to be defined as we progress.
2. The optical axis of the module (which alternatively may be called the module normal) is always assumed to pass thru the center of the arc and thru the focus of all symmetric optical elements.

Figure 3-14 depicts the source defining plane (in the plane of the paper) and a generalized disc. The disc is the projection of the vectors T upon the defining plane. The center point is the vector R from the arc center to the point from which the arc is being viewed (P_r). Since the disc is normal to R , the disc

FIGURE 3-13
MODULE COORDINATE SYSTEM

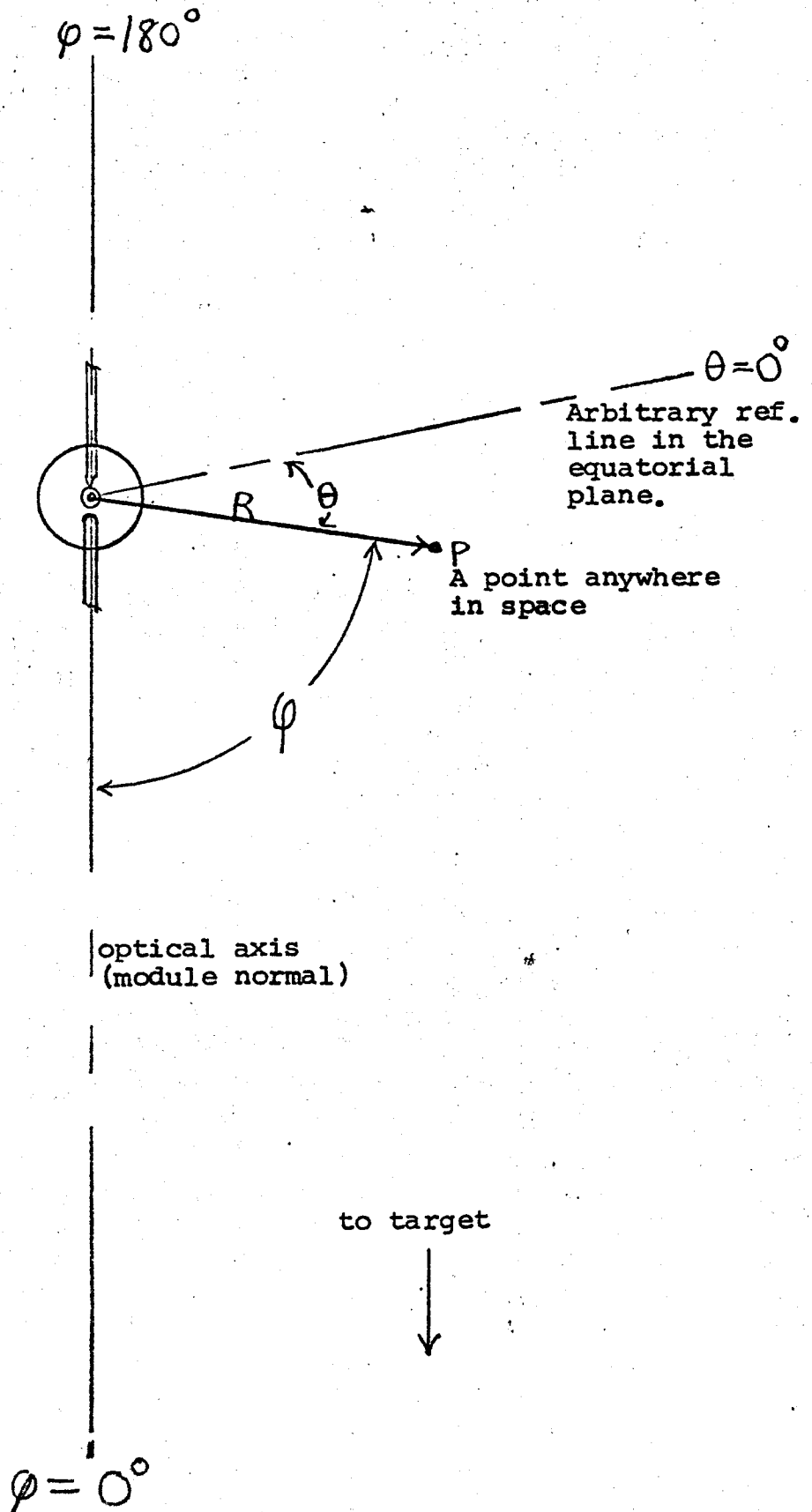
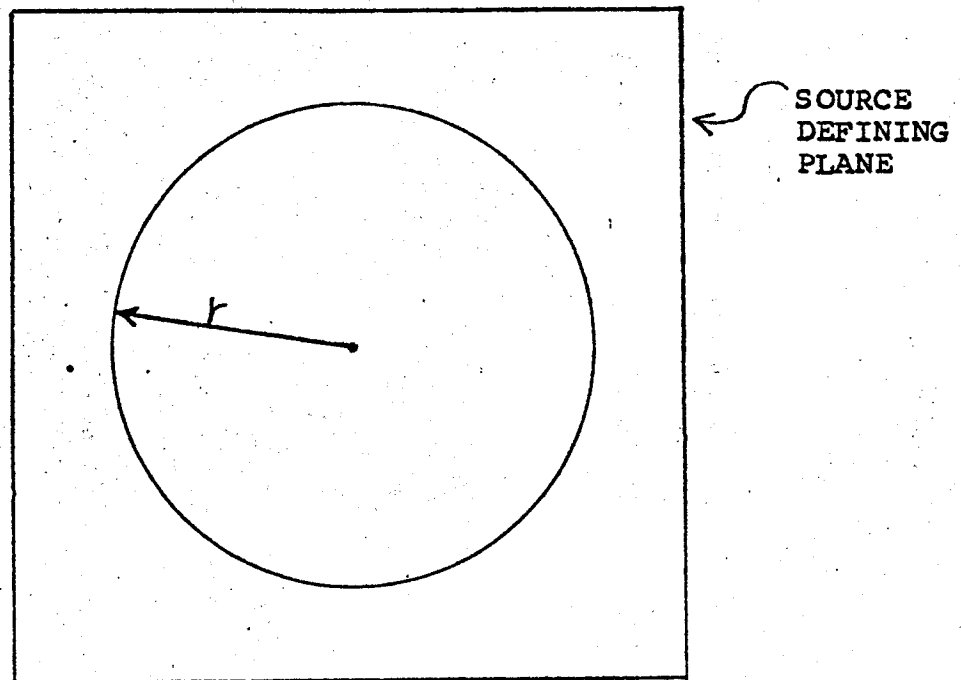


FIGURE 3-14

SOURCE-DEFINING-DISC COORDINATE SYSTEM



assumes angles ϕ , θ with respect to the module and source. Since θ is an angle of symmetry the disc will be independent of θ . However, it appears that we must define a different disc for every possible angle ϕ and distance $|R|$. In theory, we would require a new disc for every ϕ and $|R|$. In practice we shall show that for the range of interest a disc can be defined which will be reasonably accurate for any $|R|$, and the change in disc with ϕ can be applied to the entire disc as a scalar multiplier. These results are most valuable because they reduce the source representation to a single disc and a scalar function of ϕ .

Let us assume a disc has been derived for some point P (ϕ , θ , $|R|$). Now suppose we hold ϕ and θ constant and vary $|R|$, and suppose we ask how the disc will change. It is obvious that the vector to any given point on the disc will assume a new angle with respect to R as we change $|R|$. Thus this vector T no longer cuts the same set of points in the arc volume. Further, this vector T now has a new direction with respect to the normal R, and this angle (α) relates irradiance to intensity with the function $\cos \alpha$. The change in radiation which occurs due to the new set of points pierced by T depends on the nature of the arc. A surface radiator would produce one function and a volume radiator another. We have already assumed the arc to be in between. We are going to assume that the total change in I' as $|R|$ is changed is proportional to $\cos^4 \alpha$ where α is the angle between R and T. We note that the \cos^4 assumption is made by General Electric. (3)

Also, the results are better for \cos^3 so \cos^4 represents a severe test of our thesis. The arc radius will be assumed at 8 mm maximum. The optics will be assumed to be 40 mm from the arc at the closest point. This is quite close to the bulb and it is doubtful if any optical element could be placed appreciably closer. The distance used by General Electric to measure I' is 165 mm. The farthest possible distance is infinity. The mean power weighted angle in the prototype optics is $2^{\circ}18'$. Now refer to table 3-2. $\cos^4 \alpha$ is shown for several values of R and r . For infinity the term is 1.0000. For the near point of 40 mm and an arc radius of 8 mm the \cos^4 is 0.9247. Thus the deviation is only 8% for the highest and lowest $|R|$. At the near point of 40 mm and an arc radius of 6 mm the deviation is less than 5%. And for the mean power-weighted $\alpha = 2^{\circ}18'$ \cos^4 is 0.9968. This is a trivial deviation. Thus, we have shown that we can use a single model for all $|R|$ and the $\cos^4 \alpha$ term can be eliminated.

Now suppose we hold θ and $|R|$ constant and vary ϕ . Two things will happen. The total flux dF from the arc to area dA_r is a definite function of ϕ as shown by the Westinghouse source data, figure 3-3. And second, the arc shape is a function of ϕ because the arc is not symmetric with respect to ϕ . In fact, the arc is elongated along the $\phi = 0^{\circ}$ axis (see figure 3-4).

To accommodate the change in dF_r with ϕ , we shall use relative values for the disc and multiply by a factor which will vary with ϕ . We shall call this factor $G_1(\phi)$, where G_1 represents a general function. The earliest available data for flux as

TABLE 3-2

 $\cos^4 \alpha$ AS A FUNCTION OF R and r

| R | r | $\tan \alpha$ | α | $\cos \alpha$ | $\cos^4 \alpha$ |
|----------|------|---------------|----------|---------------|-----------------|
| 40 mm | 8 mm | 0.2000 | 11° 19' | 0.9806 | 0.9247 |
| 40 mm | 6 mm | 0.1500 | 8° 32' | 0.9889 | 0.9563 |
| 165 mm | 8 mm | 0.4850 | 2° 47' | 0.9988 | 0.9952 |
| ---- | ---- | ---- | 2° 18' | 0.9992 | 0.9968 |
| Infinity | ---- | 0.0000 | 0° 0' | 1.0000 | 1.0000 |

a function of θ was a curve of total radiation versus angle θ . The ratio of 'arc radiation' to total radiation at $\theta = 90^\circ$ was also available. The flux versus θ total radiation curve was multiplied by the arc-to-total-radiation ratio at $\theta = 90^\circ$ and the new curve was assumed to be arc radiation versus θ . Later in the program a curve of arc radiation versus θ was received from Westinghouse (figure 3-3.) This curve differed somewhat from the curve derived earlier.

During the early phase of the program, we realized that the arc defining disc would have a different shape as θ changed. We also realized that the problem of where to place arc center was complex. However, the data available at that time was limited to arc-iso-brightness contours at $\theta = 90^\circ$ (figure 3-4.) Therefore, a model was constructed on the following basis:

1. The arc was assumed to be spherically symmetrical,
2. Differential radiance was assumed to follow brightness,
3. Arc center was placed on the point of maximum brightness, and
4. A radius vector was drawn on the $\theta = 90^\circ$ iso-brightness plot, thru the point of maximum brightness, along the the line labelled A-A (perpendicular to the source normal). The iso-brightness was plotted along this vector and the vector was then rotated thru 360° to generate a symmetric disc.

As we have stated earlier, the actual arc is elongated. Further, the iso-differential radiance contours are not equivalent to the iso-brightness contours. And the arc center on a power centroid basis is not at the point of maximum brightness (nor

these factors, the model produced a very respectable prediction. Moreover, it is now possible to refine the model. With data developed during the course of this program, we can now define the arc center as the centroid of the differential-radiance-radius product. The model can be further refined by making the differential radiance a function of both the disc radius and the angle ϕ . Finally, the model can be based on the iso-differential radiance contours which differ somewhat from the iso-brightness contours.

If the differential radiance is developed as a function of ϕ and r , thus $g_2(\phi, r)$, then the function $g_1(\phi)$ which was used to cause the integral over the disc to be correct in value for any angle ϕ can be omitted. However, we believe it is more useful and more revealing to normalize g_2 and retain g_1 . Thus,

$$\left[\int_r g_2(r, \phi) dr \right]_{\phi} = 1 \text{ for all } \phi \quad (3-14)$$

Data developed during the program showed two discrepancies in the original model:

1. The original model extrapolated the differential radiance exponentially toward zero. This caused the arc to appear quite large. The data indicated that the differential radiance drops rapidly to zero at the edge of the arc. Thus the total arc is smaller than the first model assumed.
2. The data indicated that the (radiance) X (radius) moment was further from the center than indicated by the model.

Thus, the moment must move out, but the cutoff moves in.

The module behaviour predictions made in this program were all based on the original model. As the program progressed, a refined model was often used in a semi-quantitative manner to gain further insight into module behaviour. Thus the model, the predictions, and the data constantly interacted.

The model which we have described has some noteworthy properties. The simple basic form allows rapid computation and is remarkably accurate. Even the more refined form lends itself to computation. A highly-sophisticated, three-dimensional model could probably be derived after many months of measurement and study, but we doubt that such a model is in any way desirable. The problem would get involved in a maze of computation and all insight would disappear. We believe that the disc model we have developed is completely adequate for the task of designing a solar simulator module. (9) (10) (12) (13) (14)

3.3.7 Integration over the Arc Disc. - (14) (15) We

noted earlier (equation 3-13) that

$$d^2 F = I_s' d\omega dA_s = \frac{\partial^2 F_s}{\partial \omega \partial A_s} d\omega dA_s$$

We shall now integrate over the source disc to find dF_R .

$$dF_R = \left\{ \iint \frac{\partial^2 F_s}{\partial \omega \partial A_s} dA_s \right\} d\omega \quad (3-15)$$

$$dF_R = \left\{ \int_{r=0}^{r_{max}} g_1(\psi) g_2(r) 2\pi r dr \right\} d\omega \quad (3-16)$$

$g_1(\psi)$ is the weighting function for ψ

$g_2(r)$ is a function expressing $\frac{\partial^2 F_s}{\partial \omega \partial A_s}$ along r for the transformed symmetric disc.

If the radiation in some spectral increment ($d\lambda$) is of interest, then we can write

$$d^2 F_{R\lambda} = \left\{ \int_{r=0}^{r_{max}} g_1(\psi) g_2(r) g_3(\lambda) 2\pi r dr \right\} d\omega d\lambda \quad (3-17)$$

Since g_1 has been defined as a function of ψ only, it can be removed from the integral. However g_3 has not been shown independent of r and must remain inside the integral.

$$d^2 F_{R\lambda} = \left\{ 2\pi g_1(\psi) \int_{r=0}^{r_{max}} g_2(r) g_3(\lambda) r dr \right\} d\omega d\lambda \quad (3-18)$$

3.3.8 Integration over a Defining Surface. - (14) (15) The integral of equation 3-18 over $d\omega$ and $d\lambda$ gives the total flux from the source. Thus

$$F = \int_{\omega} \int_{\lambda} \left\{ 2\pi g_1(\varphi) \int_{r=0}^{r_{max}} g_2(r) g_3(\lambda) r dr \right\} d\omega d\lambda \quad (3-19)$$

This output will be P_r , the usefully radiated power. Note that the integration with respect to λ , ω , and r can be carried out over limited domains in order to provide the useful flux within any desired wavelength limits, arc volume, and solid angle. This equation can be rewritten

$$P_r = F = 4\pi^2 \int_{\lambda} \int_{\varphi} g_1(\varphi) \left\{ \int_{r=0}^{r_{max}} g_2(r) g_3(\lambda) r dr \right\} \sin \varphi d\varphi d\lambda \quad (3-20)$$

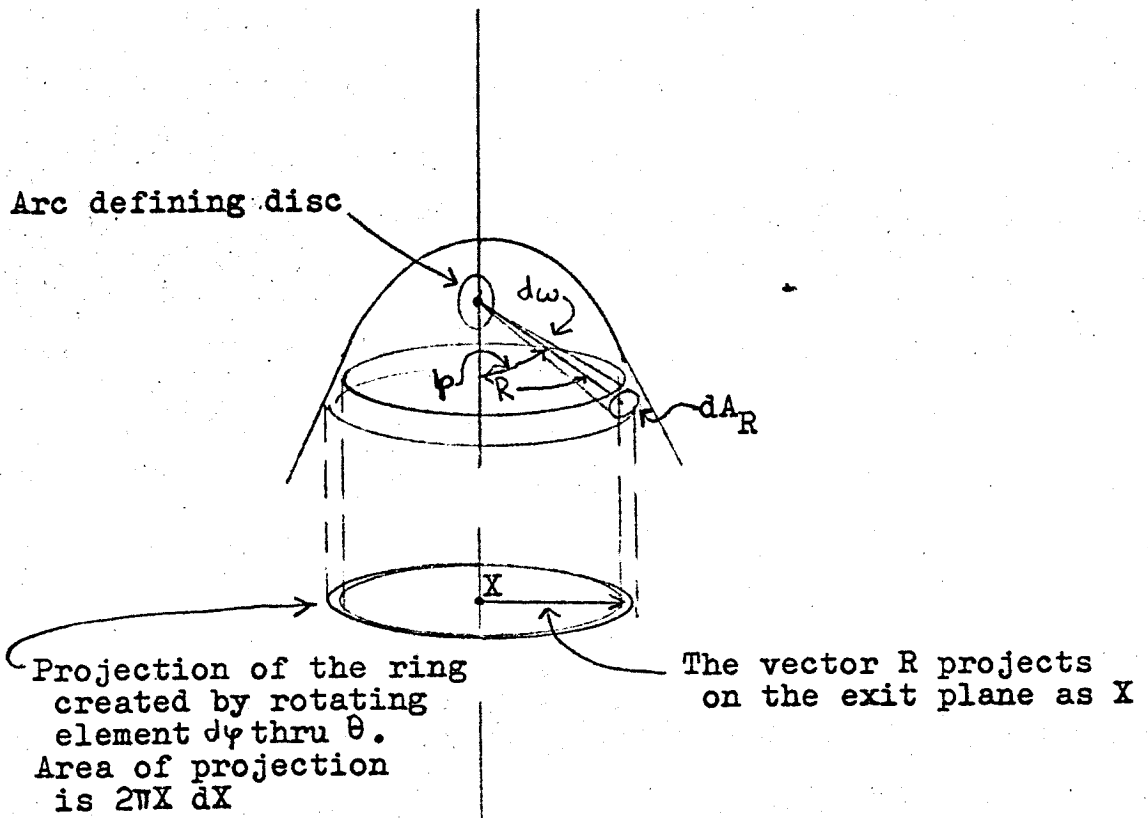
Equation 3-20 is obtained by performing the integration over a sphere. This equation allows us to compare the measured P_r from a source with the value computed from the functions.

The flux may be integrated over any surface which intercepts all of the flux to be accounted for. When optical elements are placed around the source, several possible surfaces can be considered. The integration could be performed over the surface of one or more of the elements, or the integration could be performed over the surface of an image plane. In general, the form of the equations will differ for different systems, and there will be several possible forms for any given system.

As an example, suppose we consider a source at the focus of a paraboloid of focal length f . Figure 3-15 shows a small

FIGURE 3-15

Integration Over a Parabolic Reflector



area on this reflector (dA_R) receiving flux from the arc defining disc. The area dA_R subtends solid angle $d\omega$. Thus, modifying equation 3-17 slightly

$$dF_R = \left\{ \int_r \int_\lambda g_1(\varphi) g_2(r) g_3(\lambda) 2\pi r dr d\lambda \right\} d\omega \quad (3-21)$$

The position of the area dA_R is described by a vector R from the arc center. θ is a symmetry angle. Thus only $|R|$ and φ are of interest. A parabola with focus at the origin, in polar coordinate is defined by

$$R = \frac{2f}{1 - \cos \varphi} \quad (3-22)$$

where f is the focal length of the parabola. (16)

This equation relates R and φ . Thus, we have only one independent variable of interest. The flux striking the reflector on the ring described by rotating an element $d\varphi$ thru all θ is

$$dF_\varphi = \left\{ 2\pi \sin \varphi \int_r \int_\lambda g_1(\varphi) g_2(r) g_3(\lambda) 2\pi r dr d\lambda \right\} d\varphi \quad (3-23)$$

Now we project the reflector ring subtending $d\omega$ onto the module exit pupil (figure 3-15). A radius vector projected onto the exit plane is defined by

$$X = R \sin \varphi \quad (3-24)$$

We eliminate R by using equation 3-22.

Thus

$$X = \frac{2f \sin \varphi}{1 - \cos \varphi} \quad (3-25)$$

And

$$\frac{dX}{d\varphi} = \frac{(1 - \cos \varphi) 2f \cos \varphi - 2f \sin \varphi \sin \varphi}{(1 - \cos \varphi)^2} \quad (3-26)$$

The area covered by the projection of the ring of the parabola which subtends $d\varphi$ rotated thru θ onto the exit plane is

$$dA = 2\pi X dX \quad (3-27)$$

The intensity at the exit plane is

$$E_{\varphi} = \frac{dF_{\varphi}}{dA} = \frac{\left\{ 2\pi \sin \varphi \int_{\lambda} \int_r g_1(\varphi) g_2(r) g_3(\lambda) g_4 2\pi r dr d\lambda \right\} d\varphi}{2\pi X dX} \quad (3-28)$$

where g_4 is the reflectivity.

Now let us substitute for X from equation 3-25:

$$E_{\varphi} = \frac{2\pi \sin \varphi (1 - \cos \varphi) \left\{ \int_{\lambda} \int_r g_1 g_2 g_3 g_4 2\pi r dr d\lambda \right\} d\varphi}{2\pi 2f \varphi dX} \quad (3-29)$$

Cancel and substitute for $d\varphi/dX$ from equation 3-26 and multiply by -1 due to reflection of the limits,

$$E_{\varphi} = \frac{-(1 - \cos \varphi)^3 \left\{ \int_{\lambda} \int_r g_1 g_2 g_3 g_4 2\pi r dr d\lambda \right\}}{4f^2 \left[(1 - \cos \varphi) \cos \varphi - (\sin \varphi)^2 \right]} \quad (3-30)$$

$$E_{\varphi} = \frac{(1 - \cos \varphi)^2 \left\{ \int_{\lambda} \int_r g_1 g_2 g_3 g_4 2\pi r dr d\lambda \right\}}{4f^2} \quad (3-31)$$

$$E_{\varphi} = \frac{\left(2 \sin^2 \frac{\varphi}{2} \right)^2 \left\{ \int_{\lambda} \int_r g_1 g_2 g_3 g_4 2\pi r dr d\lambda \right\}}{4f^2} \quad (3-32)$$

$$E_{\psi} = \frac{\sin^4 \frac{\psi}{2} \left\{ \int_0^X \int_0^r g_1 g_2 g_3 g_4 2\pi r dr d\lambda \right\}}{f^2} \quad (3-33)$$

Equation 3-33 expresses intensity at the exit pupil as a function of ψ . Equation 3-25 relates ψ to X . Equation 3-33 can be stated in terms of X by developing $\psi(X)$ as a power series, but the complexity would limit the value of the equation. The $(\sin^4 \frac{\psi}{2})$ term of equation 3-33 shows a very steep fall in intensity for points away from the optical axis.

3.3.9 Flux Collection. - One of the tasks of the optical system is to gather the flux radiating in all directions and send it in the desired direction. In classical optics, this is easily accomplished for a point source and an infinitely large paraboloid. We do not have a point source and the infinite paraboloid will not fit in our module, so for us the problem is somewhat more difficult. In particular, the following restrictions apply to the solution:

1. The radius of the collecting system must agree with R_u as defined by equation 3-9. This equation establishes an upper radius limit.
2. The flux which is initially directed away from the desired exit plane must be brought around the source without returning through it.
3. The collecting elements must be clear of the source and its supports.
4. The collecting element supports must not interfere excessively with the transmission path.
5. The collector should mate with the rest of the optical system to produce the desired beam pattern.

In addition to the requirements above, the collector elements must be fabricated at reasonable cost, must have a reasonable cost, must be alignable, and must be alignable without undue complexity or criticality.

There are an unlimited number of possible collection systems. We will not attempt to classify them or to survey them. We will briefly discuss a very few basic types where the discussion bears upon the designs we have used.

The ellipsoid with the source at one focus is one type of basic collector. The source is imaged at the other focus. Since the ellipsoid creates an image at a finite distance, another element is required to complete the collimation* .

* Collimation is used here to mean that if the source were a point, then all flux would exit parallel. There is no implication that flux from a finite source will be parallel, because in fact it won't.

The use of an ellipsoidal collector has several difficulties:

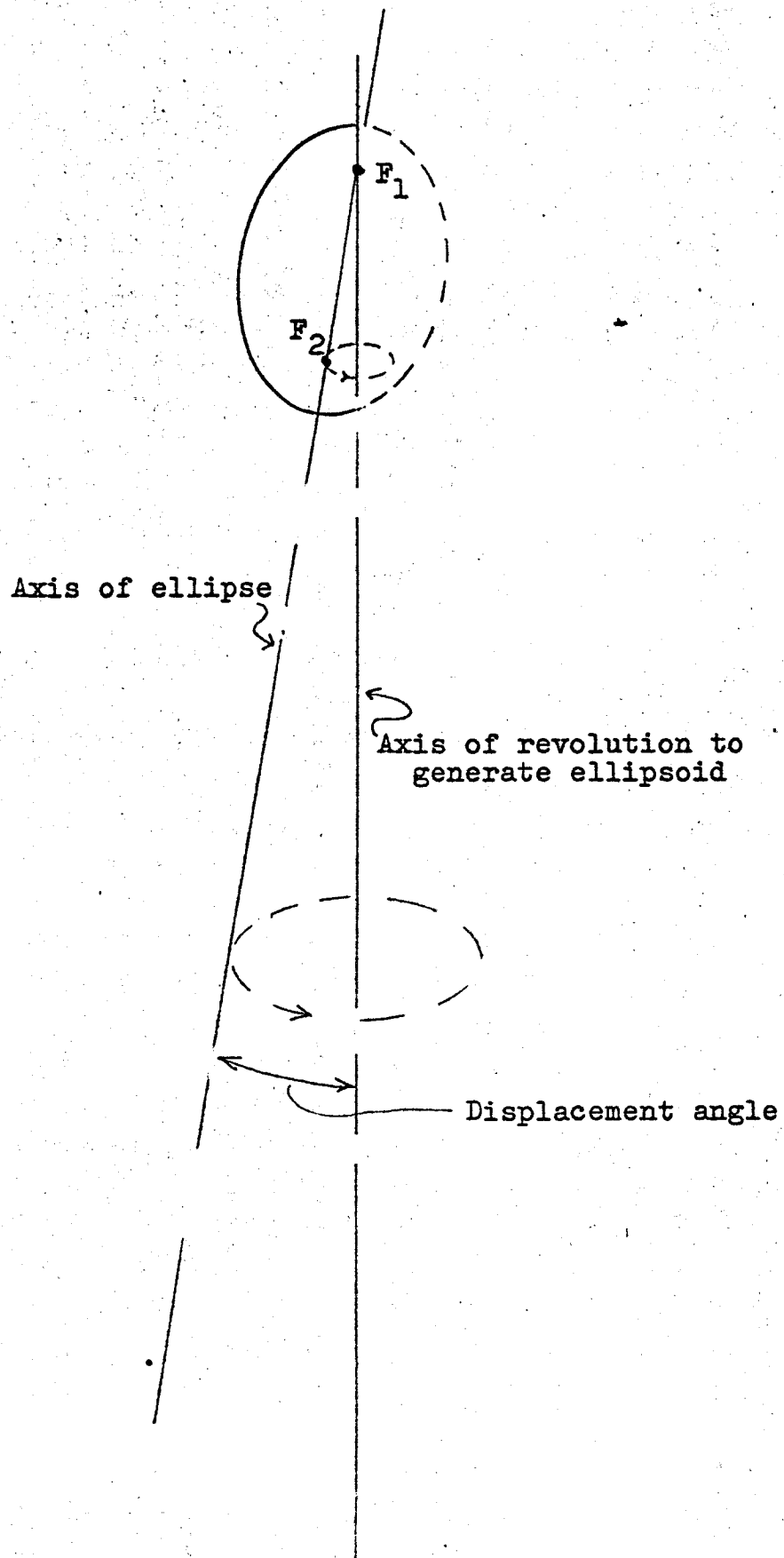
1. The flux radiating at large values of ψ will be returned through the source,
2. If the ellipsoid is large enough to clear the source and to view most of the arc volume, the radius becomes excessive, and
3. The flux is brought to focus at a considerable angle, and the second element must bend the flux through a large angle to complete the collimation.

These problems can be alleviated by using an angularly displaced ellipsoid. (An ellipse is drawn with the top focus on the source, but the bottom focus is displaced from the optical axis. This ellipse is then rotated about the optical axis to produce the angularly displaced ellipsoid. See figure 3-16.) Further progress can be made with a segmented reflector, but we shall discuss segmented reflectors in connection with paraboloids.

The paraboloid has some very attractive features and some major problems. The major advantage of the paraboloid is that all flux which it intercepts is collimated.* Thus, if the

FIGURE 3-16

Angularly Displaced Ellipsoid



paraboloid can be made large enough to intercept the required amount of flux, then we do not have to use a second element to complete the collimation. In terms of efficiency this

*Collimation is used here to mean that if the source were a point, than all flux would exit parallel. There is no implication that flux from a finite source will be parallel, because in fact it won't.

is a significant advantage. A second large advantage is freedom from chromatic aberration. Since the flux exits from the paraboloid already collimated, there is no need to use refractive elements to bend the rays. Reflectors are substantially free from chromatic dispersion, whereas with refractive elements made only from quartz dispersion becomes a major problem. The advantages of the paraboloid are major, and it is desirable that an attempt be made to solve the difficulties so as to realize these advantages. The difficulties are as follows:

1. The flux radiating at large values of φ will be returned through the source.
2. If the paraboloid is large enough to clear the source at the top and to view the majority of the arc volume, then the maximum radius becomes excessive (if the flux at small values of φ is to be collected.)
3. The intensity is very high at the center of the parabola and falls as $\sin^4 \frac{\varphi}{2}$ as the edges are approached.

The basic problem with the paraboloid can be restated as follows:

1. If the focus of the paraboloid is short, the arc

volume subtends an excessively large angle at reflector points ^{near} the vertex, and much flux will be returned through the source.

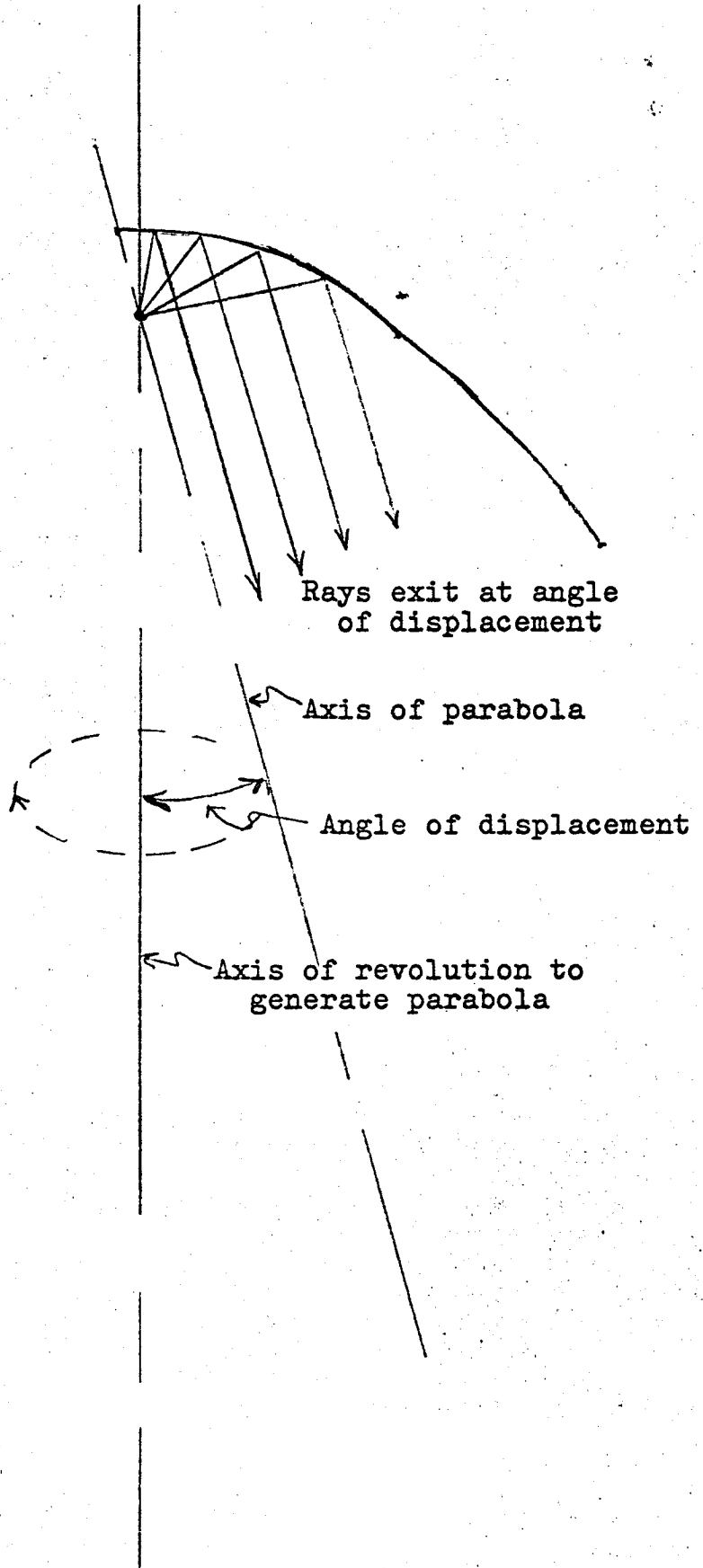
2. If the focus of the paraboloid is long, the mouth end cannot collect flux at small angles of ψ without exceeding the allowable module radius.

Fortunately, two excellent methods may be brought together to solve the problems of the paraboloid. One method is tipping and the other is segmenting. Refer to figure 3-17 to observe a tipped paraboloid. A tipped paraboloid is generated by rotating a parabola around its focus in its own plane (through ψ), and then rotating the plane about the optical axis (through θ). The rays of light are angularly tipped at the same angle as the parabola. The light must be tipped back parallel to the normal. This can be done with refraction or with reflection from a cone. The latter method is favorable because it does not produce chromatic dispersion.

Segmentation can have a number of meanings. As used here, we mean a reflector system with different segments for different zones of ψ . Segmented reflector systems include fresnel reflectors with hundreds of elements as well as systems with only two or three elements. Also, the edges of the elements may join or may be separated. The statement is sometimes seen that segmented reflectors have high loss. Like most generalizations this statement is not very good. When speaking of loss one must first define the ground rules. For example, consider two hypothetical reflector systems A and B.

System A intercepts 95% of the available flux and 85% of all intercepted flux is brought down. Thus,

FIGURE 3-17
Tipped Parabola



this system has an overall efficiency of
 $.85 \times .95 = .81$.

System B intercepts only 75% of the available flux,
 but brings down 92% of all intercepted flux
 for an overall efficiency of $.75 \times .92 = .69$

System B has lower 'loss' if the per cent of flux intercepted
 is ignored. But by any criterion of value in solar
 simulation, system A is better.

The losses in a fresnel reflector with hundreds of steps may
 get very high. Segmentation loss in a segmented system of
 three to six elements may be zero for a point source and less
 than 10% for a typical arc. The gain due to additional flux
 collection can easily outweigh the loss.

The beauty of the segmented system is in its ability to deal
 with the specialized problems of collecting flux over a solid
 angle of almost 4π . The flux from the region of high ψ can
 be caught in a tipped reflector and brought to the outside to
 clear the source. The flux from intermediate values of ψ
 can be brought straight down by ^aparaboloid. And at low values
 of ψ , where an extended paraboloid would reach very large
 diameter, a new reflector segment can be used. In other words,
 near optimum collection occurs for all values of ψ . In
 particular, at values of ψ where the flux is strongest the
 value of $|R|$ can be made optimum for the desired beam pattern.
 $|R|$ will then be non-optimum in regions of weak flux.

An area where we feel some remarks are in order is in the use of
 complex, multi-element systems. For example, the aconic systems
 which require dual elements, one aconic correcting another,

and the highly refined collimating systems which have been designed for projectors are included in this group. We are mindful of Occam's Razor* which advises us that, 'when two or more hypotheses cover all the known facts, choose the simplest of them', and we paraphrase the Razor thusly, 'when two or more systems meet the requirements of a problem choose the simplest system.' We feel that the consideration of complex methods should begin only if and when it is clear that simpler systems cannot succeed. And, as we shall see, more complex solutions do not appear to be required.

*Ockham, William of, 1300?- 1349?

3.3.10 Beam Determination. - Consider a source and an optical system. The output can be defined by stating the flux going in every direction for every point on the exit pupil. The beam can be described by the following parameters.

1. Total power in the beam.
2. Initial diameter of the beam.
3. Half-angle of the cone which will contain a defined per cent of beam power at infinity.
4. Beam power as a function of angle (β) and origin on the exit pupil.

The beam profile for any distance from the module can be determined from these parameters.

We shall examine the beam from a source at the focus of a paraboloid. The total power can be found from the following equation

$$F = \int_{\varphi} \int_{\lambda} \int_{r} 4\pi^2 g_1 g_2 g_3 g_4 \sin\varphi r dr d\lambda d\varphi \quad (3-34)$$

The initial diameter will be the diameter of the paraboloid. The equation 3-34 can be rewritten to find the total power in angle $d\beta$. Equation 3-34 integrates over the source defining disc using r as the variable. If a reflector element is R distance from the source disc, and if a vector to a point on the disc is at angle α to R , then

$$r = R \sin\alpha$$

And by differentiation

$$dr = R \cos \alpha d\alpha \quad (3-36)$$

We can use the equation relating R and $\cos \varphi$ (3-22) to write

$$r = \frac{2f \sin \alpha}{1 - \cos \varphi} \quad (3-37)$$

and

$$dr = \frac{2f \cos \alpha}{1 - \cos \varphi} d\alpha \quad (3-38)$$

We can now express the flux in angle $d\alpha$ by

$$dF_{\alpha} = \int_{\varphi} \int_{\lambda} 4\pi^2 g_1 g_2 g_3 g_4 \sin \varphi \frac{(2f)^2 \sin \alpha \cos \alpha}{(1 - \cos \varphi)^2} d\lambda d\varphi d\alpha \quad (3-39)$$

The flux incident on a reflector element dA_R at angle α will be brought down at angle α off the normal, if the reflector is a paraboloid (non-tipped.) Thus, for the case of the basic paraboloid angle α is angle β as defined earlier. Thus we write

$$dF_{\beta} = \int_{\varphi} \int_{\lambda} 4\pi^2 g_1 g_2 g_3 g_4 \sin \varphi \frac{(2f)^2 \sin \beta \cos \beta}{(1 - \cos \varphi)^2} d\lambda d\varphi d\beta \quad (3-40)$$

The total flux at all angles from β_1 to β_2 is

$$F_{\beta} = \int_{\beta_1}^{\beta_2} \int_{\varphi} \int_{\lambda} 4\pi^2 g_1 g_2 g_3 g_4 \sin \varphi \frac{(2f)^2 \sin \beta \cos \beta}{(1 - \cos \varphi)^2} d\lambda d\varphi d\beta \quad (3-41)$$

The half-angle of the cone which will contain K_1 per cent of beam power (at infinity) is formed by solving 3-42

for β_2 :

$$\frac{F_\beta}{F} = K_1 = \frac{\int_0^{\beta_2} \int_0^{\pi/2} \int_0^\lambda 4\pi^2 g_1 g_2 g_3 g_4 \sin \psi \frac{(2f)^2 \sin \beta \cos \beta}{(1 - \cos \psi)^2} d\lambda d\psi d\beta}{\int_0^{\pi/2} \int_0^\lambda \int_0^\lambda 4\pi^2 g_1 g_2 g_3 g_4 \sin \psi \frac{(2f)^2 \sin \beta \cos \beta}{(1 - \cos \psi)^2} d\lambda d\psi d\beta} \quad (3-42)$$

The distribution of flux by β is given by equation 3-40, and this equation can also be used to yield flux as a function of exit position and β .

A paraboloid with a point source at its focus maps every possible view of the point onto the exit pupil. This map will be translated without transformation to all planes perpendicular to the optical axis, out to infinity. If the point source is replaced by a finite source, the paraboloid maps the center of each view onto one point of the exit pupil. Each view is mapped around its center point. Thus the views overlap. A small section of the exit pupil is thus an overlap of a series of views over some $\Delta\theta$ and $\Delta\psi$. We call the region near the exit pupil the near field. In the near field region we find a correlation between position (from the optical axis) and view (θ and ψ). Since θ is a symmetry angle, we can consider this a correlation between X , the perpendicular distance from the optical axis, and ψ the angle of view measured from the optical axis.

A region very far from the paraboloid is termed a far field region. In the far field, we find that a portion of the arc

at angle α with respect to vector R will be mapped into angle β . Thus in the far field, we find a correlation between the radius r (the angle α is $\arcsin \frac{r}{R}$) and the angle β . We noted earlier that for a paraboloid α and β are equal. The correlation is complex, because each part of the reflector is at a different distance $|R|$ from the arc, and thus different parts of the reflector will map a particular area of the source dA_s at different angles β .

Between the far field and the near field, the mapping is a hybrid of both ψ and α . The test volume in a typical solar simulation problem will be in the near and the mid field. The far end of the volume may be considered to approach far field. Because most of the volume is near or mid field, far field simplifications cannot be made.

The manner in which the reflector system maps the arc defining disc described by parameters $g_1(\psi)$ and $g_2(r)$ into the beam described by $E(X, \beta)$ determines what the beam profile will be at any distance Z from the source.

Let us restate the previous paragraph. The source ^{is} completely described by $g_1(\psi)$ and $g_2(r)$. The beam is completely described by $E(X, \beta)$. The reflector system maps $g_1(\psi)$ and $g_2(r)$ into $E(X, \beta)$, thus completely determining the beam profile for all distances Z .

In designing a collector system, our goal is to design a system which will:

1. Collect as much flux as possible,
2. Bring this flux to the exit pupil with the highest possible efficiency, and

3. Establish a mapping of q_1, q_2 into E (χ, β)
which will produce the desired beam profile.

It may not be possible to satisfy these three conditions completely with a single element system. (By a single element system we mean a system where each ray touches only one element.) If a single element will not suffice then we wish to select a set of collector elements to satisfy the conditions to the greatest possible extent with '1' and '2' having maximum priority. We can then use a second element to complete the satisfaction of '3'.

3.3.11 Beam modification. - There are numerous ways in which a beam can be modified. We shall discuss three methods:

1. the single lenticular plate,
2. the dual lenticular plate, and
3. the baffle assembly.

The lenticular plate is an assembly of lenses (figure 3-18). The lenses can be bound together or molded into a single plate. The lenses may all be identical or they may differ. The parameters for each lens are:

1. shape,
2. size,
3. thickness,
4. focal length, and
5. prism angle (if any).

Since the lenticular plate is normally mounted very near the exit pupil of the collector system, the collector system maps a certain view $\Delta\theta$, $\Delta\psi$ onto a given lens. That particular view will have a β distribution determined by $R(\psi)$ for that part of the reflector system. The lens can do either of two things separately or together:

1. The concentric-conical β distribution can be transformed by spheric lens action.
2. The concentric-conical β distribution can be tipped by some angle through prism action.

From the foregoing description, it should be obvious that this is a very general and very powerful method, and that it cannot be characterized by simple statements. A lense is a very flexible tool, and a plate of lenses has this flexibility manifold. As an example of the versatility of this method, note that a particular problem might be solved by a few lenses at the center and holes or flat plate for the other areas. Or a single row of lenses might be placed around the rim with a large hole in the center. Or prisms of differing angle might be placed selectively on different lenses. Or the lenses might have different focal lengths.

Since each lense intercepts a view region $\Delta\theta$, $\Delta\varphi$ and remaps the β distribution for this region, the lense plate can serve as a scrambler or integrator. Thus, points in the near field will no longer map to a given $\Delta\theta$, $\Delta\varphi$ and points in the far field will no longer map to a given Δr in the arc volume. This is very valuable, because it avoids the following problems:

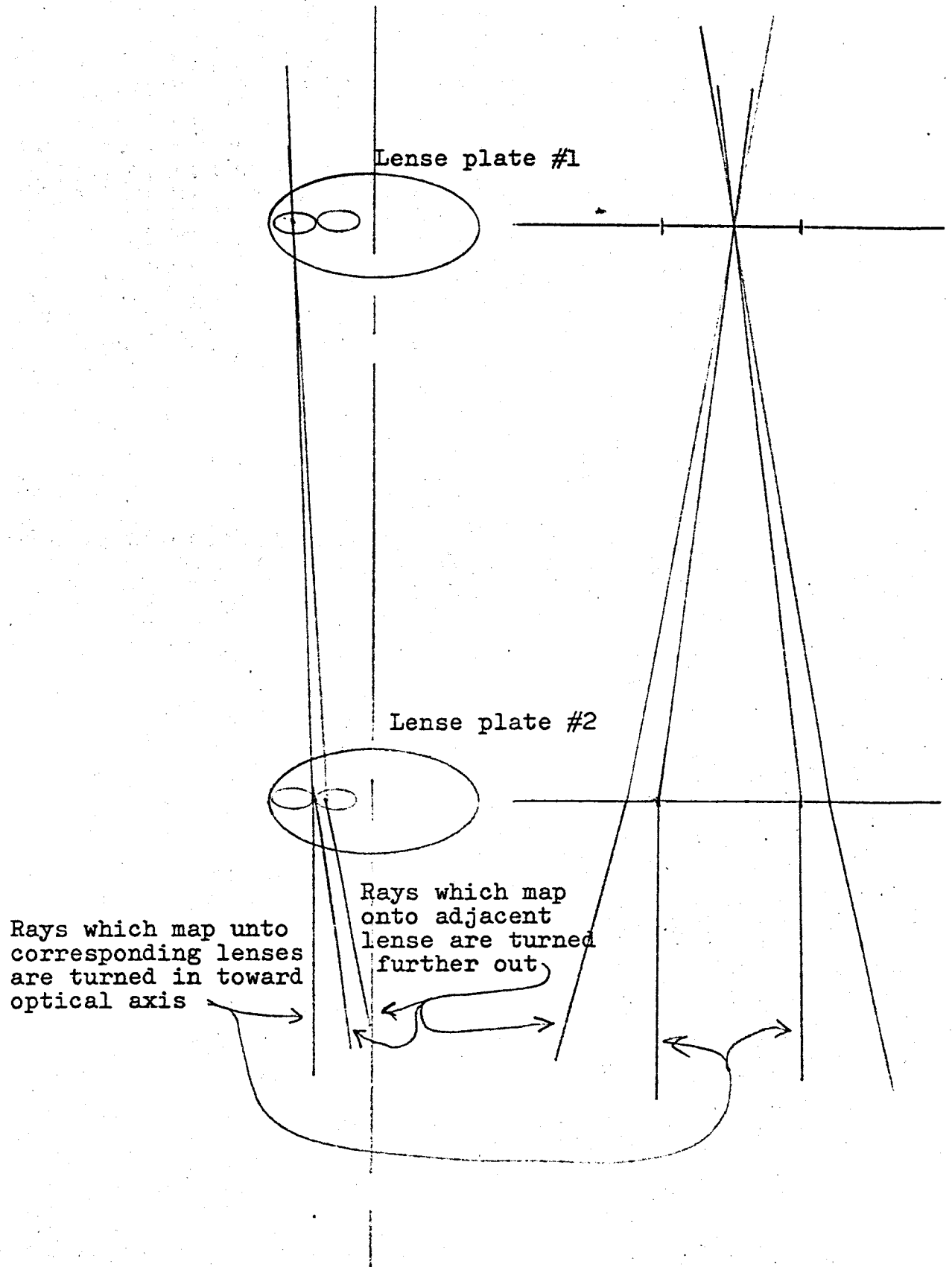
1. Spectral structure in the test volume due to correlation between λ and r, φ , or θ .
2. Intensity structure in the test volume due to correlation between I and r, φ , or θ .

We have assumed that θ is an angle of symmetry, but in practice we must expect some variation with θ . The lenticular lense system will integrate such variations.

Consider the special case of two identical lenticular plates mounted on a single optical axis, spaced one focal length apart, and oriented so that corresponding lenses are coaxial. A lense on the first plate receives a view described by a function of θ , ψ , and r , and maps it onto the corresponding lense on the second plate. This mapping is a function of α and thus of r , but it is not a function of θ or ψ . All rays which are incident on a plate one lense at angle α will be mapped to a ring of radius r_L on the corresponding plate two lense. Since rays of angle α will be incident upon the entire surface of the plate one lense, the ring on plate two receives rays over an angular range. The plate two lense will map this angular distribution into a new angular distribution. The net effect is to take all rays leaving the reflector at angle α through a very complex mapping into an angular distribution β . This system is thus an excellent scrambler. However, it has a further function. Note in figure 3-20 that all rays within a certain angle will be mapped onto the corresponding lense, and that rays incident at a greater angle will be mapped onto the next lense over. This adjacent lense will turn the stray ray further out. The ray will now have considerable angle and can be easily removed by a stop or baffle. The net effect of the two plate system described above is to create a hard beam profile due to sharp angular selection.

FIGURE 3-19

Sharp Angular Selection



Consider a lenticular plate at the mouth of a collector system. Assume all lenses have a focal length f_L and a radius r_L . All rays which are incident upon the lense at an angle α where

$$\alpha \leq \arctan \frac{r_L}{f_L} \quad (3-43)$$

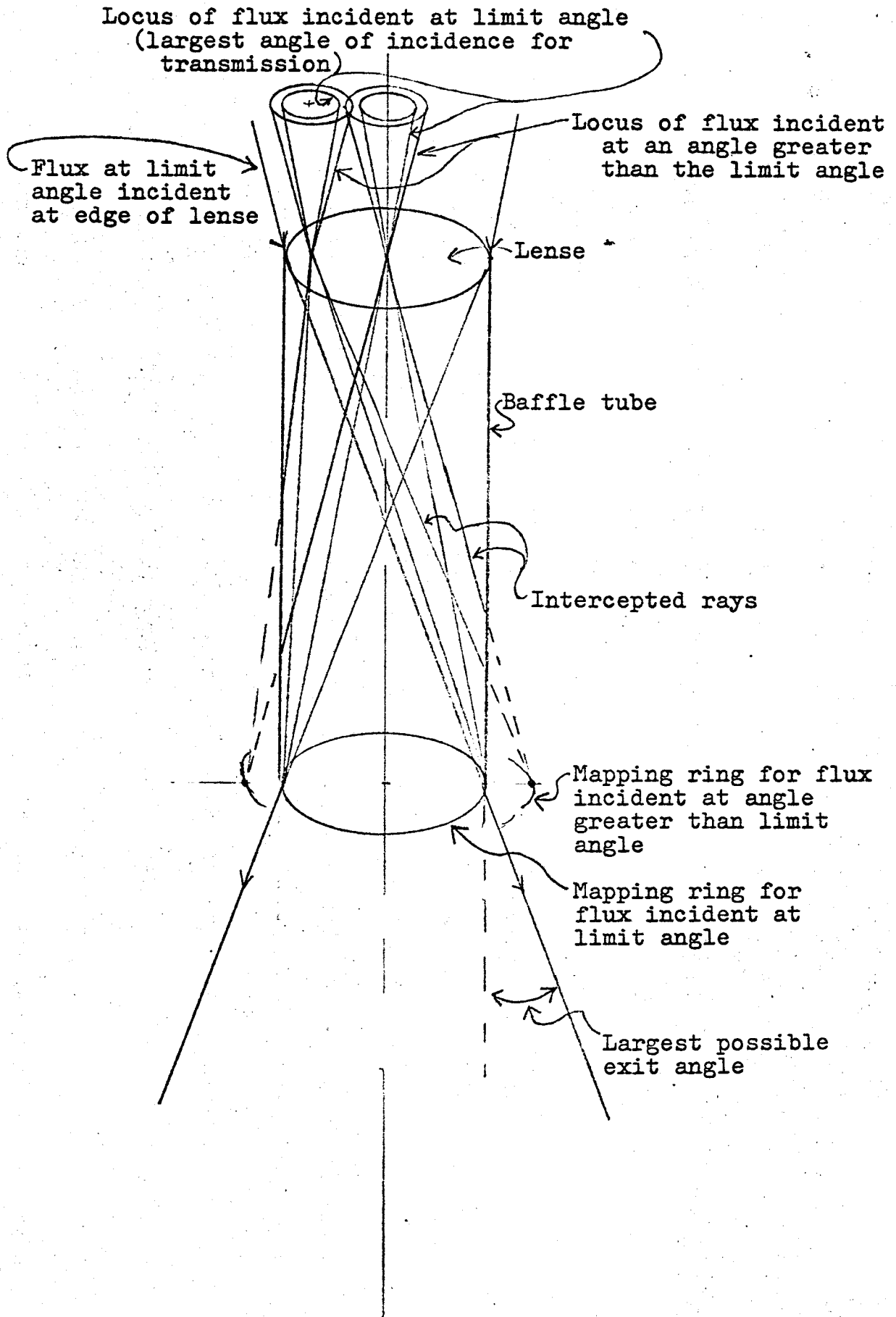
will be imaged in the image plane within an area which is bounded by the projection of the lense circumference upon the image plane. All rays which are incident upon the lense at a greater angle are imaged outside of the aforementioned area.

Now suppose we place a tube between each lense and the focal plane. The tube is the locus of the projection of the lense circumference. Thus, the tube crossection has the same shape as the lense circumference, and the tube length is the focal length of the lense. Assume that the tube will absorb all radiation incident upon its walls. Then all rays which leave the collector system and are incident upon the lense at an angle $\alpha \leq \arctan \frac{r_L}{f_L}$ will remain entirely within the tube and will be transmitted without loss. All rays which are incident upon the lense at a greater angle will strike the tube wall and be absorbed. Figure 3-21 illustrates the operation of such a baffle tube.

A system of such tubes forms a baffle. The baffle properties can be varied by changing the length and position of the baffle tubes and by changing the focal length and diameter of the lenses.

FIGURE 3-20

Baffle Tube



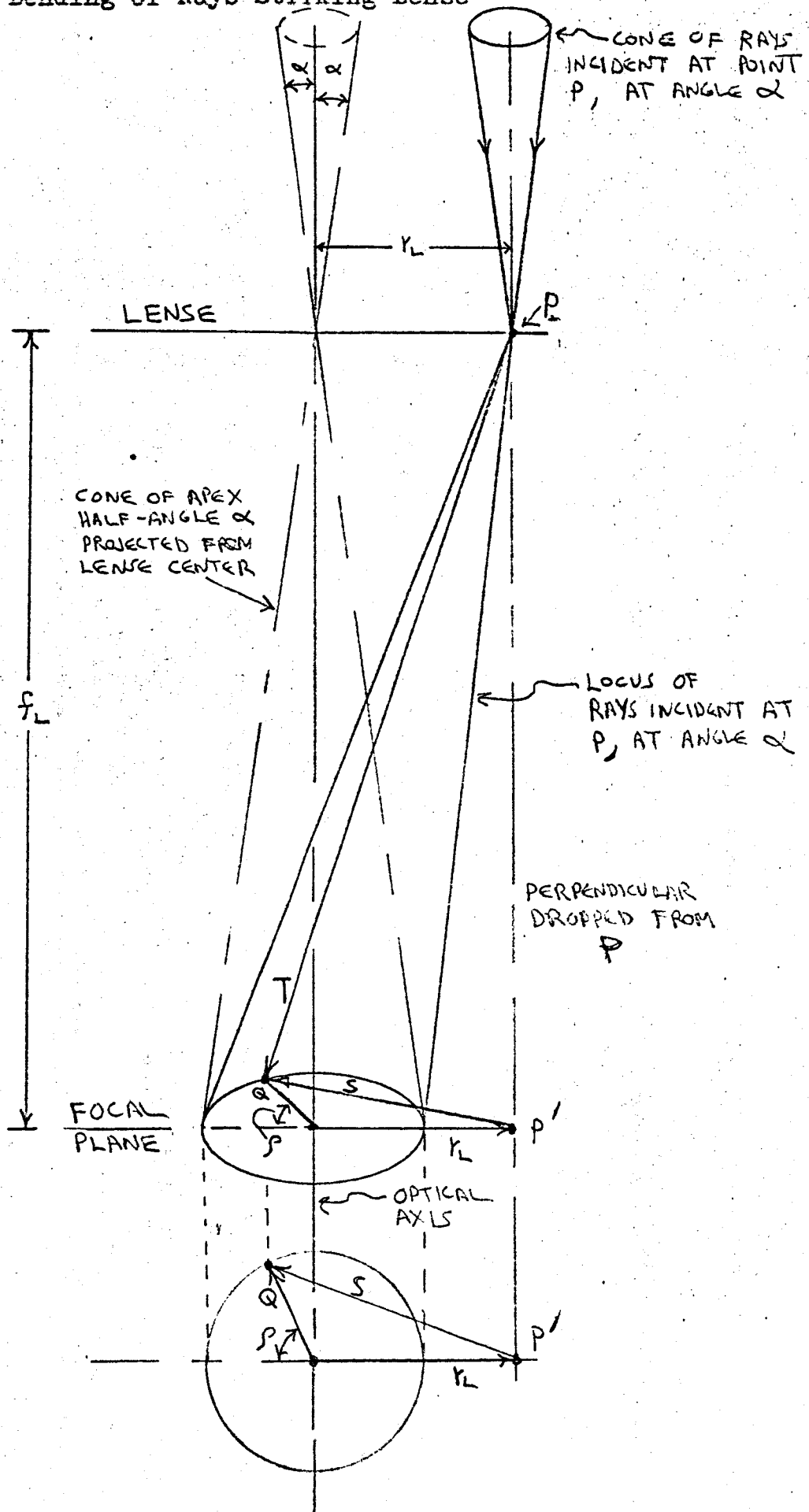
The operation of the baffle system described above with respect to α , the angle of incidence, is very simple. Below a certain α all rays are transmitted, and above that α all rays are absorbed. However, because of the action of the lense, the rays which transmit will have an angular distribution from an angle of zero to an angle of $\arctan \frac{2r_L}{f_L}$.* In the absence of further optics,

*This is a straightforward derivation based on geometric optics.

this is the angular distribution which will irradiate the target, and thus we will refer to it as the β distribution.

Equation 3-11 noted that rays of flux from an incremental area of the arc defining disc at a distance r from the disc center, reflecting from a point on the paraboloid which is at distance R from the arc center, will have an angle with respect to the optical axis of $\alpha = \arctan \frac{r}{R}$. The distribution of flux by α for a paraboloid was given by equation 3-39. In the absence of further optical elements, 3-39 can be rewritten as in 3-40 where β is set equal to α . If a lenticular plate is present, then α and β will be functionally related. The function relating α and β can be derived from the lense action. Figure 3-21 shows a conical surface which is the locus of all rays striking the lense at a single point P and at an angle α . All rays incident upon the lense at angle α will image on a ring formed by the intersection of the

FIGURE 3-21
 Bending of Rays Striking Lens



focal plane with a right circular cone of half angle α , with its apex at the lense center and its axis coincident with the optical axis. (This is first order optical theory and is based on the $\sin L = L$ approximation. At 8° the error is 0.33% - less than $2'$.) Now a conical surface is projected from the point P on the lense to the image ring in the focal plane. This surface is the locus of all rays which were incident upon the lense at point P and at angle α . Consider the ray T on the conical surface. S is the projection of T onto the focal plane. S meets a normal dropped from P which will have length f_L . Thus, by basic trigonometric consideration

$$\beta = \arctan \frac{S}{f_L} \quad (3-45)$$

A triangle is formed by S, a line formed by the displacement of P from the optical axis (r_L), and a line formed by the displacement of T from the optical axis. The length of the latter is

$$Q = f_L \tan \alpha \quad (3-46)$$

Referring to the view of the focal plane in figure 3-21,

$$S = \left[(r_L + Q \cos \rho)^2 + (Q \sin \rho)^2 \right]^{1/2} \quad (3-47)$$

where ρ is the angle between Q and r_L .

But then

$$S = \left(r_L^2 + f_L^2 \tan^2 \alpha + 2r_L f_L \tan \alpha \cos \rho \right)^{1/2} \quad (3-48)$$

And

$$\beta = \arctan \left(\frac{r_L^2}{f_L^2} + \tan^2 \alpha + \frac{2r_L}{f_L} \tan \alpha \cos \rho \right)^{1/2} \quad (3-49)$$

ρ is determined by the angular position of vector r on the arc defining disc. Thus, ρ is an angle of symmetry, and for the arc model we are using, the flux is equally weighted for all values of ρ . Therefore, β is a function of three variables:

- r_L , position along the lense diameter, with a range from zero to half of the lense diameter,
- α , the angle between the incident ray and the lense axis, with a range from zero to a maximum established by r of the defining disc and R of the reflector, and
- ρ , the angle between the projection of the ray upon the focal plane and the projection of r_L upon the focal plane, with a range from zero to 2π .

Equation 3-49 can be manipulated to yield a variety of results, but in many instances the form becomes so complex that the result is not clear by inspection. The flux as a function of β can be written by substituting β and its derivatives into previously derived equations. Rather than introduce more complex equations at this point, we shall inspect 3-49 for its significance. For angles of very small α (approaching 0) equation 3-49 reduces to

$$\beta = \arctan \frac{r_L}{f_L} \quad (3-50)$$

Since rays of a given α are assumed incident in approximately even intensities over the surface of the lense, the distribution of β follows the area. Thus, the mean β is given by

$$\bar{\beta} = \arctan \sqrt{.5} \frac{r_{LM}}{f_L} \quad *(3-51)$$

where r_{LM} is the maximum possible lense radius.

*This and other results in this section are based on circular lenses. The results will differ somewhat for square or hexagonal lenses. However, the circular result provides a very good guide. Square or hexagonal lenses operate quite satisfactorily.

Let us define a constant K_L ,

$$K_L = \frac{r_{2m}}{f_L} \quad (3-52)$$

We can rewrite 3-49,

$$\beta = \arctan \left(\eta^2 K_L^2 + \tan^2 \alpha + 2\eta K_L \tan \alpha \cos \rho \right)^{1/2} \quad (3-53)$$

where $\eta = \frac{r_L}{r_{LM}}$ and thus has a range of 0 to 1.

Then

$$\bar{\beta} = \arctan \sqrt{.5} K_L = \arctan .707 K_L \quad (3-54)$$

Now let us consider rays of $\alpha = \arctan 4K_L$,

$$\bar{\beta} = \arctan \left(\eta^2 K_L^2 + \tan^2 \arctan 4K_L + 2\eta K_L \tan \arctan 4K_L \cos \rho \right)^{1/2} \quad (3-55)$$

$$\beta = \arctan \left[\eta^2 K_L^2 + (4K_L)^2 + 2\eta K_L 4K_L \cos \rho \right]^{1/2} \quad (3-56)$$

$$\beta = \arctan \left[\left(\eta^2 + 16 + 8\eta \cos \rho \right)^{1/2} K_L \right] \quad (3-57)$$

Since η ranges from 0 to 1 and $\cos \rho$ ranges from 0 to 1, equation 3-57 can be simplified, with an error of less than 10%, to

$$\bar{\beta} \sim \arctan 4K_L \quad (3-58)$$

Since α was set equal to $\arctan 4K_L$, $\bar{\beta}$ is approximately equal to α .

We can summarize the effect of the lenses upon the mean angular distribution thusly:

1. For very small angles of incidence

$$\bar{\beta} = \arctan .707 K_L$$

2. For large angles of incidence ($\arctan 4K_L$ or greater)

$$\bar{\beta} \sim \alpha$$

3. As the angle of incidence increases from zero to $4K_L$, $\bar{\beta}$ increases in a non-linear fashion, beginning with $\arctan .707 K_L$. $\bar{\beta}$ will be greater than α but the difference will asymptotically approach zero.

We can see that flux which initially had a very low α is mapped to a substantial mean angle. Flux which initially had a high α is remapped, but the mean angle will not increase substantially.

3.4 Design Adaptation

The optical portion of the module must collect the greatest possible amount of flux, must direct this flux into the test volume, must establish the desired beam pattern, and must remove radiation which is at undesirable angles. It would be erroneous to identify each of the various optical elements with only one of these functions, because most of these functions are performed by two or more elements operating together.

The tendency to consider the optical functions separately has often led to undue complexity because of an attempt to force each section of the optical system to fulfill a function by itself. This leads to various sections opposing each other instead of aiding each other. Full use is not made of the optical properties of the various elements.

3.4.1 Collection. - The object of collection is to direct the greatest amount of flux possible into the target volume with the desired angular distribution. It will be recalled from the discussion of 3.3.4 that in order to achieve uniformity, a distribution over a finite angle is desirable. The total flux leaving the reflector within an incremental angle $d\alpha$ is expressed by the equation

$$dF_{\alpha} = \int_{\varphi} \int_{\lambda} 4\pi^2 g_1 g_2 g_3 g_4 \sin \varphi \frac{(2f)^2 \sin \alpha \cos \alpha}{(1 - \cos \varphi)^2} d\lambda d\varphi d\alpha$$

(3-39)

The problem is to maximize the flux while maintaining an angular distribution which allows efficient modification to meet the uniformity requirement.

The first element can be either reflecting or refracting, and in each case a wide choice of elements is possible. In work prior to this contract, Linear, Inc. established to its satisfaction, that the first element should be reflective. Because this decision occurred prior to this program, the factors involved will only be mentioned in passing. Of primary importance is the fact that reflectors do not produce chromatic dispersion due to change of index with wavelength, or in other words, reflectors are free of chromatic aberration. A reflective coating such as Liberty Mirror #747 provides a mean reflection coefficient of about 89% integrated over the wavelength range from .2 to 2.5 microns so that the transmission loss is comparable to that of one fairly thin lens. Finally, the back of the reflector provides a dark space, where supports can be placed without causing loss.

An infinite variety of reflector shapes can be used. Prior to this program, the basic classes of reflectors were examined. The criterion used was that all other factors being equal, the reflector system which requires the least subsequent lense path will produce the highest efficiency. Aconic elements require at least one extra element, and therefore to justify the use of an aconic, one must prove that the aconic gained more flux than the extra element (s) lost. Thus, the designer should start with a single element system, optimize it and compute the flux collected within acceptable angles. Since a second element immediately introduces a loss of about 10%, the second element should not be considered unless at

least 10% more collection is possible.

Linear module #0430 was based on a segmented reflector of which the main element was an offset ellipsoid. The use of the SAHX-2500F source in Linear module #0430 was examined and several problems became apparent.

1. The SAHX-2500F is an anode-down source and thus has higher flux distribution at higher values of ϕ than the anode-up source for which #0430 was designed.
2. The manufacturer advises against returning flux thru the SAHX-2500F, but this would occur if an SAHX-2500F was placed in the #0430 module.
3. The arc radius used in the design of the #0430 module was 5.5 millimeters, but the arc radius of the SAHX-2500F source was computed to be nearer 8 millimeters.
4. The rounded anode of the SAHX-2500F source spreads the flux over wider angles, thus making collection of a high percentage of flux more difficult.

Two further problem areas had to be dealt with in accomplishing the design adaptation.

1. Requirements on the lense elements for significant changes in flux direction created greater losses due to the method of lense plate fabrication than had previously been indicated by information on the fabrication process.
2. Specification of target zone as 20 feet to 60 feet from the module increased the problem of achieving uniformity at the near distance. The #0430 module with an eight-inch exit pupil was designed for a target zone 30 feet to 100 feet from the module.

Patterns from this module in single array on 27-inch centers with an effective two-degree half-angle would not even meet for nearly 23 feet from the modules.

The limitations of single element reflectors such as ellipsoids and paraboloids were discussed in section 3.3.9. The higher flux distribution, at higher values of φ , from the anode-down source, will be intercepted by zones on the single element reflector having smaller values of $|R|$, thus producing higher values for $\bar{\beta}$ (the mean of the angular distribution) than would be the case for the anode-up source. The necessity to decrease the focal lengths to achieve the same percentage collection of total flux (which is now distributed over wider values of φ) also increases $\bar{\beta}$. Of course, a larger arc radius also increases $\bar{\beta}$.

The problem areas delineated the adaptation task and pointed to joint solutions through:

1. emphasizing the segmentation of the reflector system. It was pointed out in section 3.3.9 that the segmented reflector has many advantages for overcoming the problems of flux collection,
2. using "maximum flux within an angle β of three degrees" as the criterion for balancing of total collection as well as balancing between reflector segments. The resulting distribution would produce uniformity in a shorter distance than the previous two-degree target, and
3. maintaining maximum reflector diameter within dimensions for side-by-side multiple array

placement and using paraboloid segments to effectively eliminate requirements on lenses for directional changes of flux.

Once this approach was justified and adopted the remainder of the reflector adaptation task consisted of balancing the relationships discussed in 3.3.

We must emphasize that we can write no equation and we know of no algorithm for the design of the best possible segmented reflector system. In this sense, the design is an art. Of course, once a particular configuration is designed, the equations can be used to compute its output with high accuracy. But the selection of a configuration is at least partly intuitive.

The flux from the highest angles ψ must be brought around the bulb, and a tipped paraboloid operating into a cone proved superior to solutions which would bring this flux through the center of the module. The next region of ψ is that where $dF/d\psi$ is the highest for any region around the source. It was, therefore, handled with a paraboloid of the longest focal length of any of the segments. This paraboloid was fitted between the tipped paraboloid and the cone. Note in figure 3-22 that the use of the tipped paraboloid provides a dark space near the source, and the lower angles of ψ can be handled by one or two paraboloids operating in the dark space left by the tipped paraboloid. Table 3-3 lists the reflector elements and their basic parameters. The positioning of the breaks and extent of each segment zone must be determined by careful, laborious

evaluation of the change in the total flux integral over β when each break is moved.

We emphasize that the reflector system as designed would have zero loss due to segmentation for a point source and has less than 10% segmentation loss when the SAHX-2500F source is used. The loss is due to some of the rays from the finite image reflected from element one missing the cone and some of the rays reflected from 1, 2 and 3 spilling onto the backs of elements 3 and 4.

We decided that for purposes of evaluation of the basic optical design, the reflectors should be fabricated from #416 stainless steel. Recommendations of vendors indicated that the accuracy of fabrication would be more predictable, and it is desirable to separate questions of losses due to fabrication method from those of basic design performance.

Detailed drawings for segmented slumped glass reflectors were made, in accordance with the inclusion of this type of reflector in the #0430 module. If it is not necessary to grind and polish the slumped glass reflectors, they will, in quantity fabrication, cost only about 20 percent of the cost of stainless steel or aluminum reflectors. It is the belief of design personnel, that such grinding and polishing will not be necessary and that required fabrication accuracy can be achieved. As the program progressed, time and fund limitations predicated the relegation of this approach to future system engineering.

3.4.2 Beam modification. - Once the extent of flux collection has been established and this flux has been

directed into the test volume, the remaining requirements of the optical system are the establishment of the desired beam pattern and the removal of radiation which is at undesirable angles.

It is important to remember that it is erroneous to identify the various optical elements with only one specific function. While the segmented reflector was discussed in the previous section on Collection, one of the primary functions accomplished during the design balancing of this element was the establishment to the fullest extent possible, of the desired beam pattern.

As discussed in section 3.3.11 the beam pattern is established by the combination of two flux distribution factors. The distribution of the flux across the exit pupil is the primary factor in the very-near field, while the angular distribution becomes almost the sole determinant in the very-far field. Throughout the region of interest established by the test volume, we are concerned with the combination of both factors.

Use of the segmented reflecting element facilitates the elimination of undesirable extreme deviations both in distribution of flux across the exit pupil of the module and in distribution of flux angularly. Further, the segments serve a significant function in breaking up the continuous one-to-one mapping around the arc, thus eliminating continuous and extreme changes across the exit pupil due to change in nature of the flux with angle φ .

The remaining beam modification requirements are, therefore of smaller magnitude and consist mainly of small changes in angular distribution and the integration of flux in a manner which will offset undesirable changes across the beam due to change in nature of flux with angular distribution from the arc.

As we have seen in section 3.3.11, the relatively higher dispersion of flux distributed within lower angles and the further breaking up of the mapping of the arc make lenticular lenses a powerful element for final refinements of the beam pattern. As in model #0430 the final adapted module design incorporates one or two lenticular lense plates molded from Vycor.

The Vycor lense plates are molded from a high-grade fluxed glass which melts at a much lower temperature than quartz. These molded pieces are then put through a leaching process to remove the fluxing elements. They are finally fired to close holes left by the leaching process. The resultant material is almost identical to fused quartz.

This process involves two principal problems:

1. The leaching and firing processes naturally cause shrinkage. The original mold must be made oversize to produce a completed item of the proper dimensions. When there are wide variations, especially in plate thickness, the leaching process takes longer and can be inconsistent. Compensation for dimensional shrinkage on a plate with wide variations in thickness becomes very complex.

2. The second problem is a limitation of the molding process in forming the lense edges. This problem occurs mainly with the use of significant prisms or torroids which cause sizeable variations in plate thickness. The manufacturer insists that for successful molding, lense edges rising above the plate must slope a minimum of 7° rather than rise vertically. This slope over the height of the lense edge above the plate creates a zone of unusable lense edge and losses which are comparable to fresnel losses.

The difficulties of dimensional control and lense edge losses are, of course, relative problems to be carefully considered in balancing for overall optical efficiency. They do provide obvious incentive to minimize the extend of prismatic or torroidal work required of the lenslets.

The two main functions which are varied in the design of the lenses are focal length and lateral focus. As we have previously seen, focal length is intimately tied to lense size and baffle dimensions and to lense size and plate to plate distance (where two lens plates are used.) Lateral focus is varied by the use of prisms or torroids and can be a very powerful tool in making smaller refinements in beam intensity crossection.

Both of these variables are most efficiently used when varied radially across the lense plate to operate in conjunction with the specific flux distribution in the particular radial zone. Careful consideration of the wide range of legitimate possibilities for the system and the degree of speculation

involved in the representation of the arc, led to the conclusion that these refinements should be deferred until after verification of the actual beam pattern from the reflectors and a review of specifications for the final system.

The course was facilitated by assembly of the lense plates from individually fabricated lenses which were supported mechanically. This assembly provides the flexibility for the evaluation of any number of lense plate adaptations and the modification of the lense plate to correspond to any other system modifications. Fabrication of lense plate molds is costly, and even slight changes in plate design would require a complete repetition of the process.

Thus, the initial lense plate design consisted of lenses of uniform focal length without torroidal or prismatic shaping but with provision for incorporating later changes. The remaining decisions were concerned with size and shape.

Size of lense and number of lenses in a plate of given dimensions are inversely related. The considerations in determination of lense size are basically four in number.

1. The extent of integration or scrambling of flux is a function of the number of lenses. It is important in this respect, however, to differentiate between the integration or scrambling mechanisms. The degree of modification of angular distribution and the elimination of variations in flux which correlate with original angular distribution is a function only of the half angle of the lense or the lense radius to focal length ratio. Thus, one

lense over the whole plate will accomplish the same angular scrambling as 100 lenses of the same half-angle. In this connection, the fallacy in the statement that multi-faceted lense systems change field or collimation angle is clear. The number of lenses has no effect on field angle, collimation angle or angular distribution.

The number of lenses does determine the extent of integration which reduces difference in nature of flux due to view point around the arc. And, it will be remembered that this facet of integration affects the very near field with less and less effect as distance is increased from the exit pupil of the module. In general, the closer to the module it is desired to achieve uniformity, the greater the number of lenses predicated. Conversely, beyond a certain number of lenses, there will be no real added advantage for a given distance from the module.

2. Thickness of the lense plate and variations in the thickness will be determined by number of lenses for a given lense half-angle and by the prismatic and torroidal work requirements of the lenses. Therefore, as lense half-angle and prismatic or torroidal work requirements increase, the advantages of a larger number of smaller lenses increase.
3. Edge loss between lenses increases as the number of lenses increases.
4. The length of baffles to be used in conjunction with the lense elements for a given angular cut-off are

directly proportional to the lense focal length. On the other hand, the smaller the lense size for a given lense half-angle, the greater the number of tubes in the baffle element. This consideration alone is one of the strongest, since the ease of fabrication of the baffle element for efficient operation is of vital importance. Shape of the lenses is the other matter to be decided. No matter what the shape of individual lenses, the lense surface itself is spherical and therefore has lines of equal lense action in circles increasing in radius from the center. Circles will not, however, fit together exactly on a plate. The only three regular geometrical figures which will fit together on a plane are the equilateral triangle, the square, and the hexagon. Generally the hexagon is utilized to fit lenses together since it is the one of the three figures which most nearly approximates a circle. There are unquestionably advantages to minimizing the difference in lens action which exists at the radius of the circle inscribed in the lense and the larger radius at the corner of the lense. Likewise, the area of the lense outside the circle inscribed in the lense can be used as a measure of the amount of energy subjected to the greater lense action. This is greatest for the triangle, less for the square, and least for the hexagon.

However, it is a fallacy to state that the area

outside the inscribed circle represents a system inefficiency or loss. This is a misconception of the lense operation and would only be the case where an absolute angular cutoff at the half-angle represented by the inscribed circle radius was mandatory. As we have seen in prior discussion of beam irradiance crossection, this will never be the case for a solar simulator module where beams must be matched between modules. All energy incident upon the corner of a lense outside the inscribed circle on that lense and within an angle of incidence $\alpha \leq$ the lense half-angle at the inscribed circle radius, will pass through the inscribed circle which is projected to the focal plane of the lense. Overriding the somewhat smaller angular deviations to be achieved by use of heagonal lenses, three considerations led to the adoption of square lenses for the prototype.

1. Square lenses could be fabricated individually much more easily and later incorporation of prisms would be simpler.
2. Shape of baffle tubes is determined by lense shape and the square tubes would be much simpler to fabricate, particularly in the prototype stage.
3. Square lenses can be arrayed symmetrically by quadrants so that later fabrication of plates in quadrants and sealing of quadrants could be accomplished without creation of additional partial lenses. This is of great importance in two plate operation, but of lesser importance with one plate.

The effective half angle of the lense was settled upon as somewhat of a compromise between the target 2° half-angle and the 3° half-angle recognized to be necessary as a criterion for reflector balancing. The effective half-angle at the inscribed circle radius was set at 2.67° and the corner at approximately 3.3° half-angle. *This was definitely a mistake in terms of two plate configuration efficiency as will be seen from the results. The effective half-angle at the inscribed circle radius is definitely the overriding angular cut-off.

The size of the lenses was determined more in terms of workable module length than of required integration. The sixty lenslets resulting from use of approximate 2 inch squares are well in excess of the number required for a useable test volume starting 20 feet from the module. The resulting 20-inch focal length did, however, establish 20 inches as a plate-to-plate distance for the two plate operation which was a reasonable addition to module length. This focal length also established baffle lengths of 20 inch magnitude. The 20 inch length was workable and 2 inch square baffle tubes were reasonable to fabricate and align. Dimensions of much smaller size would not have been as workable.

3.4.3 Removal of radiation at undesirable Angles. - Finally, radiation which would otherwise leave the module at angles in excess of those desired must be stopped. The second lense plate in a two plate configuration actually acts as a series of stops, but the energy of higher angle is merely diverted to even larger angles and not stopped from entering the test

volume.

Baffles represent the best method of stopping and removing higher angle energy to the extent desired, and when used in conjunction with lenticular lense plates, they can remove high angle energy very efficiently.

Final baffle design depends upon actual beam parameters selected and especially upon the nature of angular cut off specified. Since this area of specification needs further review, we decided that a short baffle, of six-inch-long tubes, square-shaped to correspond to the square lenses, would be the most useful in prototype evaluation. The six-inch baffle depth was selected to permit evaluation of baffle operation in several different zones along the optical path.

The prototype baffle was fabricated from thin aluminum sheet which was black anodized. While in final module operation the baffle would be cooled, no cooling was provided for prototype evaluation.

Cooled baffles used below the last lens plate will be an extremely valuable element in preventing stray radiation and re-reflection of radiation reflected from the test object.

3.5 Prediction of Module Performance

Throughout the program, mathematical descriptions of various phases of module operation were formulated and calculations *were made in accordance with these descriptions* for the balancing of design variables. These formulations have been discussed in section 3.3.

Generally, due to the complexity of the calculations, the operation of the module was studied in three stages.

1. From the arc representation, flux intensity and angular distribution of flux were determined at the reflector system exit pupil. Basic predictions of module performance could be made from this stage.
2. From the resulting distributions across the projected reflector exit pupil radius (X) a description of beam irradiance crosssection at a given distance from the module could be derived.
3. From the exit pupil description and the lenticular plate parameters, the beam irradiance crosssection at a given distance from the module could be derived for the one or two plate configurations.

Information available to serve as a basis for design adaptation and prediction of module performance, particularly on the short-arc lamp, was partial and, in many respects, not directly applicable. Most of the basic functions involved had to be inferred from the partial information.

The module performance predictions made at the conclusion of the design adaptation phase were all based on the original functions. As the program progressed, more adequate data which became available, results of calculations, and measurement results were often incorporated in phases of the calculations to improve insight into particular areas of module behavior. The model, the calculations and the data interacted constantly throughout the program.

The two primary predictions of module performance were concerned with the total flux output of the module and the angle within which this flux would be included. Beam irradiance cross-section and modified distribution after lens plates are both subject to any errors inherent in these basic predictions, and comparison with actual data becomes much more difficult. Since the program was dealing with variations of four configurations and refinements were constant, it has not been possible to incorporate all refinements and review the complete calculations of a particular configuration.

Therefore, we shall concern ourselves with the basic predictions of total output and of angular distribution of flux. A typical beam pattern prediction will be shown as an example.

3.5.1 Function $g_1(\varphi)$ - radiance weighting as a function of φ . - Source output data, describing the spatial and directional distribution of radiant energy within the applicable spectral region, is essential to a prediction of the

performance of a solar module. Short-arc lamps commonly have symmetrical radiance distributions around the lamp axis (through the angle we have called θ .) The radiance distribution about the axis we have called Φ is a strong function of Φ . The polar plots of this distribution are variously referred to as polar radiation distributions, polar luminance distributions, meridional flux distributions, radiation distributions, or candlepower distributions.

Since lamp manufacturers are usually concerned with measurements of visible radiation in photometric units, the earliest data for $q_1(\Phi)$ was inferred from polar diagrams of luminous intensity and from partial information on radiant intensity for the flat anode version of the Westinghouse SAHX 2500-C lamp. The function was revised when polar diagrams of radiant intensity for total lamp radiation (including bulb and electrode radiation) were received for the SAHX2500F lamp.

The function $q_1(\Phi)$ used in the predictions in this section is actually a third version and is derived from the polar radiation diagram in Figure 3-3 which includes curves for both total lamp radiation and for electrode and bulb radiation. Arc radiation obtained from the difference between the two curves is the best approximation of the actual distribution function which was available. While this data has generally corresponded with results, it has some shortcomings which should be noted:

1. The method of measuring bulb and electrode radiation has very likely understated the bulb and electrode radiation. Thus, useable radiation has been overstated for certain directions.

2. The arbitrary separation of electrode radiation from arc radiation understates the useable radiation for certain directions especially those which view the hot electrode centers at favorable angles (small α).
3. The directional radiation measurements have no stated band-pass other than the radiometer band-pass of .2 to 7.5 microns.
4. The definition of arc center for these measurements could make a directional difference of up to 2° when optics are placed close to the bulb.

It is possible, from data developed during the course of this program to refine the q_1 function further. The use of the reflector segments to study zones of ϕ has greatly increased insight into this area.

The function has generally been utilized in tabular form, but it is also possible to write an equation for it. The equation will be most useful when $q_1(\phi)$ is used in conjunction with $q_2(r)$ and, as indicated in section 3.3.6 the two functions could be expressed as one equation.

3.5.2 Function $q_2(r)$ - differential radiance as a function of arc disc radius. - The significance and derivation of function $q_2(r)$ was discussed at length in section 3.3.6. Luminance was integrated by contours over the arc brightness disc in figure 3-4 and restated as concentric circular contours. The power curve for this revised disc is shown in figure 3-23. This data, extrapolated exponentially toward zero, is the basis for function $q_2(r)$ used in the predictions in this section.

Figure 3-~~34~~²³ is a graph of $q_2 2\pi r dr$ as a function of V . The radiance in solid angle $d\omega$ is given by equation 3-16 as

$$dF_R = \left\{ \int_{r=0}^{r_i} q_1(\varphi) q_2(r) 2\pi r dr \right\} d\omega$$

where r_i is the upper limit of integration.

The per cent of total flux for a given r_i can be stated as

$$\% \frac{F_{Ri}}{F_{Rmax}} = \frac{\int_{r=0}^{r_i} q_2(r) r dr}{\int_{r=0}^{r_{max}} q_2(r) r dr} \quad (3-59)$$

~~(3-59)~~

Equation 3-59 is graphed as a function of r_i in figure 3-24.

~~The radiance in solid angle $d\omega$ is given by equation 3-16.~~

~~$$dF_R = \left\{ \int_{r=0}^{r_i} q_1(\varphi) q_2(r) 2\pi r dr \right\} d\omega$$~~

The function $q_2(r)$ was utilized in tabular or graphical form for most calculations, but it was also found to be closely approximated by the equation:

$$q_2 = 100 \left[1 - e^{-(.077r + .093r^2)} \right] \quad (3-60)$$

The shortcomings of the above derivation of $q_2(r)$ were discussed in section 3.3.6. Discrepancies in the characterization of q_2 account for the major portion of the discrepancies in performance predictions. The largest source of error was in the assumption of the arc center.

3.5.3 Function $q_3(\lambda)$ - weighting function over wave-length. -

Data for this function has been most unsatisfactory. As indicated in section 3.5.1 there is little assurance that available spectral data corresponds with the other lamp data which has been used. No data is available on the correlation of $q_3(\lambda)$ with arc radius and there most certainly is a correlation.

Four different sets of data were available on spectral distribution and agreement between them was poor. Some of these became available later in the program, so that for different portions of the calculations, different data was used for $q_3(r)$. The data utilized for this function in the predictions in this section is the spectral data tabulated in reference (2). The function q_3 for a HgXe lamp is quite discontinuous and can only be utilized in tabular form. Measurements in this area are quite difficult and subject to relatively large errors. However, some general refinements in the function are possible utilizing some of the data obtained during the measurement phase of this program.

3.5.4 Function q_4 - reflectivity. -

The data for this function is graphed in Figure (3-25) which is the reflectivity curve for Liberty Mirror Front Surface Aluminum coating No. 747. This coating was applied to all reflective surfaces. This function was always utilized in graphical or tabular form.

3.5.5 Module Total Flux output. -

With the functions derived, the prediction of total flux output is a matter of solving the equation for total power (equation 3-34).

$$F = \int_{\Phi} \int_{\lambda} \int_{r} 4\pi^2 q_1 q_2 q_3 q_4 \sin \Phi r dr d\lambda d\Phi$$

This equation can be re-written as:

$$F = \sum_{i=1}^4 \int_{\Phi} \int_{\lambda} \int_{r} 4\pi^2 q_1 q_2 q_3 q_{4i} \sin \Phi r dr d\lambda d\Phi \quad (3-61)$$

where i = reflector number
 q_{4i} = reflectivity for reflector
 and Φ is integrated between the limits
 intercepted by each reflector

Since we are forced to assume that q_3 is independent of Φ and r (because of lack of data), then we can separate

3-61 and solve independently:

$$\int_{\lambda} q_3 q_{41} d\lambda = .805$$

$$\int_{\lambda} q_3 q_{42} d\lambda = \int_{\lambda} q_3 q_{43} d\lambda = \int_{\lambda} q_3 q_{44} d\lambda = .897$$

Relating the total flux collected by the four reflectors (from $\Phi = 158^\circ$ to $\Phi = 31^\circ$) to total useful power radiated by the lamp (from $\Phi = 180^\circ$ to $\Phi = 0^\circ$) the percentage of total useful power radiated (P_r) which is intercepted by the reflectors is 96.97%. When the summations over all reflectors are completed it is found that the total power directed into the target volume by the reflectors will be 994 watts.

However, losses will be incurred on the lens plate(s) and baffles where used and a slight amount of this flux will be at angles which exceed the acceptance angle of the radiometer

and will not be seen even for the open reflectors. Therefore, let us defer system efficiency predictions until we have the prediction of angular distribution of the flux.

3.5.6 Angular distribution of flux output. - If we now return to the description of total flux in terms of β (equation 3-41):

$$F_{\beta} = \int_{\beta_1}^{\beta_2} \int_{\phi} \int_{\lambda} 4\pi^2 q_1 q_2 q_3 q_4 \sin \phi \frac{(2f)^2 \sin \beta \cos \beta}{(1 - \cos \phi)^2} d\lambda d\phi d\beta$$

and integrate for power over 1° intervals of β we secure a rough angular distribution of the same total flux secured in the previous summation. The results of this integration are plotted as cumulative watts as a function of β_2 (the upper limit of integration) in figure (3-26).

From this distribution it can be seen that only 980 watts are within the radiometer acceptance half-angle and that approximately 790 watts are within 3 degrees of half-angle.

3.5.7 Prediction of Module Efficiency. - With the total flux output and the angular distribution determined, it is now possible to predict efficiency for different module configurations and for different limiting half-angles for each of these configurations.

For example using a .895 transmission factor for each lenticular plate, to account for the two surfaces, slight quartz transmission losses, and lenslet edge losses, we can make the following output predictions:

| <u>MODULE CONFIGURATION</u> | <u>HALF-ANGLE LIMIT</u> | <u>WATTS OUTPUT</u> |
|-----------------------------|-----------------------------|-------------------------|
| REFLECTORS-ONLY | 30 | 790 |
| | 4° | 882 |
| | 5° | 932 |
| | T O T A L | 980 |
| TWO LENS PLATES | 30 | 633 |
| | 4° | 706 |
| | 5° | 746 |
| | T O T A L | 785 |
| ONE LENS PLATE | 30 | 624 |
| | 4° | 717 |
| | 5° | 796 |
| | T O T A L | 877 |

3.5.8 Beam irradiance crossection. - Beam irradiance crossection for a given distance from the module is determined from beam power as a function of angle (β) and origin on the exit pupil.

The methods used to transform the flux distribution to a plane at a given distance from the module exit pupil are in most respects the same or analogous to those used in transformation from the arc defining disc to the reflectors. Only the limits and the coordinate systems change.

The beam irradiance crossection at 60 feet from the module which results from the flux distribution across the reflectors described in sections 3.5.5 and 3.5.6 is shown in figure (3-27). It will be noted that for values below about 0.5° the

prediction is extrapolated from the progression of adjoining values. Extrapolation was used for this region, because the available description of flux at very small half-angles did not have the required resolution.

4 MEASUREMENT PROGRAM AND RESULTS

4.1 Parameters to be Measured. - The measurement portion of the program, as it was originally conceived, was concerned with total module output power, angular distribution of the energy, and uniformity of intensity in an infinite array. As the wider range of attractive alternatives for the final system was indicated, the measurement task was expanded. The additional data provided a broader basis for evaluation, including review of the specification, and target parameters, before proceeding with any adjustment of final design. Planning of the expanded measurement task provided for securing data relating to:

1. Efficiency relative to angular distribution.
2. Beam pattern modification achieved with various module configurations including one lens plate, two lens plates, and lens plate with baffles.
3. Effect on efficiency in achievement of beam pattern modification.
4. Angular distribution of energy from various module configurations.
5. Spectral distribution across the beam for the different module configurations.
6. Contributions to efficiency, beam pattern, angular distribution and spectral distribution by individual reflectors.

These measurements were taken at distances of 15, 30, and 60 feet from the module.

4.2 Measurement Facility and Instrumentation

4.2.1 Module Housing and Mounting. - A 9 X 9 X 8-foot room was constructed to house the solar simulator module and the turning mirror. The front wall of this room has a double door that is remotely opened and closed. This door gives rapid, safe access to the measurement area when the module is operating. The interior surfaces of the room and the module supports are painted optical black.

Mounting frames, attached to the rear wall of the room, support the module. The output of the module is directed down because of the anode-down operational requirement of the HgXe bulb. The turning mirror, which is mounted at a 45-degree angle to the simulator normal, directs the flux into the measurement area. The mirror dimensions are 32 X 45 X $\frac{1}{2}$ inch and the mirror has a front surface Liberty Mirror 747 coating. The mirror is flat to within 7 fringes/radial inch. The reflectivity curve is shown in Figure 3- .

4.2.2 Measurement Area. - The measurement area is approximately 50 feet long, measured from the front of the room. The length of the beam path inside the room adds about 10 feet to this distance. The area is about 10 feet wide and more than 10 feet high. One side of the area is enclosed with heavy, black curtains. The other side is a wall which is painted optical black.

4.2.3 Module Supports. - A system of frames support the module reflectors (See Figure 3-22). The individual reflectors can be positioned at different locations along the optical axis of the module. This feature permits accurate focusing of individual

reflectors. (Refer to Section 4.3.2). In addition, the effect of off-focus operation of each reflector can be studied.

The lens plates are mounted below the reflector assembly. They are attached to four support bars, extending from the assembly. (Figure 4-1).

4.2.4 Radiometer. - An Eppley Mark III radiometer is used to measure the irradiance of the radiant energy. The radiometer was supplied with a calibration certificate giving the sensitivity of the instrument. A copy of this certificate along with the derived calibration curves is illustrated in figure 4-2 and 4-3. The time constant of this instrument is 0.8 second. A complete description of the characteristics of the Epply Mark III radiometer is contained in the manual supplied with the instrument. (17)

4.2.5 Radiometer Cart. - The radiometer is mounted on a cart which is motor-equipped to remotely position the radiometer at different co-ordinates on the X and Y axes. These axes are perpendicular to each other as well as to the optical axis of the simulator (See figure 4-4). Figure 4-5 shows the radiometer mounted on the cart.

The cart is also equipped with a water tank and pump to supply cooling water to the radiometer. The capacity of the tank is approximately 8 gallons. This system maintains the water temperature within $\pm 1^{\circ}\text{C}$ at about 25°C , over a period of several hours.

The cart is moved manually on the Z axis (parallel to the optical axis). Since the cart is not moved often, remote motorized operation on the Z axis is not necessary. A pair of

rails constructed from angle stock and mounted on the floor guide the cart when it is moved on the Z axis.

To position the cart, reference lines were carefully marked on each rail, 15, 30, and 58.4 feet from the module. There is another set of reference lines on the cart located, one on each side, at the base of the cart. The operators found that when the lines on the cart are brought into registration with the lines marked on the rails, the cart can be positioned on the Z axis with a repeatable accuracy of better than $\frac{1}{4}$ inch.

Two reversible single-phase induction motors are used to move the radiometer on the X and Y axes. The motor outputs are each geared to a roller chain. The X axis chain drives a trolley across the cart. The Y axis motor and roller chain are mounted on this trolley. The Y axis chain drives a smaller trolley to which the radiometer is attached. Limit switches are located at each end of the two trolley runs. Figure 4-6 is a schematic of the motor control system.

Each of these trolleys drives a precision 10-turn potentiometer. The moveable arm (pole) of each potentiometer presents a voltage which is proportional to the position of the radiometer on the X and Y axes. That is, the output from each potentiometer represents the position of the radiometer on its axis. These outputs, along with the connection to a reference voltage supply are brought out of the measurement area to a control console.

4.2.6 Control Console. - A console was constructed to house various power supplies, controls, meters, and circuits. (See figure 4-7). Figure 4-8 is a schematic diagram of the control

console circuits.

The outputs from the X and Y potentiometers are each connected to one side of a d'Arsonval movement galvanometer. The other side of the meter is connected, in series with a limiting resistor, to the moveable arm of a 10-turn potentiometer mounted on the panel of the control console. The shaft of the potentiometer is connected to a 10-turn precision dial. A four-pole, three position switch is mounted on the control panel next to the potentiometer and below the meter. When the switch is in the center position, the motor is off. The motor direction in the other two positions is indicated on the panel.

To position the radiometer in accordance with a particular dial setting, the motor switch is turned in the proper direction until the meter indicates a "null". The radiometer positions obtained using this method proved to be repeatable within less than $\frac{1}{4}$ inch. The maximum distance traveled by the radiometer on the X axis is 85.9 inches and on the Y axis 75.8 inches. This would give an error in positioning accuracy of 0.33% of total range in the case of the Y axis.

A number of additional circuits and controls were incorporated in the console to aid in automating the data collection and reduction. The output from the radiometer is amplified by a high-gain, chopper-stabilized, operational amplifier. The amplifier output is connected to a switch and an analog correction circuit. This circuit automatically corrects for the radiometer non-linearity above intensities of 190 watts per square foot. The output from the correction circuit is connected to a switch and one end of a 10-turn potentiometer with a grounded center tap.

This potentiometer is geared to another potentiometer which is designated as the radius potentiometer. The pole of the radius potentiometer is connected to one side of a galvanometer through reference circuitry. The other side of the meter is connected through a compensation circuit and a switch to the pole of either the X or Y potentiometers.

Setting a precision dial on the radius potentiometer nulls the meter. When the meter is null, the voltage on the pole of the grounded center tap potentiometer is proportional to the product of the corrected amplifier output (irradiance) and the radius from the center of the pattern. This computation is correct if the center of the beam pattern has been accurately determined. The evaluation team found that the center could be determined from peak intensity readings and symmetry of readings around the center. The accuracy of this procedure was better than 0.2%.

A switch on the control panel connects a digital voltmeter to one of four voltages, including the amplifier output, the corrected amplifier output, the product of the corrected output and the radius, and the X or Y potentiometer output. When the data was taken, some of these factors were not numerically recorded since they are included in the plotted data. (See section 4.4) They were necessary, however, in the initial evaluation of the instrumentation accuracy.

Another switch on the control panel selects either the corrected amplifier voltage (irradiance) or the irradiance radius product as the Y input to an X-Y plotter. The X or Y potentiometer outputs are switch selected to produce the X

input to the plotter. Both of these signals are attenuated to provide the proper scale for the plotter. The Y input also uses the amplifier section of a VTVM as a buffer. A manual-plot push button on the panel is used to control the plot command. In figure (4-9) the operator adjusts controls. Table 4-1 lists the major components used in the instrumentation system and includes pertinent specifications.

4.3 Measurement Technique

The procedures employed in recording the data were developed to provide rapid accumulation and accurate results.

At the beginning of the measurement period, the effect of radiometer operation with its shutter open and closed was investigated. The peak intensity of the beam which was being measured was quite high in most cases. For example, the irradiance at the center of the beam was approximately 1.8 solar constants in the case of the reflectors without lens plates measured at a distance of 30 feet from the module. With the amplifier gain set to place this reading near the top of the digital voltmeter range, there was no measureable output, with the shutter closed. Since high peak intensities were a condition encountered during almost every measurement run, background readings were not recorded.

In the case of some of the narrow band filters, the peak intensity was relatively low. A background reading of approximately 0.001 millivolt was measured at the output of the radiometer. With the radiometer located at a fixed

TABLE 4-1
INSTRUMENTS

10-Turn Potentiometer

Clarostat Series 62JA
Linearity $\pm 0.25\%$
Resolution 0.026%

10-Turn Potentiometer Dial

Helipot RB Series
Dial Accuracy 0.05%

Amplifier (Used on Radiometer Output)

Dymec Model DY-2460-A-MI
DC Gain Accuracy $\pm 1.0\%$
DC Gain Stability $\pm 0.01\%^{\circ}\text{C}$
 $\pm 0.01\%$ per week at constant temperature

Zero Drift 1 microvolt per week maximum at constant temperature
0.5 microvolt $^{\circ}\text{C}$ maximum temperature coefficient

Input Noise 4 microvolts p-p max., 0 to 1 cps, referred to summing point.

Digital Voltmeter

Digitec Model 210
Accuracy 0.2% Full Scale
Resolution 0.05% full scale

Point Plotter

Moseley Model 7590A
Accuracy 0.1% full scale

Polar Planimeter

Keuffel & Esser Model 62 0000
Accuracy 0.3%

Radiometer

Eppley Model Mark III Serial No. 6897-D compared with the Eppley group of reference standards, at a radiation intensity of approximately 76 watts/ft.². The derived calibration curves were provided.

position the reading fluctuated about this value. The average value of 0.001 millivolt background remained constant across the beam except at the outer fringes. In the case of a few of the narrow-band filters, the radiometer output readings on the fringes with the shutter open were the same order of magnitude as the background readings. In other words, the intensity is quite low. Since the significance of the measurements in the fringe areas is questionable, these areas were not included for purposes of power computations.

The amplifier which was used has a zero correction control. This control was adjusted to offset the average 0.001 millivolt background. The fluctuations represent a small error in the reading. As an example, the peak reading for a filter with wavelength limits of 295 to 332 millimicrons, measured at 30 feet, is 0.470 millivolt at the radiometer output. The maximum amplitude of the fluctuations was approximately 0.001 millivolt. This produces a reading error of $\pm 0.2\%$ of full scale.

At the beginning of the measurement program, it became obvious that it was convenient to relate the position of the radiometer on the X and Y axes to control panel dial settings. 6.45 units on the potentiometer dial are equal to one inch of movement on the X or Y axis. The dial is divided into 1000 units.

Data were recorded and plotted at intervals of 20 potentiometer dial units and, in some cases, 10 units. The radiometer was positioned as described in section 4.2.6. After a setting period of 5 seconds, the data were recorded. The

radiometer time constant is 0.8 seconds. (See section 4.2.4)

4.3.1 Individual Reflector Measurements. - The evaluation team determined the output of each reflector by removing the other reflectors and, in some cases, blocking a portion of the output of a reflector. As an example, reflector number 4 normally blocks a portion of the output from reflector number 3. Reflector 4 was replaced with a section of black stove pipe with the same size and shape as number 4. This pipe blocked the same amount of flux as reflector 4 did, without contributing to the output as 4 normally would.

4.3.2 Module Alignment. - The focus of each parabola was checked by using a G.E. 1493 projector lamp. The light output was projected on a screen about 30 feet away. The lamp was moved on the optical axis to obtain the sharpest circle on the screen. This procedure was followed with the reflectors mounted in the module support frames. The HgXe lamp was then positioned with the arc intensity peak at the common focus of the reflector segments.

In experimenting with the effect of moving the individual reflectors off focus, it was found that the moment of angular power distribution (mean β) could be decreased. The information derived from this study proved invaluable in determining the true shape of the arc as well as its power centroid. The segmented reflector is a powerful tool for studying the arc shape.

This led to a realignment of the reflector elements in the module. The segments were then aligned to give the minimum

composite moment of angular distribution. Once this was done the position of each reflector and the bulb with respect to the base plate of the module support was recorded. Module alignment for this design is then simply a matter of positioning the reflectors and the bulb in accordance with these measurements.

4.3.3 Wide Angle Energy. - The maximum aperture half angle of the radiometer is 7.5° . All measurements were taken in a plane perpendicular to the optical axis with the radiometer normal always parallel to the optical axis.

The total power output from the module did not increase after the module had been realigned. However, more power was contained within a smaller angle, i. e. the moment of angular power distribution decreased. This indicates that there is virtually no flux present at angles greater than 7.5° .

4.4 Data Processing and Reduction

The data obtained from a measurement run appears in two forms.

1. An X-Y plot of the irradiance and power as a function of position (Figure 4-10), and
2. A data sheet with entries recorded by the operator for each point plotted. (Figure 4-11).

Pertinent information about the experiment, such as radiometer aperture, filter wheel position, etc., is recorded on both data sheets. This particular experiment was an X axis run. The potentiometer dial setting and amplified radiometer output are recorded for each point plotted. The corrected amplifier

output, and the product of the corrected output and the radius were not recorded, since these factors appear in the plotted data. A few of the radius potentiometer readings were recorded for use in computing the power plot scale factor.

The points of the irradiance and power plots were connected with straight line segments. A sufficient number of points were plotted to produce a good approximation of the actual curves. Dashed lines are used to differentiate the irradiance curve from the power curve. The power dips to zero at the center because the radius is zero at this point.

4.4.1 Scale Factor. - The horizontal scale on the plotted data is always related to actual position of the radiometer on the X or Y axis. The horizontal axis scale factor describes this relationship.

$$K_H = \frac{41.07}{6.45} = 6.37$$

(4-1)

The numeral 41.07 represents the number of potentiometer dial units per inch on the plot. Since 6.45 potentiometer units represent one inch of radiometer movement, each horizontal inch on the plot equals 6.37 inches of radiometer travel.

A voltage divider on the vertical input to the plotter was adjusted to accommodate different peak intensity signals. This was necessary in order to place the plot of the peak power and irradiance readings near the top of the graph without going off scale. Greater reading ease and accuracy make this requirement essential. Therefore, the vertical scale factor is not a constant and must be computed for each measurement run. A vertical scale factor for the irradiance curve is

shown in figure 4-11. The computation of this factor is similar to the power curve scale factor calculation.

Four points on each graph were chosen to obtain the vertical scale factor for the power curve. One point near the top of each lobe of the curve, and one point near the bottom of each lobe were selected. The amplified radiometer output reading was multiplied by the corresponding radius at each of the four points. This numeral was divided by the vertical height, measured in inches on the plot, at each point. These factors are designated by mv, R, and vertical inches in the scale factor equation. The computations from the four points were averaged.

$$K_{VP} = \left(\frac{R}{6.45}\right) \left(\frac{mv}{300}\right) \left(\frac{1}{\text{vertical inches}}\right) \left(\frac{1}{0.0844}\right) \left(\frac{1}{144}\right) \quad (4-2)$$

Where

$$\begin{aligned} \frac{R}{6.45} &= \text{the radius converted to inches} \\ \frac{mv}{300} &= \text{Radiometer output voltage (the amplifier gain was 300) millivolts} \\ \left(\frac{1}{0.0844}\right) \left(\frac{1}{144}\right) &= \text{The slope of the radiometer calibration curve mv/watt/in}^2 \end{aligned}$$

The dimensions of the vertical scale factor are watts/in²

4.4.2 Total Power Computation. - Each lobe of the power curve was integrated using a polar planimeter. The power

$$P = \pi K_H K_{VP} \text{ Integrated Area} \quad (4-3)$$

If a filter had been used, this result would be multiplied by a filter factor. This represents the power measured after the turning mirror. The reflectivity of the mirror was determined from the lamp spectral data supplied by the manufacturer. (2) and the reflectivity curve for the turning mirror and the reflectors. (Figure 3-). This factor was computed to be 89% . Thus the actual module output power is higher than the measured output by the reciprocal of this factor.

4.4.3 Filter Factors. - A filter factor was not received from Eppley with the UG-11 filter. This filter is most useful, since it covers a broad region of the ultraviolet. Project personnel computed a filter factor using the method described by Eppley in their radiometer manual. (17) The spectral curve (supplied by Eppley) for a HgXe lamp was carefully replotted on a large sheet of graph paper. The transmittance curve for the UG-11 filter was also handplotted on the same sheet, and the product of the transmittance and spectral curves was plotted. The integrations with the planimeter were performed several times, producing a filter factor of 2.11. In communication with the Eppley firm, measurement personnel obtained from them a filter factor of 1.53. When the discrepancy between this figure and our calculated filter factor was pointed out, Eppley recomputed the factor and arrived at 1.90.

Project personnel checked some of the other filter factors, and they were in close agreement with our calculations, with the exception of the filter covering the region from 386 to 423 millimicrons. The Eppley factor for this filter is 3.39, as opposed to our computed factor of 2.53. A list of filters appears in table 4-2 and table 4-3.

The data obtained from the filter measurements was used in evaluations of spectral uniformity and distribution. Because this data was used to determine the relative contribution by spectral region, the use of the filter factor is not necessary.

4.4.4 Automatic Data Reduction. - Since this instrumentation system provides an accurate and rapid plot of the power and intensity functions, it is a powerful tool in the evaluation of a solar simulation module. The engineers feel that the system can be further automated if future evaluations of this type are undertaken. By automatically integrating the power curve, the efficiency of data reduction can be increased. This can be accomplished with a number of scalers. The output from the scalers can be displayed, plotted or printed out.

Computation of the scale factor also can be incorporated in the instrumentation. If this is done, the power can be read directly. A printer with a totalizer could read out the total power at the end of each data run.

4.5 Estimate of Data Accuracy

Each step in the design of the instrumentation was carefully studied to minimize measurement errors. Precision components such as the 10-turn potentiometers and dials were used throughout. (See table 4-1) The technique of using the meter nulls to indicate position eliminates many possible sources of error.

The stated accuracy of the planimeter is 0.3% with repeated careful measurements, except where the area is less than 10 square inches. Almost all of the data plotted produced areas larger than 10 square inches, and the integrations were performed several times on each curve.

In section 4.2.6, the error in positioning the radiometer was stated as $\frac{1}{4}$ inch or 0.33% of the radiometer travel. This was determined by carefully measuring the position of the radiometer for a particular dial setting. The procedure was repeated many times at the same dial setting and at a number of different settings. The error includes the effects of mechanical slip between various gears, hysteresis, and erroneous null reading or dial setting by the operator.

The error in plotting a given point is a function of the accuracy of each component in a chain of instruments and circuits starting with the radiometer and ending with the X-Y plotter. Another source of error is noise contributed by the various components in the system. The effect of this can be seen as a slight vertical modulation of the character printer. With the radiometer positioned at a fixed location, the point is plotted several times. From the distribution of these points,

the maximum error due to the system noise was found to be $\pm 0.5\%$.

The accuracy of the radiometer is not stated in either the manual or the calibration certificate. An estimate of system error will be computed without the radiometer. Table 4-4 lists the factors involved in computing the power and their relative accuracy figures. The gain of the amplifier was checked using a Calibration Standards precision voltmeter with a specified accuracy of $\pm 0.05\%$. The gain accuracy of the amplifier was found to be within $\pm 0.3\%$. The noise does not enter into the power computation since it is averaged in the integration with the planimeter.

It can be seen from equations 4-2 and 4-3 that these factors (with the exception of the voltage dividers, the VTVM amplifier, and the X-Y) combine as a product to compute the total power. The three exceptions listed are combined in the amplitude of the vertical plot. The fractional error of the product of two (or more) numbers is the algebraic sum of their fractional errors. In the case of division, the error of the quotient of two numbers is the algebraic difference of their fractional errors. Therefore, the system error (without the radiometer) is within $\pm 1.9\%$, i.e. the computed power is within $\pm 1.9\%$ of the true reading.

TABLE 4 - 4

Components Used in Estimate of Error

| FACTOR | ACCURACY |
|------------------|-------------|
| Radius | $\pm 0.5\%$ |
| Amplifier | $\pm 0.3\%$ |
| Voltage Dividers | $\pm 0.3\%$ |
| VTVM Amplifier | $\pm 0.1\%$ |
| X-Y Recorder | $\pm 0.1\%$ |
| K_H | $\pm 0.3\%$ |
| Planimeter | $\pm 0.3\%$ |

4.6 Measurement Data

The execution of the expanded measurement task outlined in section 4.1 was accomplished through 345 measurement runs on various configurations and elements of the module. Prior to receipt of the actual reflector elements, 92 of these runs were made using an approximate 4 inch focal length paraboloid to make preliminary studies of the source and the operation of the lense* plates.

One of the main reasons for the large number of runs was the number of module configurations to be measured. 72 of the runs were made upon the complete prototype reflector system without plates, 33 runs were made on the two plate configuration, and 29 runs were made on the one-plate configuration.

Since the individual reflector segments were so powerful a tool in studying directional distribution of flux about the source and spectral changes over φ , 119 runs were made using the individual reflector segments or sometimes combinations of them. These runs were used to balance the final module alignment and to verify individual segment performance.

For the study of angular distribution, as opposed to merely determining collimation angle, 55 runs were made with apertures, and to investigate the uniformity of intensity by spectral regions, 89 runs were made with filters. In addition 6 runs were made using both apertures and filters.

A typical series of runs on a particular configuration was as follows:

| <u>NO RUNS</u> | <u>FILTER</u> | <u>AXIS</u> | <u>Z</u> | <u>PURPOSE</u> |
|----------------|---------------|----------------|----------|-------------------------------------|
| 2 | ----- | X,Y | 15 | Irradiance Crossection |
| 2 | ----- | Y-80, Y+80 | 15 | (Intensity Only) Verify Symmetry |
| 2 | 12 | X,Y | 15 | Infra Red Crossection Index |
| 2 | 8 | X,Y | 15 | Visible Crossection Index |
| 2 | 3 | X,Y | 15 | U.V. Crossection Index |
| 2 | ----- | X,Y | 30 | Irradiance Crossection |
| 2 | ----- | Y-80 Y+80 | 30 | (Intensity Only) Verify Symmetry |
| 1 | 12 | X | 30 | I.R. Crossection Index |
| 1 | 8 | X | 30 | Visible Crossection Index |
| 1 | 3 | X | 30 | U.V. Crossection Index |
| 2 | ----- | X,Y | 60 | Irradiance Crossection |
| 2 | ----- | Y-120 Y+120 | 60 | (Intensity Only) Verify Symmetry |

As the measurement program progressed, some of these runs were dropped and others substituted. For instance, the off-axis, intensity-only runs proved to be unnecessary after the three basic configurations had been checked. We found that no additional information was obtained by running filters on both axes at 15 feet so these runs were dropped. The irradiance crossection on Y axis was retained for one value of Z rather than the three values used initially.

Later the broad band filters for the U.V. and I.R. were used instead of the three narrow band filters, particularly on the individual reflector segment runs. The apertures, which were not included in the typical runs, were added, and many special runs were made to check for certain losses, to check

5. MODULE PERFORMANCE

We shall present the results of measurements made on the prototype, we shall compare these results with the performance predictions, and we shall discuss the significance of any differences. We shall concentrate on

1. total output,
2. angular distribution, and
3. beam irradiance crosssection

for each of three configurations:

1. prototype reflectors only
2. prototype reflectors and two lenticular plates, and
3. prototype reflectors and one lenticular plate.

We shall discuss the uniformity of intensity for total flux and by spectral region for each configuration.

5.1 Reflectors Only Configuration

An understanding of the performance of the reflectors only (without the lenticular plates) is basic to an understanding of the other configurations. Figure 5-1 shows the reflectors and the source, without the lenticular plates, in operation. Reflector #4 was not in place at the time figure 5-1 was taken. Reflector #4 overheated, due to flux intercepted by its back from reflector #³~~4~~. The coating of #4 darkened considerably, and it was removed from the system. The power measurements are thus for reflector #1, 2, 3, and 5. If reflector #4 is to be retained in the system, it will have to be much thinner, and it may require special cooling.

special spectral regions, and to measure effects of element positional changes.

While the data from only about 25 of these runs is directly included in the following section, almost all of the runs were brought to bear upon the evaluation of the module, the refinement of the mathematical model, and the cross verification of data. The normalizing, clear description and interpretation which would be necessary to make all 345 runs suitable for publication is clearly beyond the scope of this program.

5.1.1 Total output. -

| | |
|--------------------------------------|------------|
| MEASURED TOTAL OUTPUT (WITHIN 7.5°) | 1000 WATTS |
| PREDICTED TOTAL OUTPUT (WITHIN 7.5°) | 933 WATTS |

Total flux brought down by the reflectors only (with #4 removed) was measured in runs #529, #535, and #582 as 1000 watts $\pm 3.9\%$ *. The measured total output should be

*For this estimate, the Eppley radiometer is assumed to have an error of $\pm 2\%$ of reading.

adjusted upward because of the following factors:

1. Reflectors #2 and #3 had some surface porosity and thus had a lower q_+ than the value used in computation.
2. Reflector #3 had some loss due to a turned-down edge.

These fabrication faults would be avoided by the use of glass reflectors. The extent of the loss due to these faults is extremely hard to estimate, and we prefer not to speculate on the amount of this loss.

A logical explanation of the differences is contained in the previous discussion of electrode radiation in section 3.5.1.

It seems likely that electrode radiation is understated in zones not having a direct view of the ~~cathode~~^{electrode} tips causing an overstatement of the ~~next~~^{net} arc radiation in those zones. Hence, reflectors 2 and 4 should be below prediction which they were.

On the other hand, output from zones viewing the electrode tips at favorable angles should exceed predictions and reflectors 1 and 3 do this. (Further corroborating evidence for this explanation will be seen when spectral peculiarities by zones are considered.) Reflector #4 had a predicted output of 47 watts, but when operated alone it produced only 34 watts.

The intensity in watts per square foot and in percentage relative to beam center as a function of radial distance from beam center is tabulated in Table 5-1. The data was derived from runs #529, #535, and #582.

5.1.2 Angular Distribution. -

| |
|--------------------------------|
| MEASURED MEAN β - 2.15° |
| PREDICTED MEAN β - 1.70° |

Angular distribution was measured using apertures on the radiometer and was also calculated from beam pattern and system geometry. The agreement between measurements and calculations was remarkably good with the largest deviation being 3.2% and mean deviation of 1.9%. The final aperture runs on the reflectors only were runs #561, #563, #565, #567, and #569.

The breakdown of the flux output of the reflectors by one-degree half-angle increments is as follows:

5.1.2 cont.

| <u>HALF-ANGLE INCREMENT (DEGREES)</u> | <u>WATTS INCLUDED</u> | <u>CUMMULATIVE WATTS INCLUDED</u> |
|---|---------------------------|---------------------------------------|
| 0 to 1 | 195 | 195 |
| 1 to 2 | 280 | 475 |
| 2 to 3 | 164 | 639 |
| 3 to 4 | 129 | 768 * |
| 4 to 5 | 67 | 835 |
| 5 to 6 | 65 | 900 |
| 6 to 7.5 | 100 | 1000 |

This distribution is compared in figure 5-2 to the predicted design theoretical distribution. An adjusted prediction curve is also shown which removes the reflector 4 contribution from the original prediction and substitutes a .89 reflectivity in the prediction instead of the .897 figure originally used.

The flux is definitely distributed over wider angles than predicted. The mean flux half-angle is 2.15° versus a prediction of 1.7° . The flux within 2° is 20.7% less than the adjusted prediction and that within 3° is 15.2% less.

Some contribution to wider angular distribution came from the fact that the outer rim of reflector 1 protrudes too far inside reflector 2 when both segments are on focus and vignettes approximately two degrees of that reflector's view. This segment was therefore aligned relatively high. This aggravated a problem with reflector 1 which already existed. This segment was designed very close to the bulb and because of time limitations was not offset, although this step was considered. This was a mistake. The segment focus should be

offset. By offsetting we mean making the focus of the paraboloid an angular ring by offsetting the focus from the optical axis before revolving the figure through Θ . (See Figure 5-3). Since a large portion of the view from high values of ϕ on this segment is blocked by the cathode, this course would reduce the mean resultant angle of the actual flux viewed.

From this discussion, it can also be seen more clearly that the necessity in the prototype to align this segment high increased the view of the cathode and degraded the angle of the actual flux.

Of far greater importance, however, in accounting for the discrepancies between prediction and performance are the differences between factual shape and size of the arc and assumptions made in representing the arc in the predictions. The position of the arc centroid and the non-equivalence of luminance and radiance distributions in the arc make up the major share of the discrepancy. These factors were discussed in sections 3.3.6 and 3.5.2.

5.1.3 Beam Irradiance Crosssection. - Figure 5-4 illustrates the relative beam irradiance crosssections for the reflectors-only at the three distances from the module. These plots are of the data previously included in Table 5-1.

Figure 5-5 compares the measured 60 foot pattern with that originally predicted. The main discrepancy is seen to be in the peak intensity which was predicted to be 138 watts/ft² and measured at 96 watts/ft². That this is almost solely a function of the discrepancy in predicted angular distribution can be seen

from the third curve which was secured by substituting the measured angular distribution into the prediction calculations. For this purpose it was necessary to assume that the measured angular distribution of flux was spread evenly over the module exit pupil. The prediction technique has proven to be quite satisfactory for design requirements.

5.1.4 Uniformity of Intensity. - Taking the measured beam irradiance cross-section and assuming a large hexagonal array of modules producing identical patterns, it is possible to compute the intensity at any point in the plane to which the pattern applies. If the module centers are given X and Y coordinates then a point P at X_p and Y_p will be a distance $[(X_p - X_i)^2 + (Y_p - Y_i)^2]^{1/2}$ from module i . This distance is also the radial distance from pattern center of module i and a corresponding intensity applies from the beam irradiance cross-section. Summation of the contributions by all modules within a distance of less than the radius of the beam irradiance cross-section will give the resultant intensity at point P.

A series of calculations were made for each of the planes for which the measured beam irradiance cross-sections were available.

These calculations were made for modules arrayed on 27-inch and 15.59-inch ^{module} center-to-center distances. ^{The 15.59-inch center-to-center distance is the direct} relationship of two and three array centers when each individual array is on 27-inch centers.

The resultant total array point intensities were then related to the average array intensity. Selection of the maximum point deviation over the entire pattern then gives the deviation essentially in terms of the target specification of ± 50 percent deviation, using a one-inch-diameter detector. Integrations to

~~is~~ correspond to the target specification of ± 5 per cent, using a one-foot-square detector, have not been made and this area has been treated by estimates from the maximum point deviations.

The percentage of maximum radiant intensity deviation resulting over the pattern for the reflectors only is as follows:

| <u>FEET FROM MODULE</u> | <u>27-INCH MODULE CENTERS</u> | <u>15.59-INCH MODULE CENTERS</u> |
|-----------------------------|-----------------------------------|--------------------------------------|
| 15 | 239.0 | 46.7 |
| 30 | 77.3 | 15.9 |
| 60 | 11.1 | 2.1 |

These results illustrate the effects of the basic beam irradiance cross-section and the degree to which beam modification is necessary. On 27-inch centers, uniformity of intensity would be outside the target specifications to almost 40 feet from the module. On 15.59-inch centers, however, the uniformity is within target parameters at approximately 15 feet from the module.

The problem to be overcome in dealing with this beam pattern is that the flux distributed in the low angles causes hot spotting under the module center and the point on the optical axis is the point of maximum deviation throughout the target volume. It is interesting to note that at 60 feet from the module it is energy distributed within less than 0.6° which is causing the peak in the beam irradiance cross-section.

5.1.5 Spectral Uniformity. - Detailed spectral distribution measurements and evaluation were beyond the scope of this program. Still, approximately one-third of all runs made on

actual module configurations utilized interference filters to study variables by spectral region. This approach is based upon the premise that uniformity of irradiation must include uniformity within spectral regions as well as in total. In many cases, the importance of spectral uniformity may become more significant than total uniformity.

Again in this area, filtered measurements by zones utilizing the individual reflector segments were especially effective in demonstrating both chromatic changes with changes in the view of the arc (through ϕ) and in demonstrating chromatic changes across the arc (along ν) and therefore with angular distribution.

Spectral beam patterns and deviations for the reflectors only are graphed in figure 5-6. The beam patterns, based on runs #180, #182, #184, and #186, are presented in terms of the percentage of flux in the particular spectral region to the total flux for points at regular intervals across the module beam. The data for these curves was taken at 30 feet from the module.

The region from 295 millimicrons to 332 millimicrons (filter 3) was used as an indicator for ultraviolet, the 515 millimicrons to 573 millimicrons region (filter 8) for visible, and the 1100 millimicrons to 1900 millimicrons region for infra-red.

The deviations of region point intensities from region average intensities over the entire pattern were then weighted on the basis of contribution of the point deviation to non-uniformity of that region at that point in a one solar constant array.

The deviations across the beam from the reflectors only are substantial with the UV contributing over 20 percent excess near the beam center and IR low by almost 18 percent.

Examples of a couple of the more spectacular chromatic peculiarities by zones around the arc are seen in both the UV and the IR peaks near the center of the beam. The UV peak is largely contributed by reflector 1 and probably has as its source the edge of the small hot plasma ball. The IR peak is made up by the combination of two peaks from reflector 1 and reflector 3. The sources for these are very probably the hot cathode tip in the case of 3 and the hot anode center in the case of 1. There is no evidence of high contributions in this area by reflectors 2 or 4 at all.

Note also that the UV excess and the IR deficiency in the center of the beam tend to mask each other in the total intensity.

5.2 Two Lens Plate Configuration

Figure 5-7 shows the operating module with two lens plates in position. Although this view shows the bottom of both lens plates, the angle of the view of the top lens plate from the optical axis is less than the angle at which the bottom plate is viewed. For this reason more visible flux can be seen from the top plate. Of course, in final configuration, the whole module would be enclosed in a cylindrical housing and only the bottom plate would be visible.

5.2.1 Total Output. -

5.2.1 Total Output. -

| | |
|--------------------------------------|-----------|
| MEASURED TOTAL OUTPUT (WITHIN 7.5°) | 635 WATTS |
| PREDICTED TOTAL OUTPUT (WITHIN 7.5°) | 785 WATTS |

Total flux brought down by this configuration measured in runs #207, #227, and #239 was 635 watts, but only 465 watts of this total were in the basic square pattern. The remaining output was in the throw-out squares adjacent to the flats of the base square, and this flux would be removed by baffles for strict adherence to the prescribed pattern. The absolute and relative intensities along the beam radius are tabulated in Table 5-2.

Figure 5-8 shows the beam pattern for this configuration at a distance of 60 feet from the module. The throw-out squares can be seen off the sides of the base square. Integration of total flux for this pattern had to be done specially since the simple intensity-radius product was not applicable over the whole beam radius. The restatement of coordinates of intensity points in terms of the square pattern was straight forward even if time consuming. The verification of this procedure provided one of the main reasons for the early off-axis intensity runs.

The predicted total output for this configuration which is comparable to the 635 watts measured was 785 watts. The discrepancy of 150 watts or 19.1% is substantial and accounted for by the following facts:

1. Loss of energy on the prototype lens plates was higher than would be the case with molded plates because the surface is interrupted by the support structure of pins and bands. Frosted and darkened lenslet edges also contributed to these higher lens plate losses.

The visible flux being scattered by the pins and lenslet edges is quite evident from the bottom plate in figure 5-7 where the bulk of the flux is not within the view angle. Also, the vignetted corners of the square pattern from this configuration seen in Figure 5-8 are caused by the supporting pins at lenslet corners in the prototype plates.

The excessive losses due to support structure including the pins, bands, and lenslet edges was calculated to be 93 watts based on the energy incident on the two plates and the actual angular distribution of that energy. These unusual prototype losses were not taken into account in the prediction.

2. Another factor not contemplated in the original prediction is concerned with the fact that the lens plates tip some of the energy originally distributed within 7.5° to larger angles and this flux is not, therefore, within the radiometer view angle. This factor is calculated to account for 41 watts.
3. In two plate operation the partial lenslets become very ineffective. The absence of the opposite side of the full lens at the second plate causes vignetting

of essentially all flux diverging from the optical axis of the module and even some of the smaller angle converging flux received from the corresponding lenslet in the first plate.

This factor caused excessive losses of approximately 16 watts. These losses would have been closer to 20 watts if the support and tip losses had not been netted out of incident flux previously. This factor was also not taken into account by the prediction. However, this can be corrected easily by two techniques. The lens size and plate shape can be coordinated to minimize the edge partial lenses, making the plate slightly out of round if necessary. The major portion of this loss can be avoided by use of prisms on the first plate partial lenslet to slightly offset its image on the second plate partial lenslet.

5.2.2 Angular Distribution. -

| | |
|---------------------|-----------------------|
| MEASURED 465 WATTS | $(\beta = 2.5^\circ)$ |
| PREDICTED 633 WATTS | $(\beta = 2.8^\circ)$ |

Since this configuration produces an abrupt angular cut off and in this particular case at a low half angle, aperture runs were not applicable to its output. Neither were predictions made directly in terms of angular distribution. However, the predictions of module output for configurations operating at different half angles are based upon this type of data.

Unfortunately, for the two plate system, we can only directly

verify operation at one half-angle for each set of lenses used. Actually, none of the predictions correspond directly to this set of lenses, but since the system was treated nominally as a three degree system let us compare the predicted 633 watts output for a 3° half-angle two lens plate system to the 465 watts measured in the basic pattern for the prototype. Three factors must be considered.

1. The prediction was based on a three degree half-angle lens and the assumed conditions for the prediction would be satisfied if the lens were a round one having the relationship $\frac{r_L}{RFL} = \tan 3^\circ$. However, the actual lens used is square having a 2.67° relationship at the radius of the inscribed circle and a 3.77° relationship at the corner of the square. If we re-calculate from the predicted angular distribution for this lens we find that the prediction becomes 624 watts so that shape causes only a 9 watt discrepancy in the prediction.
2. If we again re-calculated using the measured angular distribution out of the reflectors and the square lens shape the answer produced is 506 watts. Thus, the angular distribution difference is by far the largest factor of difference between predicted and measured performance accounting for 120 watts.
3. If we now compute the unusual prototype losses applicable to the transmitted energy it is found that they account for 41 watts which is also the difference between the 506 watts in 2 above and the 465 watts measured.

It should be noted that while unusual prototype losses calculated in 5.2.1 amounted to a total of 150 watts these were from all energy down and the 41 watts relates only to the energy accepted by the pair of square lenslets. Thus, for this particular lens design, the unusual losses of 109 watts are not important since the energy from which they were lost would not have been accepted by the lens plates into the base pattern. It can also be seen, however, that the unusual losses applicable will be different for each half-angle dealt with.

It can now be stated that this configuration with two molded lens plates having the same lens design would put 502 watts in the base square. This includes the adjustment of the plates to reduce partial lenslet losses.

Ninety percent of the energy in the measured pattern for this lens design is within 2.5° half-angle. However, with a molded lens plate ninety percent of the energy would be within 2.3° half-angle.

5.2.3 Beam Irradiance Crossection. - Figure 5-9 illustrates the relative beam irradiance crossections for the two lens plate configuration at the three distances from the module. These plots are of data previously included in Table 5-2.

This configuration with the image of the top plate lenticles at approximately 15 feet instead of infinity was also measured and evaluated. The beam pattern at approximately the focal plane is shown in Figure 5-10. The stepped patterns of the overlapping lenticle images, which at this distance have not yet become large enough to essentially cover the entire pattern, can be

clearly seen. Also clearly seen in this illustration are the throw-out squares and their relationship to the base pattern. These throw-out squares are more prominent in this operation because of the additional spillage resulting from the necessarily greater plate-to-plate distance. The 60 foot pattern from this higher focus is much larger as can be seen by comparison of the picture of this pattern in Figure 5-11 to the 60 foot pattern under normal operation previously shown in Figure 5-8.

5.2.4 Uniformity of Intensity. - Using the three beam irradiance crosssections, the same series of calculations as those described in section 5.1.4 were made.

The complete series of calculations for the configuration focused at 15 feet were not made since the lens acceptance angle could not be adjusted to operate in combination with the revised focus. The energy angle accepted has far more effect than the plane of focus selected.

The percentage of maximum radiant intensity ^{deviation to average array intensity} resulting over the pattern for the two lens plate configuration focused at infinity is as follows:

| <u>FEET FROM MODULE</u> | <u>27-INCH MODULE CENTERS</u> | <u>15.59 - INCH MODULE CENTERS</u> |
|-----------------------------|-----------------------------------|--|
| 15 | 90.4 | 5.8 |
| 30 | 47.2 | 8.1 |
| 60 | 7.4 | 3.9 |

On 27-inch centers the pattern is unacceptable until just beyond the 30 foot distance from the module. The pattern would be acceptable on 15.59-inch centers at approximately 11 feet from the module.

A greater energy half-angle must be accepted to provide uniformity within the target specifications at the 20 foot distance from the module with this configuration on 27 inch centers. The very uniform intensity pattern with sharp edge drop off produced by the individual module of this configuration does create standing-wave patterns or intensity ripple throughout the irradiated zone.

5.2.5 Spectral Uniformity. - Spectral beam patterns and deviations for the two lens plate configuration are graphed in Figure 5-12. The beam patterns are based on runs #227, #229, #231, and #323 which were all made at 30 feet from the module.

Local deviations across the beam have been almost entirely eliminated by this configuration. While the deviations computed for the U.V. and visible regions are still relatively high, this results, to a great extent, from making these measurements on all energy down from the un baffled configuration. The deviation curves are pretty flat and removal of IR from throw-out patterns would substantially reduce the level of these deviations by increasing the percentages of UV and visible energy in the total base pattern energy. Measurement data would have to be taken on the baffled module or in the pattern nearer to 60 feet to effectively separate the base pattern energy.

5.3 One Lens Plate Configuration

No illustration of the one-plate configuration has been included because this configuration is produced by merely removing the second plate from the two-plate configuration which

was illustrated in Figure 5-7. Of course, the support bars would be shortened and the final module would be about 20 inches shorter.

5.3.1 Total Output. -

| | |
|--------------------------------------|-----------|
| MEASURED TOTAL OUTPUT(WITHIN 7.5°) | 805 WATTS |
| PREDICTED TOTAL OUTPUT (WITHIN 7.5°) | 877 WATTS |

Total flux brought down by this configuration measured in runs #246, #253, and #267 was 805 watts. The absolute and relative intensities along the beam radius are tabulated in Table 5-3. The output of 805 watts compares with a prediction of 877 watts. In the difference of 72 watts or 8.2% of prediction, several factors have been combined:

1. Total output of the reflectors was 20 watts greater than predicted increasing the discrepancy by approximately 18 watts after plate losses.
2. Prototype lens plate support losses were excessive by approximately 50 watts
3. Energy tipped out of the view of the radiometer would be approximately 45 watts.

The energy tipped outside 7.5° would still be lost using molded lens plates and in fact would also apply on energy saved by eliminating the support structure. Therefore, the output using a molded plate with the same lens design would be 849 watts. It should be noted that there is no loss incurred due to partial lenslets in this configuration.

5.3.2 Angular Distribution. - As we have seen in section 3.3.11, with this configuration, we are dealing with a relatively

selective alteration of angular distribution in achieving the final beam. Lower half angle energy is dispersed relatively much more.

Final aperture runs were not made on this configuration nor were calculations made across all angles as they were for the reflectors-only configuration. Calculations for two zones do, however, illustrate this selective dispersion. Although in the resultant beam there is approximately 24 percent less energy within 2° half-angle than in the energy received by the plate there is in the beam only about 4 percent less energy within 5° half-angle than in the incident energy. For this configuration too, the predictions of module output for different half-angles were based upon predicted angular distribution data. With ^{the} slightly higher total ^{reflectors} output distributed over wider angles the comparison of approximate one-plate system performance to that predicted would be:

| <u>HALF ANGLE LIMIT</u> | <u>PREDICTED WATTS OUTPUT</u> | <u>WATTS MODULE OUTPUT</u> |
|-----------------------------|-----------------------------------|--------------------------------|
| 3° | 624 | 501 |
| 4° | 717 | 626 |
| 5° | 796 | 716 |

5.3.3 Beam Irradiance Crosssection. - Figure 5-13 illustrates the relative beam irradiance crosssections for the one lens plate configuration at the three distances from the module. These plots are of the data previously included in Table 5-3. The more rounded intensity peak with more gradual falloff are most efficiently achieved with the one-lens-plate configuration.

5.3.4 Uniformity of Intensity. - Again, using the three beam irradiance crosssections, the series of uniformity calculations were made. The percentage of maximum radiant intensity deviation

to average array intensity resulting over the pattern for the one-lens-plate configuration is as follows:

| <u>FEET FROM MODULE</u> | <u>27-INCH MODULE CENTERS</u> | <u>15.59 INCH MODULE CENTERS</u> |
|-----------------------------|-----------------------------------|--------------------------------------|
| 15 | 24.8 | 4.0 |
| 30 | 3.3 | .6 |
| 60 | 1.0 | .9 |

For this configuration the deviations are well within the target specifications above 15 ft. on both 27-inch centers and 15.59-inch centers. It is quite possible that it would be advantageous in conjunction with other design considerations to reduce the lens half-angle if the target uniformity is adequate.

5.3.5 Spectral Uniformity. - Spectral beam patterns and deviations for the one-lens-plate configurations are graphed in Figure 5-14. The beam patterns are based on runs #253, #255, #257, and #259 which were all made at 30 feet from the module.

This configuration produces a high degree of spectral uniformity with the maximum deviation being 4.5 percent.

6 SOLAR MODULE FUTURE

6.1 Summary of Program Results

In the course of this program, we have tested a number of design concepts and mathematical models, and have found thorough confirmation of these concepts and models. We shall summarize these concepts and models:

1. The use of the simplest system which will meet the optical requirements.
2. The use of a segmented reflector system to collect flux over a large range of angle φ and yet still maintain a small enough module diameter for packing multiple arrays and a large enough mean R for obtaining a proper distribution of flux by angle β .
3. The use of one or two lenticular plates to shape the beam as desired without introducing excessive loss or chromatic aberration, and to integrate the reflector output and destroy the adverse correlation between α and β and between φ and β or χ .
4. The use of a baffle system after the first lenticular plate to control stray flux and prevent re-reflection.
5. The use of a soft beam profile so that modules can be aligned with reasonable tolerances without the danger of holes or excessive hot spots.
6. The use of a small module so that multiple arrays can be used to extend intensity and/or operating life.
7. The use of a simple symmetric disc model to represent the arc.
8. The use of a distribution function $F(\beta)$ to describe the flux versus angle relationship.

9. The use of various mathematical techniques including mapping techniques to find the new beam after each transformation.
10. The use of individual reflector segments to study any given source.

In addition, we have developed a technique for automating certain aspects of the measurements, and we have considered possible further automation of these measurements.

The measurements made on the prototype support the mathematical models very strongly, and the measurements and models state clearly what can be accomplished with present sources and what cannot be accomplished with present sources. The following statements define these limits:

1. High module efficiency* (25 to 30 percent) can be achieved with a small (7.5 inch) module radius.

*Efficiency as here used is total module output related to total power input at the source.

2. The target of 2° half-angle requires a larger module in order to meet efficiency and uniformity targets.
3. Half-angle of 3° to 4° will allow the required efficiency and will produce a uniformity far better than the target specification.
4. The serious chromatic aberration often present in solar modules can be essentially eliminated.
5. The module can be constructed with elements which lend themselves to fabrication at a reasonable cost on a production basis.

6.2 Specification of Simualtor Parameters

Specific performances of prototype configurations have thoroughly confirmed the approach described for valuation of the operating parameters for the module and to a great extent for solar simulators more generally. Complete summarization of the combinations of results of changes in these parameters for all possible system configurations is far beyond the scope of this program. However, the direct relationship of efficiency with the angular distribution curve, of uniformity with angular distribution, and similar direct relationships, when combined with the parameters peculiar to specific configurations, begin to present a clear picture of alternatives in the selection of a particular system to meet a given group of requirements.

The results of this program provide a far sounder basis for determining the degree of accuracy which is reasonable in the simulation of each factor than has ever been available. The task now at hand is the balancing of these factors to produce specifications. This balancing must be accomplished in terms of:

1. Importance of parameter in relative to other parameters affected.
2. Initial system cost and system operation costs.
3. Test requirements.

6.2.1 Total Output - Efficiency. - High efficiency is the principle answer to holding down initial system cost and the costs of operating the system which, in the longer run, can be much more significant. Higher efficiency reduces the number of modules required, reduces the number of lamps used and the amount

of power used, and reduces the excess heat which must be removed at substantial cost in both initial equipment and in operating power.

It is suggested that this parameter has too often been traded off unwisely in over refinement of spectral distribution match and overemphasis on small β_{90} or β_{max} . The criterion suggested is that there always be a clear test requirement justification before efficiency is significantly degraded in the refinement of another factor.

6.2.2 Angular Distribution. - The angular distribution of flux must first be smooth enough and, where necessary, broad enough to produce the beam irradiance crosssection required for uniformity of irradiance. Once that requirement is satisfied, the angular distribution must be no broader in order to avoid excessive irradiance of areas which should be shadowed and avoid increasing the problem to be dealt with at array edges.

6.2.3 Representative Module Adaptations. - Having generally reviewed total output and angular distribution, the most effective approach is probably in the comparison of the approximate characteristics of several representative module adaptations. The characteristics for fourteen adaptations are tabulated in Table 6-1. These adaptations range in efficiency (Watts output/Power into lamp) from 20.5% to 33.7%. Half-Angle within which 90% of the output energy is contained (β_{90}) range from 2.85° to 7.5° and the maximum half-angle of output energy (β_{max}) ranges from 3.0° to 7.5° .

Adaptations 1 thru 4 illustrate the range of the two lenticular plate configuration between $\beta_{90} = 2.85^\circ$ and 4.74° . Adapt. 1 is not

practical, but adapt. 2 shows that the prototype will successfully operate between 15 and 17 inch centers for 2 arrays which would be on square centers.

Adaptations 5 thru 7 present the range for the one lenticular plate configuration between β_{90} of 3° and 5° . Generally, the one plate systems have outputs 11 to 12% greater than the comparable 2 plate systems and have the softer beam profile resulting in much larger values of β_{max} . It should not be overlooked, however, that the β_{90} values of the one plate adaptations range only from 15° to $.26^\circ$ above the comparable 2 plate adaptation and that only 10% of the energy is included in the much wider range beyond β_{90} .

Adapt. 8 compared to Adapt. 5 and Adapt. 9 compared to Adapt. 1 illustrate the powerful leverage exercised by arc size. As noted in the table footnote, the calculations for the Xelamps are based on comparative size of arc based on isobrightness data for the lamps related to comparable data for the SAHX2500F. While there is every reason to believe such a base is valid for comparison, these results should be confirmed by actual lamp measurements.

Adaptations 10 thru 12 take the next step in showing the advantages in higher output and smaller $\bar{\beta}$ derived from the lack of proportionate growth in arc size with growth in lamp wattage.

Adaptations 13 and 14 illustrate the effect of increasing module size while using the same source. In these adaptations the size increase is achieved by elimination of multiple array capability.

While Table 6-1 is not exhaustive in its coverage of possibilities, a careful review of it especially in combination with the preceding discussion of these parameters should give a good grasp of the interacting parameter curves.

6.2.4 Beam Pattern and Uniformity of Irradiation. - An array of solar modules will not match the uniformity of solar radiation. However, the requirement for uniformity has probably been understated. For example, what is the significance of data on output or life of a solar cell on a space vehicle if the solar cell may have been subjected to a 150% hot spot? Where irradiation of small areas within the larger test volume affects measurement data, a uniformity of something nearer $\pm 10\%$ from mean irradiance, tested with a one inch diameter sensor, would seem more reasonable. It might be noted that such a specification alone would probably suffice.

As we have seen, the soft beam profile has the greatest promise for higher degrees of uniformity.

6.2.5 Spectral Uniformity. - We have considered spectral uniformity as an essential part of uniformity of irradiation and spectral distribution match cannot be achieved without spectral uniformity. Even where spectral match is imperfect, spectral uniformity is very important. If an array does not have spectral uniformity, then calculation of the effect of spectral mis-match is not possible, for one would have to deal with a standing-wave rainbow pattern throughout the test volume.

Including uniformity by spectral regions under the same $\pm 10\%$ from mean irradiance, tested with a one-inch diameter sensor, would seem reasonable.

6.2.6 Other Factors. - Many other factors will undoubtedly enter into the balancing of specifications to some extent. Two further factors seem worth mentioning here.

Effective system running time is important since a space mission can well exceed the life of available sources. The process of selecting ^{the source} itself, however, should put emphasis on its rated life and maintenance of output. The source must be compatible with the module and it is recommended that the initial module output intensity be on the order of 1.2 to 1.33 solar constants so that sources can be utilized to the point of 80% or 75% maintenance of original output.

Spectral distribution match is the other factor and this depends on the source spectrum and on the amount we are willing to degrade efficiency by filtering to improve the match.

6.3 Complete Engineering Prototype

Once the balancing of test requirements and cost factors has resulted in a set of simulator parameter specifications attention must be centered on realizing an operating system conforming to these specifications. The design adaptation and construction of the complete engineering prototype and its evaluation is the principal requirement in accomplishing this end. A review of the requirements for the complete engineering prototype and the program to produce it seems in order.

6.3.1 Source Selection. - As we have seen, the flux source is a critical component in the system and its selection warrants first attention and thorough coverage. The short arc lamp is the only source with any degree of demonstrated capability, through adequate data and history of operation, for continuous duty application in the next few years.

Short arc sources should be evaluated using the prototype reflector segments for zonal studies of contributions to total flux, angular distribution of flux, and spectral distribution. Arc size and effective life of the source are two of the most important characteristics to be evaluated.

While spectral distribution will be far short of that desired, it would appear that lower UV content and higher continuum of the Xe lamp may be more desirable. Evaluation of some larger-wattage sources should be included.

The present automated measurement capability, which should probably be extended somewhat, and the capacity for rapid evaluation by zones will simplify this task greatly.

6.3.2 Reflector Adaptation. - The reflector system of the prototype must then be adjusted in accordance with:

1. the selected source,
2. the selected β limits,
3. the problem with reflector 4,
4. the advisability of offsetting reflector 1,
5. the selected method of sealing the module, and
6. the verification of slumped glass reflector performance.

6.3.3 Lenticular Plate Adaptation and Molding. - The new lenticular parameters depend on the β_{q_0} and β_{max} acceptable and any beam pattern adjustments required by final module array center-to-center distances. Checkout of lenticular design can probably utilize the prototype lens plates with the adjusted lenslets. These plates would then be molded once all elements have been checked out.

6.3.4 Module seals. - Several methods of sealing the module have been considered and should be investigated, including:

1. a single replaceable seal around the entire plate,
2. four replaceable quadrant seals,
3. more than four plate sections sealed separately,
4. a permanent compensated, fusion seal of the plate to the module fully tested over the full temperature range prior to further assembly, and a removeable, steel-flange, seal at another point on the module.

6.3.5 Housing and Cooling Provision. - Design of housing configuration with provision for the seals and coolant flow must also be accomplished. Orientation of the module, that is overhead or side array, must be taken into account in this phase.

6.3.6 Array edge modification. - The use of a modified lenticular plate on modules at the array edge to reduce ^{SKIRT}~~skirt~~ losses and avoid the requirement for removal of unnecessary heat load from the chamber should be very effective. A prototype of this modification could utilize the prototype lens plates with modified lenslets.

6.3.7 Power and control provision. - Power supply, ignition, and power regulation for the short arc source must be provided for each module. Provision for monitoring and control of the module should also be included.

6.4 Conclusions

This program has confirmed the concepts and mathematical models and thereby quantified the interrelationships between parameters and described the limits on what can and cannot be accomplished with present sources.

It is now required that the following parameters be balanced and specified:

1. Irradiance range.
2. Uniformity including spectral uniformity.
3. Largest tolerable and or .
4. Array orientation (side or overhead)
5. Spectral match
6. Running time requirements.

Based on these parameters, it is recommended that a complete engineering prototype be designed, fabricated, and evaluated.

The results of this program have demonstrated that an array of these modules will provide higher efficiency, will have better uniformity of irradiance including spectral uniformity, will be more flexible, will provide longer running time, and will have lower operating and initial cost, than any previous solar simulator system has provided.

REFERENCES

- (1) Handbook of Chemistry and Physics, 44th Edition, pp. 2848-2850. Chemical Rubber Publishing Co.
- (2) Freeman, George A., and Alameda, Donald J:
Short-Arc Lamps for Space Environmental Application.
Westinghouse Electric Corporation, Lamp Division,
Bloomfield, New Jersey. 1964
- (3) General Electric Xenon Compact-Source Arc Lamps.
General Electric Company. April 25, 1962.
- (4) Technitalk L15, 5/62. Macbeth Sales Corporation,
Newburgh, New York. May 1962.
- (5) Landau, L., and Lifshits, E.: The Classical Theory of Fields.
Addisen-Wesley Press, Inc., Cambridge, Mass. 1951.
- (6) Panofsky, Wolfgang K.H., and Phillips, Melba:
Classical Electricity and Magnetism. Addisen-Wesley
Publishing Co., Inc., Cambridge, Mass. 1955.
- (7) Zemansky, Mark W.: Heat and Thermodynamics.
McGraw-Hill Book Company, Inc., New York. 1951 Third
Edition.

- (8) Handbook of Chemistry and Physics, 44th Edition, Chemical Rubber Publishing Co.
- (9) Keitz, H.A. E.: Light Calculations and Measurements. English translation. Phillips Technical Library. Netherlands. 1955
- (10) Abraham, Max.; and Becker, Richard: The Classical Theory of Electricity and Magnetism, Second Edition. Hafner Publishing Company, Inc. New York. 1949.
- (11) Jenkins, Francis A., and White, Harvey E.: Fundamentals of Optics, Second Edition, McGray-Hill Book Company, Inc., New York. 1950.
- (12) Born, Ma, and Wolf, Emil: Principles of Optics, Second (Revised) Edition. Pergamon Press, The McMillan Company, New York. 1964
- (13) Set Theory
- (14) R. Courant: Differential and Integral Calculus, Second Edition, Vol. 1 and 2. Interscience Publishers, Inc. New York.

NASA CR-54479

FINAL REPORT

LINEAR SOLAR MODULE: Refinement, Measurement, and Evaluation
of Optics

by:

J. Robert Gettel

Gary F. Comiskey

Richard A. Karlin

prepared for

NATIONAL AERONAUTICS AND SPACE ADMINISTRATION

August 1965

CONTRACT NAS 3-2794

Technical Management

NASA Lewis Research Center
Cleveland Ohio
Facilities Engineering Division
Myron H. Pollyea

LINEAR, INC.

P.O. BOX 483 • EVANSTON, ILLINOIS • TELEPHONE 475-1730 • AREA CODE 312

DISTRIBUTION

OF

FINAL REPORT

National Aeronautics and Space Administration
Lewis Research Center
21000 Brookpark Road
Cleveland, Ohio 44135

Attention: Myron H. Pollyea - M.S. 60-2 (4 copies) *
John E. Dilley - M.S. 500-309
John J. Weber - M.S. 3-19
Library - M.S. 3-7 (2 copies)
Report Control Office - M.S. 5-5

National Aeronautics and Space Administration
Scientific and Technical Information Facility
P.O. Box 5700
Bethesda 14, Maryland
Attention: NASA Representative (6 copies)

WIFE BY _____ DATE _____
CHKD. BY _____ DATE _____

SUBJECT ANALYSIS DISTRIBUTION
Total Module - Reflectors Only
Measured + Theoretical

SHEET NO. _____ OF _____
JOB NO. _____

Figure 5 - 2

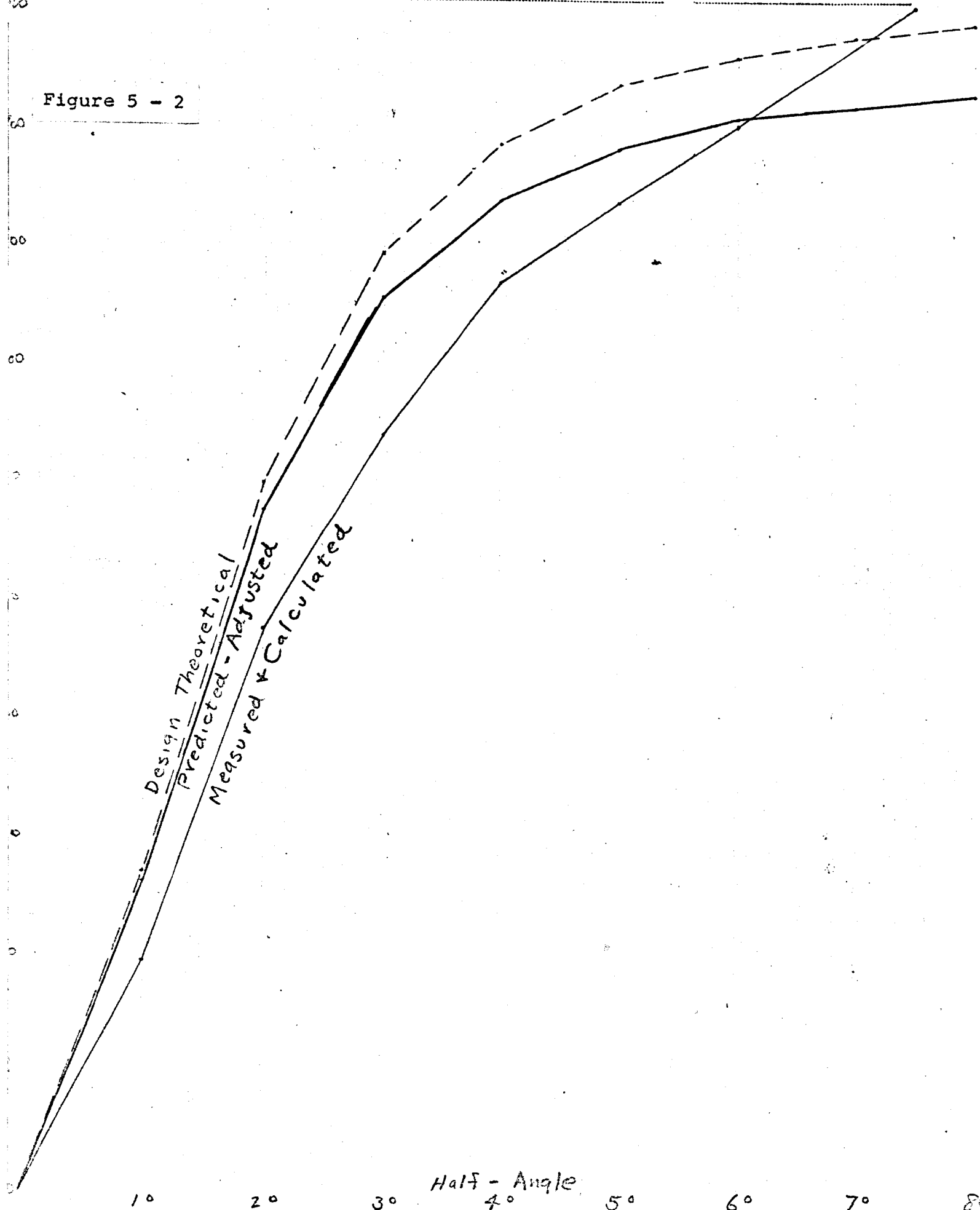
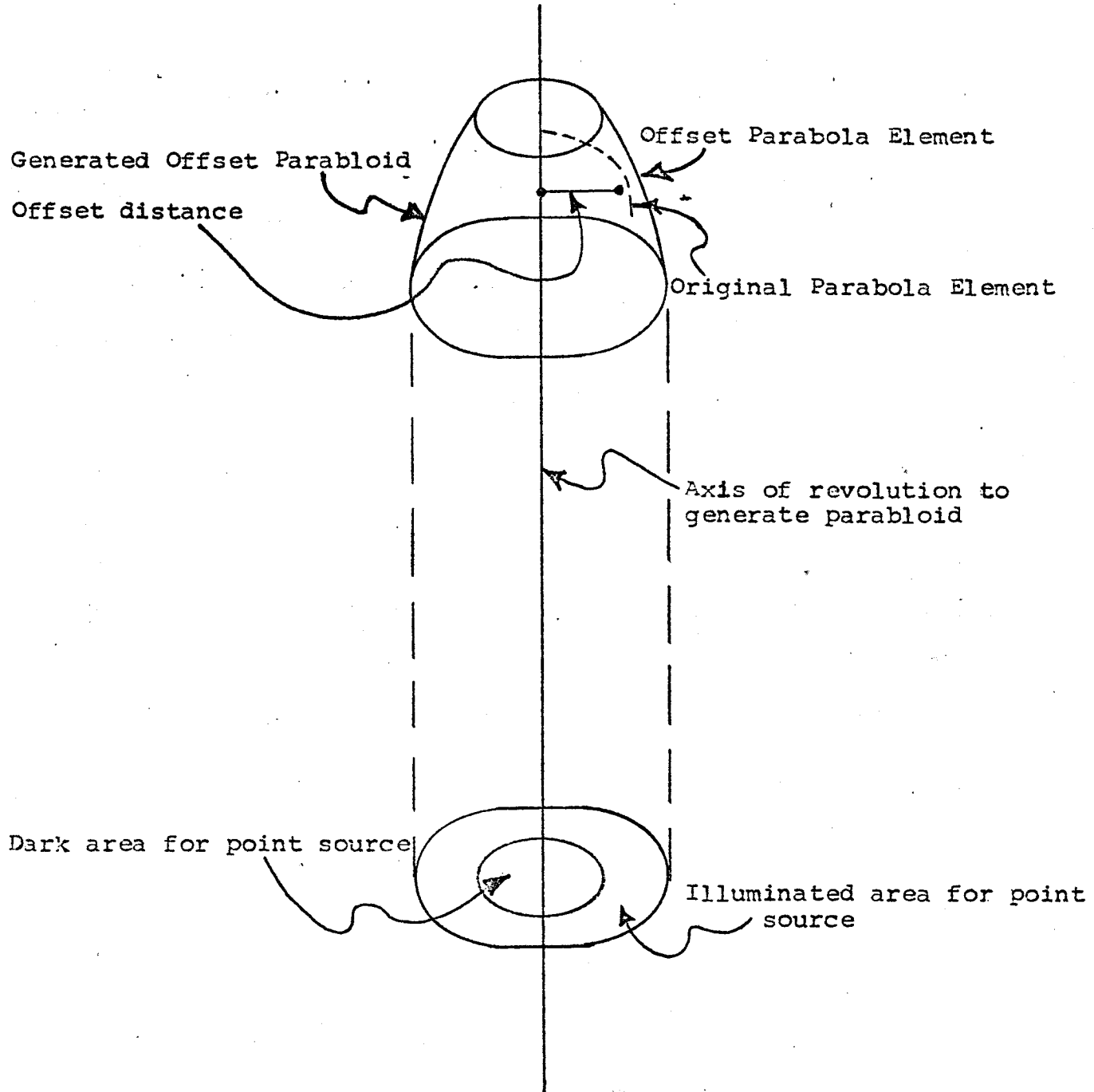


FIG.# 5-3

Offset Paraboloid



BY _____ DATE _____

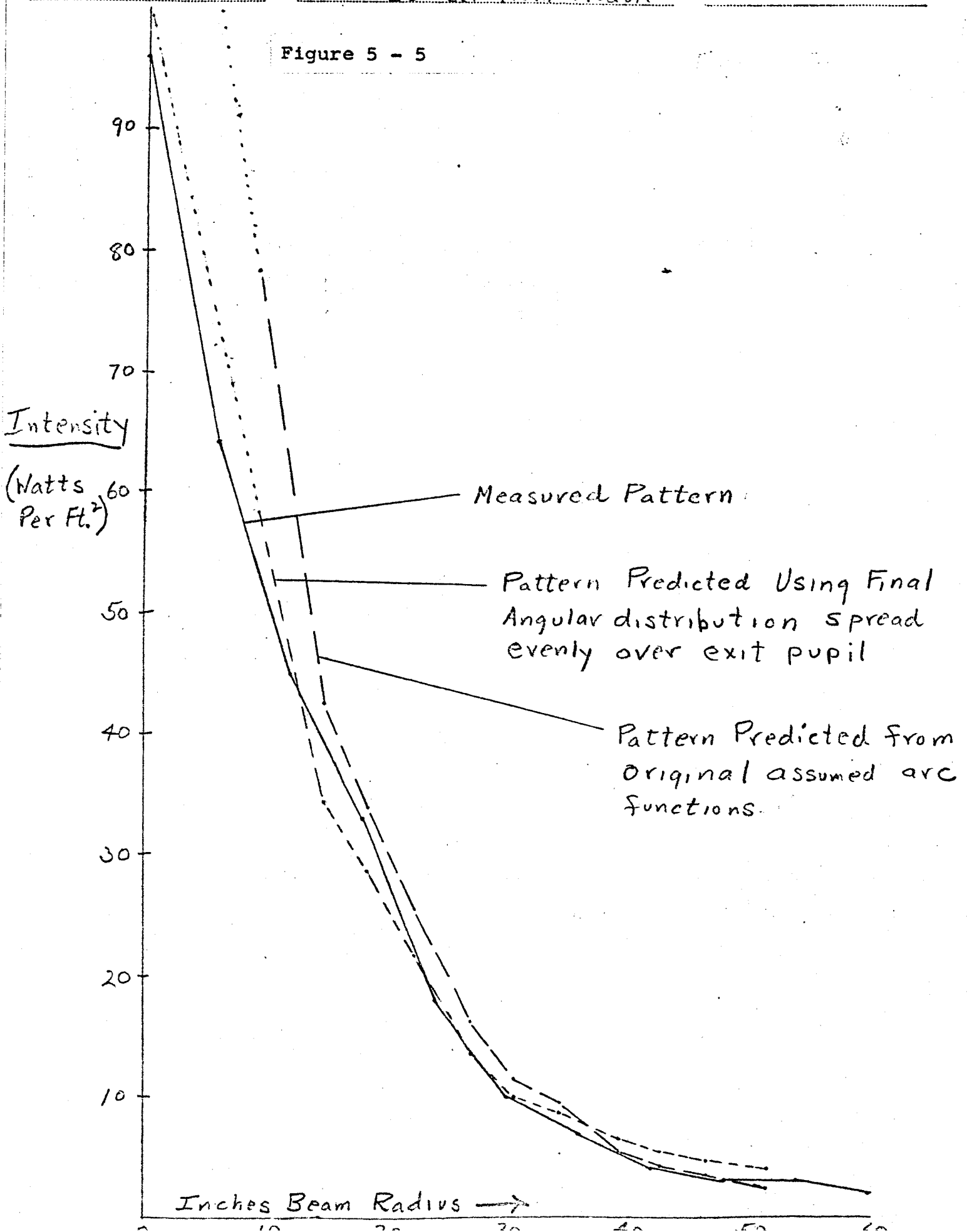
SUBJECT Predicted Beam Irradiance SHEET NO. _____ OF _____

KD. BY _____ DATE _____

Cross-section - Reflectors Only JOB NO. _____

60 Feet from Module

Figure 5 - 5

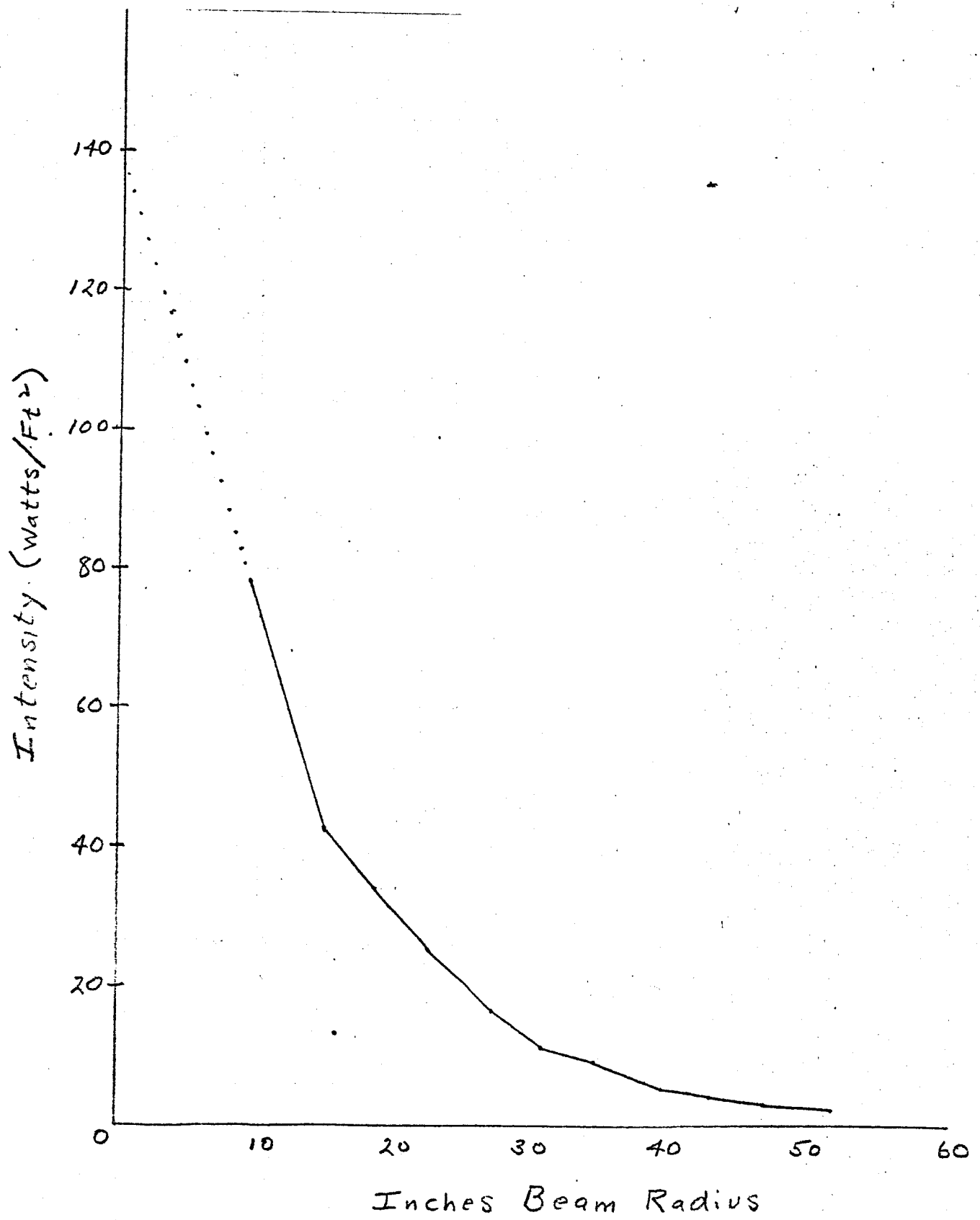


BY _____ DATE _____
CHKD. BY _____ DATE _____

SUBJECT Predicted Beam Irradiance
Cross-section - Reflectors Only
60 Feet From Module

SHEET NO. _____ OF _____
JOB NO. _____

Figure 3 - 27



BY _____ DATE _____

SUBJECT Predicted Angular Distribution SHEET NO. _____ OF _____

CD. BY _____ DATE _____

Total Modula-Reflectors Only JOB NO. _____

1000

Figure 3 - 26

900

800

700

600

500

400

300

200

100

0

Watts

θ Degrees-Half Angle

1

2

3

4

5

6

7

8

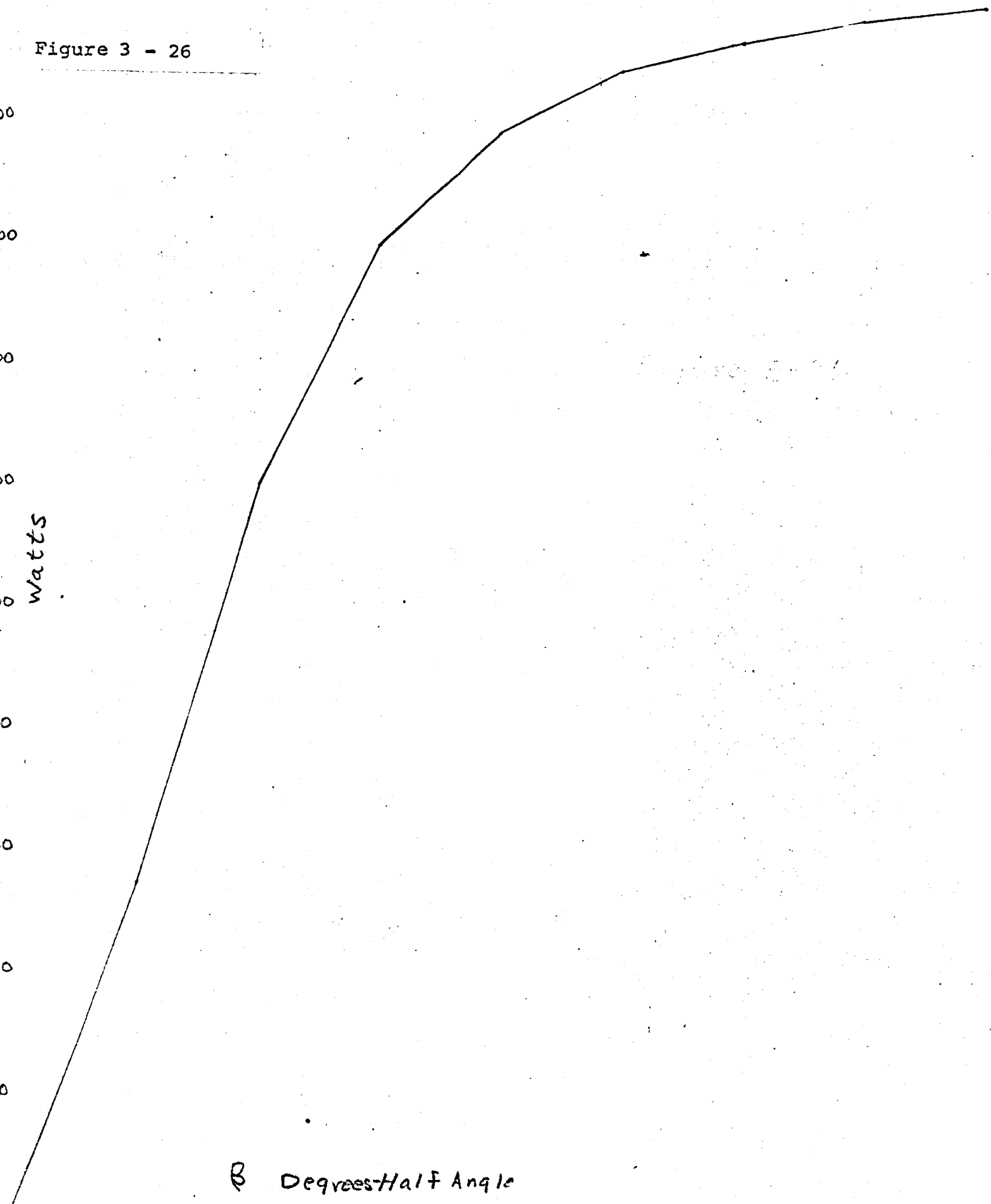
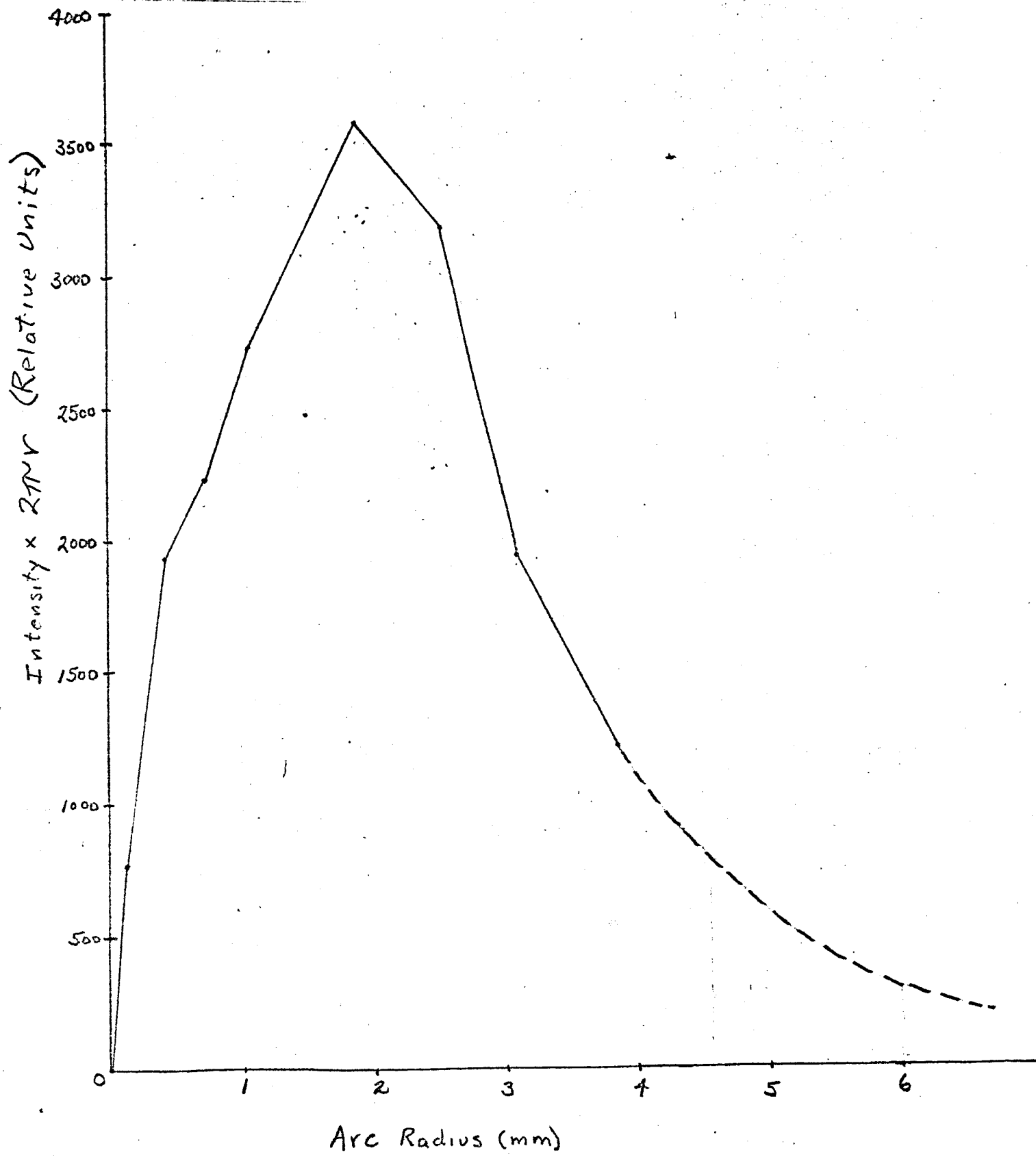
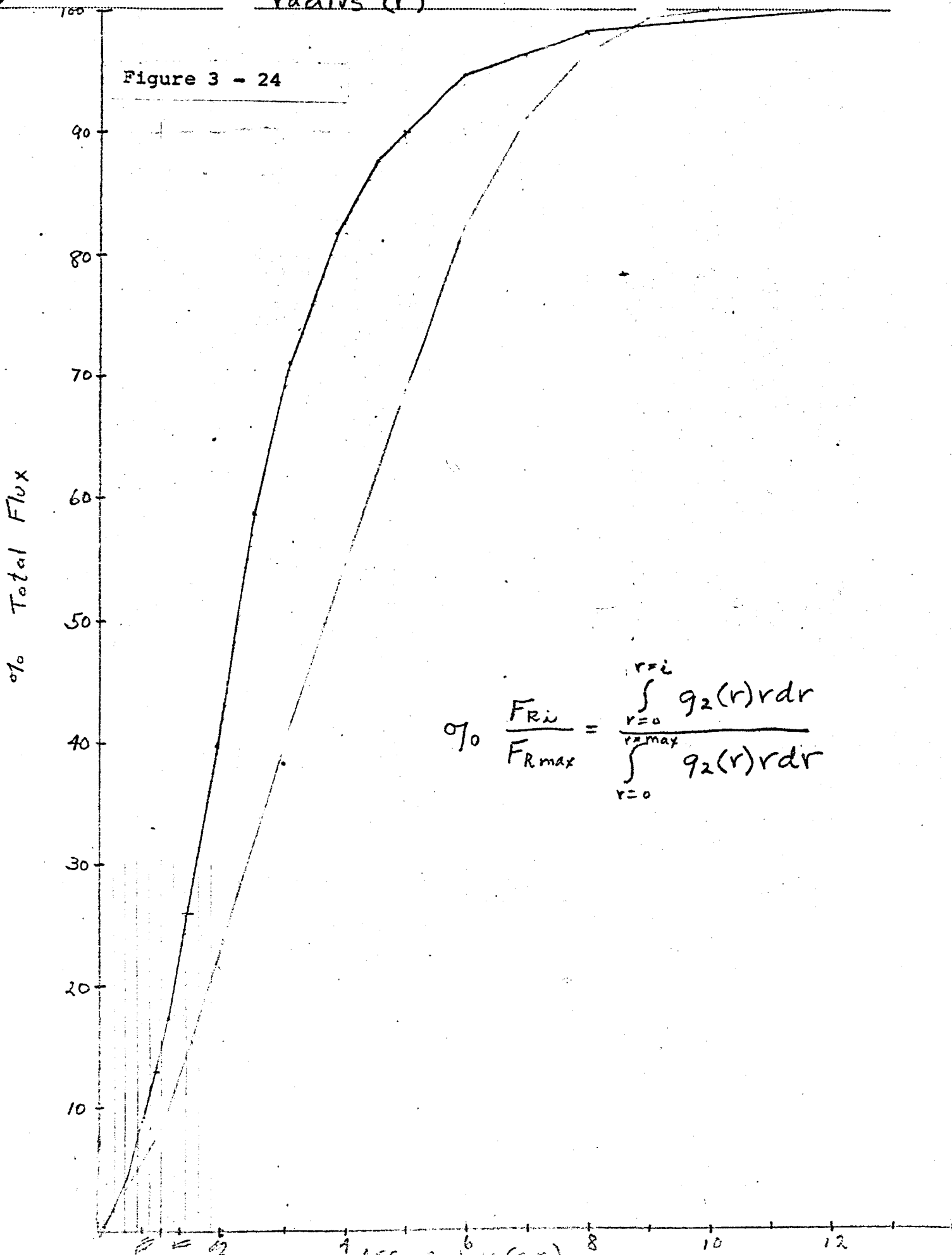


Figure 3 - 23

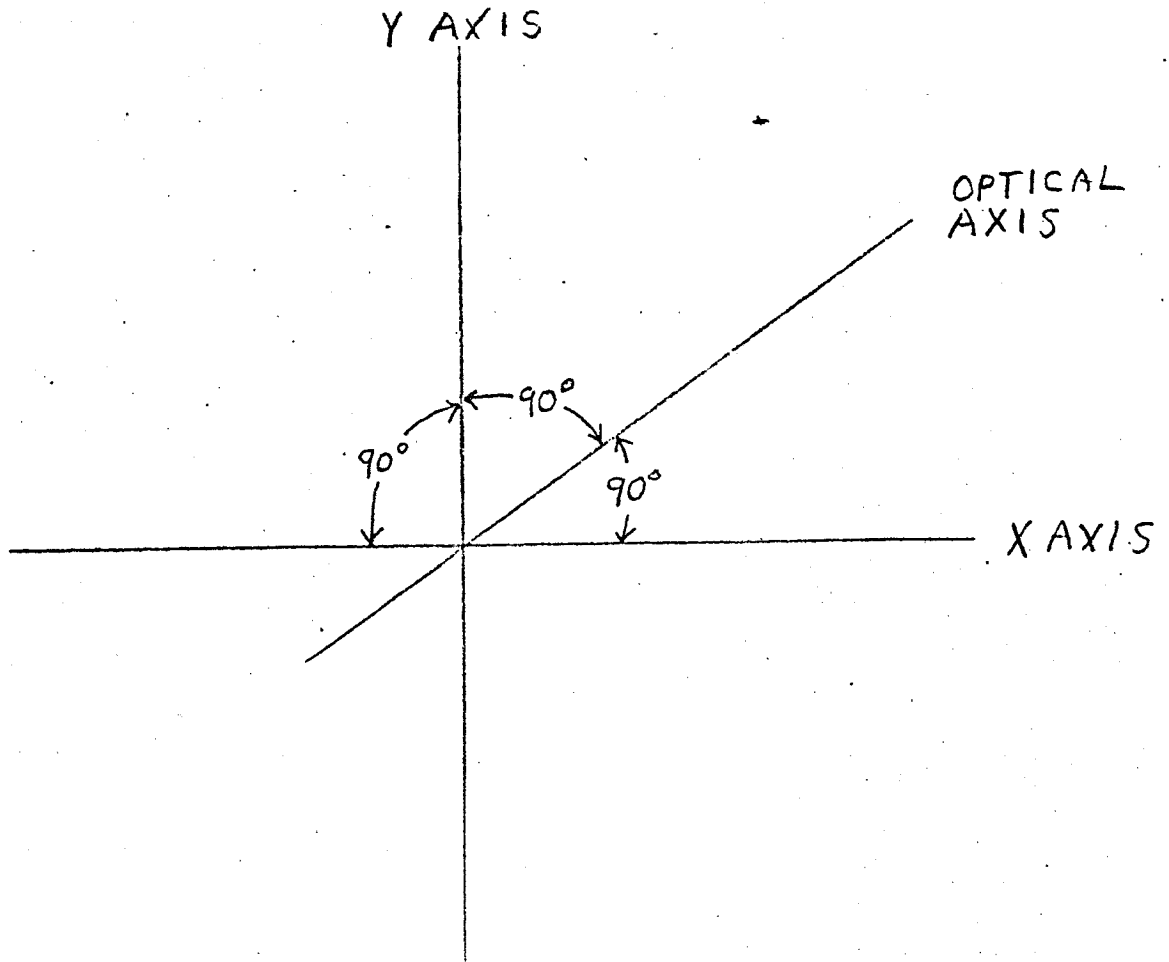




$$\% \frac{F_{Ri}}{F_{Rmax}} = \frac{\int_{r=0}^{r=i} q_2(r) r dr}{\int_{r=0}^{rmax} q_2(r) r dr}$$

X and Y Axes

Figure 4 - 4



FORM NO. 101

| DWG. SIZE | DATE | RUN No | PAGES | DESCRIPTION | BY | PAGE |
|-----------|-----------------|--------|-----------------|-------------|-----------|----------------------|
| | Figure 4 - 11 | | (617) | | T. Nelson | 617 |
| | X | R PV | V _{mV} | F | RF | |
| | 29 | 237 | 29 | | | |
| | 40 | 249 | 40 | | | |
| | 60 | | 50 | | | |
| | 80 | | 55 | | | |
| | 100 | | 72 | | | |
| | 120 | | 172 | | | |
| | 140 | | 516 | | | |
| | 150 | | 787 | | | |
| | 160 | | 1010 | | | |
| | 170 | 380 | 1162 | | | |
| | 180 | 390 | 1255 | | | |
| | 200 | | 1285 | | | |
| | 220 | | 1274 | | | |
| | 240 | | 1252 | | | |
| | 260 | | 1206 | | | |
| | 280 | | 1204 | | X | R PV V _{mV} |
| | 290 | 500 | 1206 | | 460 | 160 |
| | 300 | | 1204 | | 480 | 63 |
| | 320 | | 1264 | | 500 | 51.5 |
| | 340 | | 1290 | | 520 | 45 |
| | 360 | | 1302 | | 540 | 40.4 |
| | 380 | | 1298 | | 560 | 30.5 |
| | 400 | 609 | 1254 | | 580 | 790 16 |
| | 410 | 619 | 1150 | | 584 | 793 12 |
| | 430 | | 988 | | | |
| | 440 | | 413 | | | LENS #2 @ 16.9 |
| | APER. | 150 | V 56.5 | CENTER | | AMP GAIN 300 |
| | FILTER POSITION | 13 | A 46 | X 290 | | REFL 1, 2, 3, 5 |
| | Z | 30' | L 376 | Y 260 | | BULB @ 3.468 |

Table 3 - 1

TECHNICAL DATA FOR THE WESTINGHOUSE SAHX-2500F
MERCURY-XENON SHORT ARC LAMP

ORDERING ABBREVIATIONSAHX-2500F⁽¹⁾ELECTRICAL

| | |
|--|------------------------|
| Watts (lamp only) | 2500 |
| Starting Current | 65-80 Amperes, DC |
| Operating Current | 50 \pm 5 Amperes, DC |
| Operating Voltage | 50 \pm 5 |
| Ignition Voltage (short pulse-0.5 sec. max.) | 50,000 Volts, peak |
| Open Circuit Voltage (minimum) | 70 Volts, DC |

MECHANICAL

| | |
|---|---------------------|
| Max. Overall Length (not including flexible wire leads) | 13 inches (330 mm) |
| Max. Bulb Diameter | 2.68 inches (68 mm) |
| Electrical Terminals | Flexible wire leads |
| Arc Gap: Lamp Cold | 6.0 \pm .2 mm |

OPERATING REQUIREMENTS

| | |
|----------------------------------|---------------------------------|
| Operating Position | Vertical \pm 10° (anode down) |
| Max. Allowable Seal Temperature | 450°C ⁽²⁾ |
| Cooling (Under usual conditions) | Normal Convection |

PERFORMANCE

| | |
|--|----------------------------------|
| Initial Radiating Efficiency (Radiant Watts, 2000Å - 75,000 Å, from Arc Only) | 45% (approx.) |
| Maximum Brightness | 1050 c/mm ² (approx.) |
| Average Brightness (Measured along centerline of arc between Cathode and Anode) | 500 c/mm ² (approx.) |
| Rated Average Life (@ 8 hours per start) | 400(3) |
| Output Maintenance at 400 hours | 70% (min) (4) |

FOOTNOTES:

- (1) The SAHX-2500C differs from the SAHX-2500F only in that it has two mounting collars whereas the latter has none.
- (2) Temperature measured at the junction of the quartz glass and the graded glass seal.
- (3) Tentative - Subject to further tests.
- (4) Values up to 85% have been obtained during limited tests to date.

SECRET

THE EPPLEY LABORATORY, INC.

SCIENTIFIC INSTRUMENTS

NEWPORT, R. I.

U.S.A.

Table 4 - 2

FILTER FACTORS
AND
FILTER LOCATION

Instrument Model Mk 4

Filter Wheel Marking A-6

| Position | Wavelength Limits | Reference Wavelength | Filter Factors Source Mercury-Xenon |
|----------|-------------------|----------------------|-------------------------------------|
| 1 | 265- 298 | 270 | 10.40 |
| 2 | 276- 318 | 292 | 9.75 |
| 3 | 295- 332 | 312 | 6.08 |
| 4 | 323- 352 | 335 | 5.57 |
| 5 | 350- 384 | 365 | 3.58 |
| 6 | 386- 423 | 405 | 3.39 |
| 7 | 415- 460 | 435 | 2.27 |
| 8 | 515- 573 | 550 | 1.64 |
| 9 | 555- 600 | 580 | 1.91 |
| 10 | 600- 800 | 700 | 3.69 |
| 11 | 800-1300 | 1000 | 1.89 |
| 12 | 1100-1900 | 1500 | 2.46 |
| 13 | Blank | | |

Filter wheel is advanced by rotating in a counterclockwise direction as viewed from top.

Date of Test: 23 November 1964

IN CHARGE OF TEST

The Eppley Laboratory, Inc.

F. J. Griffin
F. J. Griffin
Senior Scientific Assistant

By: *W. J. Scholes*
W. J. Scholes
Supervising Physicist
Newport, R. I.

Shipped to: Linear Inc.
823 Emerson
Evanston, Ill.
60201

Date: 25 November 1964 S.O. 12085



THE EPPLEY LABORATORY, INC.

SCIENTIFIC INSTRUMENTS

NEWPORT, R.I.

U.S.A.

**FILTER FACTORS
AND
FILTER LOCATION**

Instrument Model Mk III Filter Wheel Marking -

| Position | Wavelength Limits | Reference Wavelength | Filter Factors | |
|----------|-------------------|----------------------|-----------------|----------|
| | | | Source | Hg Xenon |
| 1 | 1500-2250 mμ | 1850 mμ | 2.84 | (B-12) |
| 2 | 1850-2400 | 2100 | 2.11 | (C-12) |
| 3 | 2300-2800 | 2550 | 4.92 | (D-12) |
| 4 | RG8 | Cutoff 687 | 1.11 | |
| 5 | UG11 265-384 mμ | 325 | 1.53 | 1.90 |
| 6 | | | | |
| 7 | | | | |
| 8 | | | | |
| 9 | | | | |
| 10 | | | | |
| 11 | | | | |
| 12 | | | | |
| 13 | | | | |

Filter wheel is advanced by rotating in a - direction as viewed from top.

Date of Test: 15 March 1965

IN CHARGE OF TEST:

The Eppley Laboratory, Inc.

By: *W. J. Scholes*
W. J. Scholes
Supervising Physicist
Newport, R. I.

F. J. Griffin
F. J. Griffin
Senior Scientific Assistant

Shipped to: Linear Inc.
823 Emerson
Evanston, Ill.
60201

Date: 15 March 1965

S.O.13082

Table 5 - 1

Beam Intensity Pattern—Reflectors Only

| Radius (Inches) | Watts Per Square Foot | | | Relative Intensity | | |
|--------------------|-----------------------|--------|--------|--------------------|--------|--------|
| | 15 ft. (a) | 30 ft. | 60 ft. | 15 ft. (a) | 30 ft. | 60 ft. |
| 0 | 852 | 331 | 96 | 100 | 100 | 100 |
| 2 | 696 | - | - | 82 | | |
| 3 | - | 244 | - | | 74 | |
| 4 | 539 | - | - | 63 | | |
| 6 | 383 | 164 | 64 | 45 | 49 | 67 |
| 8 | 234 | - | - | 27 | | |
| 9 | - | 129 | - | | 39 | |
| 10 | 152 | - | - | 18 | | |
| 12 | 100 | 97 | 45 | 12 | 29 | 47 |
| 14 | 54 | - | - | 6 | | |
| 15 | - | 52 | - | | 16 | |
| 16 | 40 | - | - | 5 | | |
| 18 | 29 | 30 | 33 | 3 | 9 | 34 |
| 20 | 21 | - | - | 3 | | |
| 21 | - | 21 | - | | 6 | |
| 22 | 15 | - | - | 2 | | |
| 24 | 9 | 16 | 18 | 1 | 5 | 19 |
| 27 | 3 | 13 | - | | 4 | |
| 30 | 1 | 11 | 10 | | 3 | 11 |
| 33 | | 9 | - | | 3 | |
| 36 | | 8 | 7 | | 2 | 7 |
| 42 | | 3 | 4 | | 1 | 5 |
| 48 | | | 3 | | | 4 |
| 54 | | | 3 | | | 3 |
| 60 | | | 2 | | | 2 |
| 66 | | | 1 | | | 1 |

(a) Measurements in feet indicate distance from module.

Table 5 - 2

Beam Intensity Pattern—Two Lens Plates

| Radius (Inches) | Watts Per Square Foot | | | Relative Intensity | | |
|--------------------|-----------------------|--------|--------|--------------------|--------|--------|
| | 15 ft. (a) | 30 ft. | 60 ft. | 15 ft. (a) | 30 ft. | 60 ft. |
| 0 | 324 | 86 | 23 | 100 | 100 | 100 |
| 2 | 334 | - | - | 103 | | |
| 3 | - | 88 | - | | 101 | |
| 4 | 325 | - | - | 100 | | |
| 6 | 239 | 85 | 22 | 74 | 98 | 96 |
| 8 | 187 | - | - | 58 | | |
| 9 | - | 84 | - | | 97 | |
| 10 | 119 | - | - | 37 | | |
| 12 | 80 | 83 | 21 | 25 | 96 | 93 |
| 14 | 49 | - | - | 15 | | |
| 15 | - | 69 | - | | 79 | |
| 16 | 28 | - | - | 9 | | |
| 18 | 14 | 46 | 21 | 4 | 53 | 93 |
| 20 | 11 | - | - | 3 | | |
| 21 | - | 28 | - | | 32 | |
| 22 | 8 | - | - | 2 | | |
| 24 | 4 | 12 | 21 | 1 | 14 | 93 |
| 27 | 2 | 4 | - | | 5 | |
| 30 | - | 4 | 21 | | 4 | 94 |
| 33 | - | 4 | - | | 4 | |
| 36 | - | 3 | 15 | | 4 | 68 |
| 42 | - | 2 | 4 | | 2 | 17 |
| 48 | - | - | 1 | | | 2 |
| 54 | - | - | - | | | |
| 60 | - | - | - | | | |
| 66 | - | - | - | | | |

(a) Measurements in feet indicate distance from module.

Table 5 - 3

Beam Intensity Pattern—One Lens Plate

| Radius (inches) | Watts Per Square Foot | | | Relative Intensity | | |
|--------------------|-----------------------|--------|--------|--------------------|--------|--------|
| | 15 ft. (a) | 30 ft. | 60 ft. | 15 ft. (a) | 30 ft. | 60 ft. |
| 0 | 211 | 66 | 19 | 100 | 100 | 100 |
| 2 | 202 | - | - | 96 | | |
| 3 | - | 65 | - | | 99 | |
| 4 | 184 | - | - | 87 | | |
| 6 | 163 | 63 | 18 | 77 | 95 | 99 |
| 8 | 141 | - | - | 67 | | |
| 9 | - | 59 | - | | 90 | |
| 10 | 113 | - | - | 54 | | |
| 12 | 87 | 53 | 17 | 41 | 80 | 94 |
| 14 | 65 | - | - | 31 | | |
| 15 | - | 45 | - | | 69 | |
| 16 | 47 | - | - | 22 | | |
| 18 | 30 | 38 | 16 | 14 | 58 | 86 |
| 20 | 17 | - | - | 8 | | |
| 21 | - | 32 | - | | 48 | |
| 22 | 9 | - | - | 4 | | |
| 24 | 5 | 25 | 14 | 2 | 38 | 76 |
| 27 | 1 | 19 | - | 1 | 29 | |
| 30 | - | 14 | 12 | | 22 | 65 |
| 33 | - | 11 | - | | 16 | |
| 36 | - | 8 | 10 | | 11 | 54 |
| 42 | - | 3 | 8 | | 5 | 42 |
| 48 | - | 1 | 6 | | 1 | 31 |
| 54 | - | - | 4 | | | 21 |
| 60 | - | - | 2 | | | 11 |
| 66 | - | - | - | | | 2 |

(a) Measurements in feet indicate distance from module.

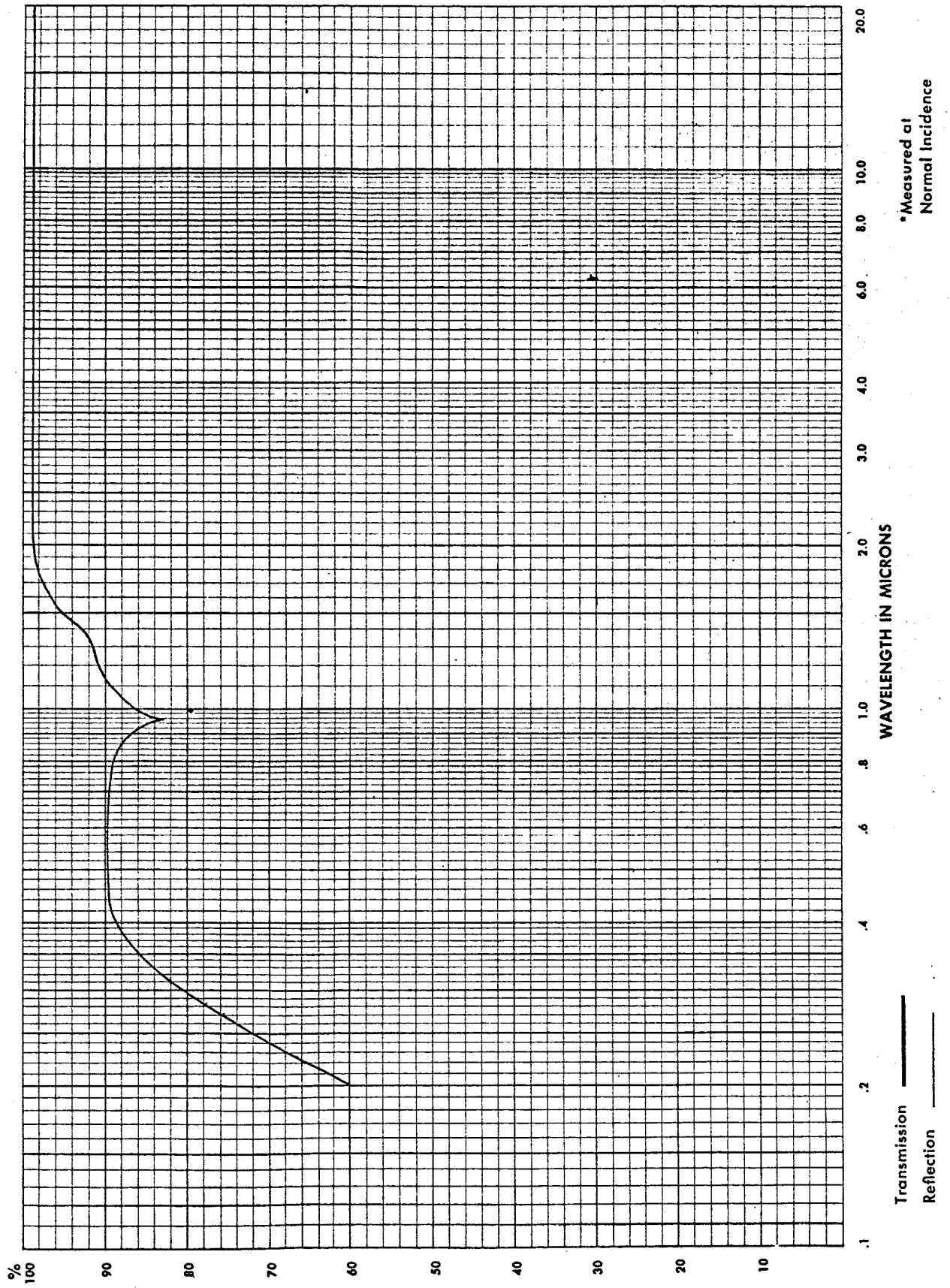
TABLE 6--1

APPROXIMATE CHARACTERISTICS OF REPRESENTATIVE MODULE ADAPTATIONS

| Adpt. No. | Lent. Plates | Inches Diam. | Source* | Degrees β 90 | Degrees β max | Watts Output | Arrays Possib. | Inches center to center distance | Solar constants on stated centers |
|-----------|--------------|--------------|---------|--------------------|---------------------|--------------|----------------|----------------------------------|-----------------------------------|
| 1 | 2 | 15 | W2500 | 2.85 | 3.0 | 514 | 3 | 27 | .90 |
| 2 | 2 | 17 | W2500 | 2.85 | 3.0 | 528 | 2 | 17 | 1.01 |
| 3 | 2 | 15 | W2500 | 3.79 | 4.0 | 618 | 3 | 27 | 1.08 |
| 4 | 2 | 15 | W2500 | 4.74 | 5.0 | 672 | 3 | 27 | 1.17 |
| 5 | 1 | 15 | W2500 | 3.00 | 6.0 | 574 | 3 | 27 | 1.01 |
| 6 | 1 | 15 | W2500 | 4.00 | 7.0 | 690 | 3 | 27 | 1.21 |
| 7 | 1 | 15 | W2500 | 5.00 | 7.5 | 750 | 3 | 27 | 1.32 |
| 8 | 1 | 15 | 0-2500 | 3.00 | 6.0 | 709 | 3 | 27 | 1.24 |
| 9 | 2 | 15 | 0-2500 | 2.85 | 3.0 | 635 | 3 | 27 | 1.11 |
| 10 | 2 | 24 | 0-6500 | 2.85 | 3.0 | 1656 | 3 | 42 | 1.23 |
| 11 | 1 | 24 | 0-6500 | 3.00 | 6.0 | 1849 | 3 | 42 | 1.37 |
| 12 | 1 | 26 | 0-6500 | 4.20 | 6.5 | 2185 | 3 | 46 | 1.32 |
| 13 | 2 | 27 | W-2500 | 2.85 | 3.0 | 693 | 1 | 27 | 1.22 |
| 14 | 1 | 27 | W-2500 | 3.00 | 6.0 | 774 | 1 | 27 | 1.36 |

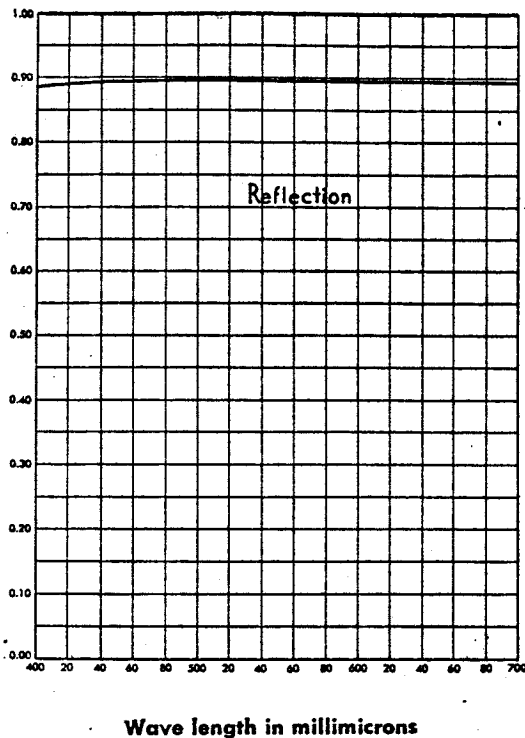
* In source designation W-2500 is the source used in this program - the Westinghouse SAHX2500F Hg-Xe lamp. 0-lamps are Osram Xe and the numbers designate the wattage. All calculations on Osram lamps are based on arc size from arc isobrightness data as compared to arc isobrightness data on the 2500F lamp used in this program.

Front Surface Aluminum Mirror No. 747



Front Surface Aluminum Mirror No. 747

Spectrophotometric curve shown in the visible region is measured at normal incidence.



*When the coated element is used at angles other than normal, curve peaks will shift toward shorter wave lengths (down scale). This variation is dependent on degree of angularity from normal incidence.

SPECIFICATION No. 1050

Reflectivity

The mirror shall have not less than 88% total reflectivity for light in the visible region as measured with a Weston photronic cell with a Viscor filter and a tungsten lamp supplying light at an angle of incidence of 22.5°. The coating has high reflectivity in the ultra-violet region.

Adherence

No visible part of the mirror coating shall be removed by the cellulose tape test described here:

Test: The tacky surface of cellulose tape shall be carefully placed in contact with a portion of the mirror surface and firmly rubbed against that surface. It shall then be quickly removed with a snap action which exerts the greatest possible stripping action on the mirror film.

Hardness

No evidence of film removal or film abrasion shall be visible to the eye when the following test is applied:

Test: A pad of clean dry cheese cloth (previously laundered) $\frac{3}{8}$ inch in diameter, $\frac{1}{2}$ inch thick, bearing with a force of one pound on the coating shall be rubbed across the coated element in any direction 25 times.

Note: During the above test, care should be exercised to prevent contaminating abrasives contacting the coated surface causing slight streaks.

Corrosion Resistance

There shall be no noticeable deterioration of the finished mirror when given the salt atmosphere test described here:

Test: The mirror shall be placed in a thermostatically controlled cabinet with a salt atmosphere for 24 continuous hours at a temperature of 95°F. The salt atmosphere shall be obtained by allowing a stream of air to bubble through a salt solution containing $1\frac{1}{2}$ pounds of sodium chloride per cubic foot of water.

Effect of Temperature

The coating shall function satisfactorily and shall not be damaged by exposure to an ambient temperature of minus 60°F and plus 500°F.

SECRET

THE EPPLEY LABORATORY, INC.
SCIENTIFIC INSTRUMENTS
NEWPORT, R.I.
U.S.A.

Figure 4 - 2

STANDARDIZATION
OF
EPPLEY RADIOMETER FOR USE AT
HIGH RADIANT FLUX DENSITIES IN VACUUM SYSTEMS

(incorporating a temperature compensating thermistor circuit)

Model Mk III Serial No.: 6897-D Resistance 350 ohms at 25 °C

This radiometer has been compared with the Eppley group of reference standards, at a radiation intensity of (approximately)

76 w ft⁻² and at an average temperature of 20 °C.

As a result of this comparison, the enclosed calibration curves were derived.

The vacuum curve is applicable at ambient pressures of 10⁻⁴ mm Hg and below.

The circuitry of the temperature compensator has been adjusted to afford best compensation over a range of ambient temperature of +10 to +50° C.

Date of Test: 20 November 1964

IN CHARGE OF TEST

F. J. Griffin
F. J. Griffin

Senior Scientific Assistant

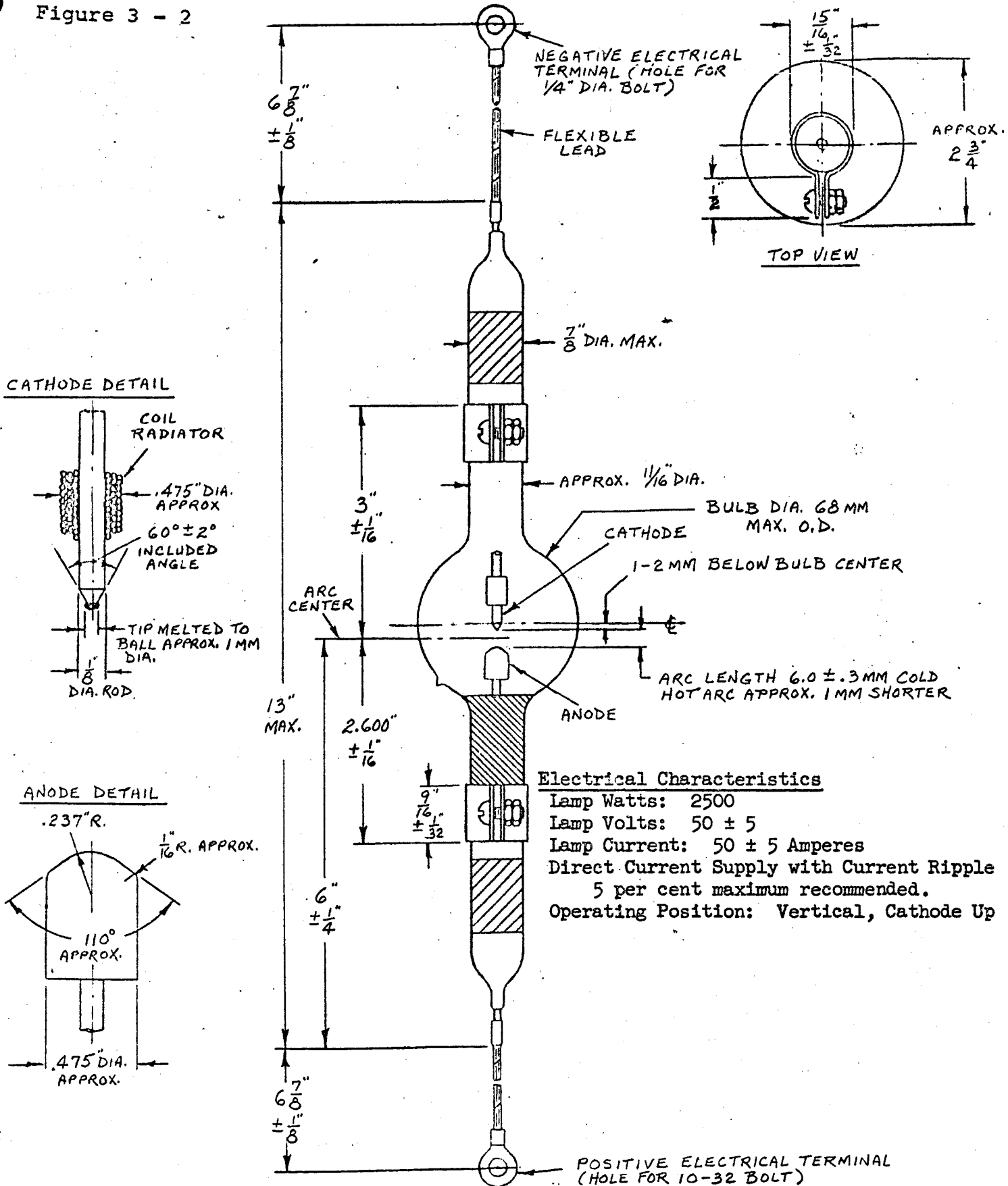
The Eppley Laboratory, Inc.

By: W. J. Scholes *W. J. Scholes*
Supervising Physicist
Newport, R. I.

Shipped to: Linear Inc.
823 Emerson
Evanston, Ill.
60201

Date: 25 November 1964 S.O. 12083

Figure 3 - 2



WESTINGHOUSE ELECTRIC CORP.
 SAHX-2500-C Mercury-Xenon Lamp

Date: 11/13/63

POLAR RADIATION DIAGRAM
of an SAHX-2500F Mercury-Xenon Lamp

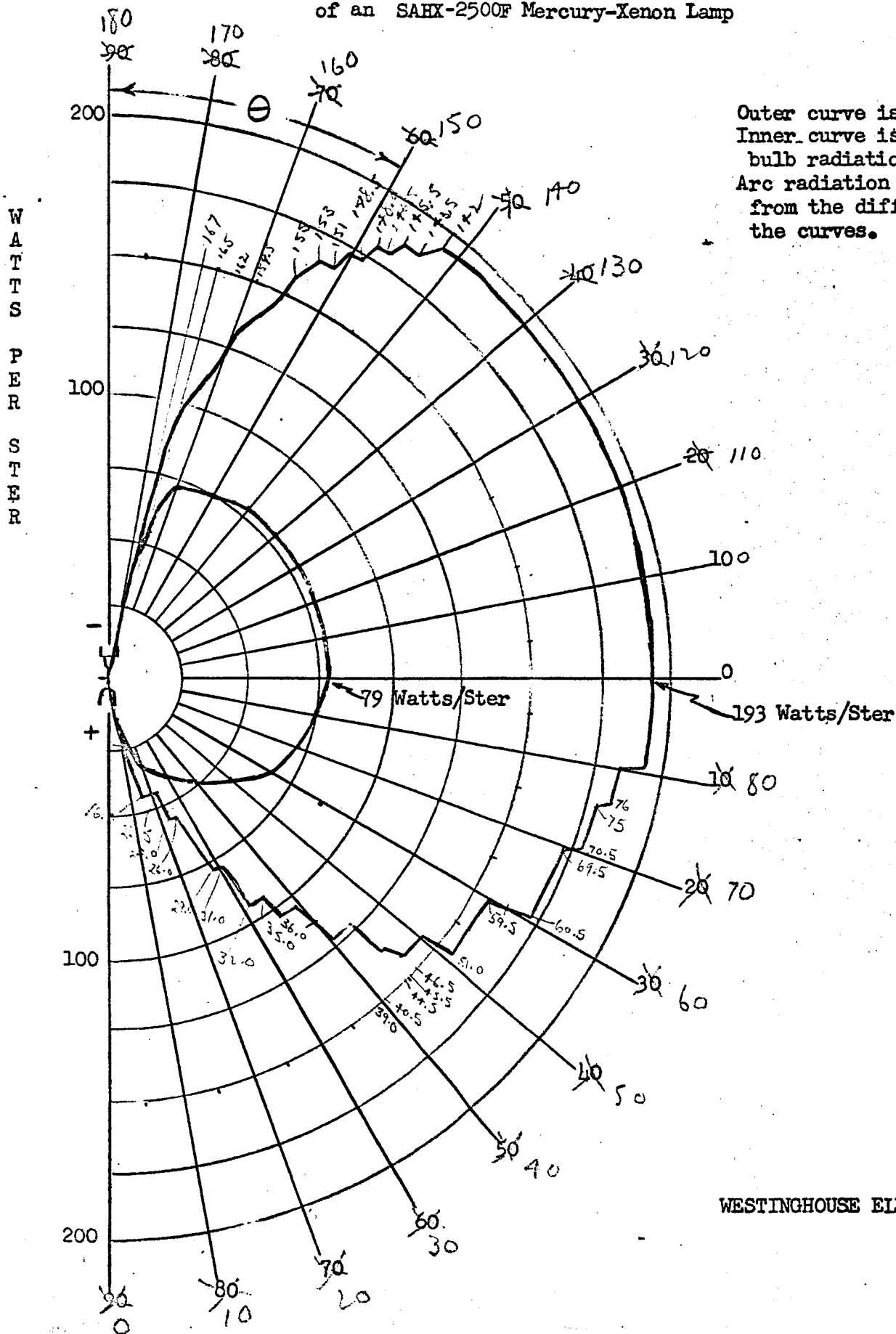
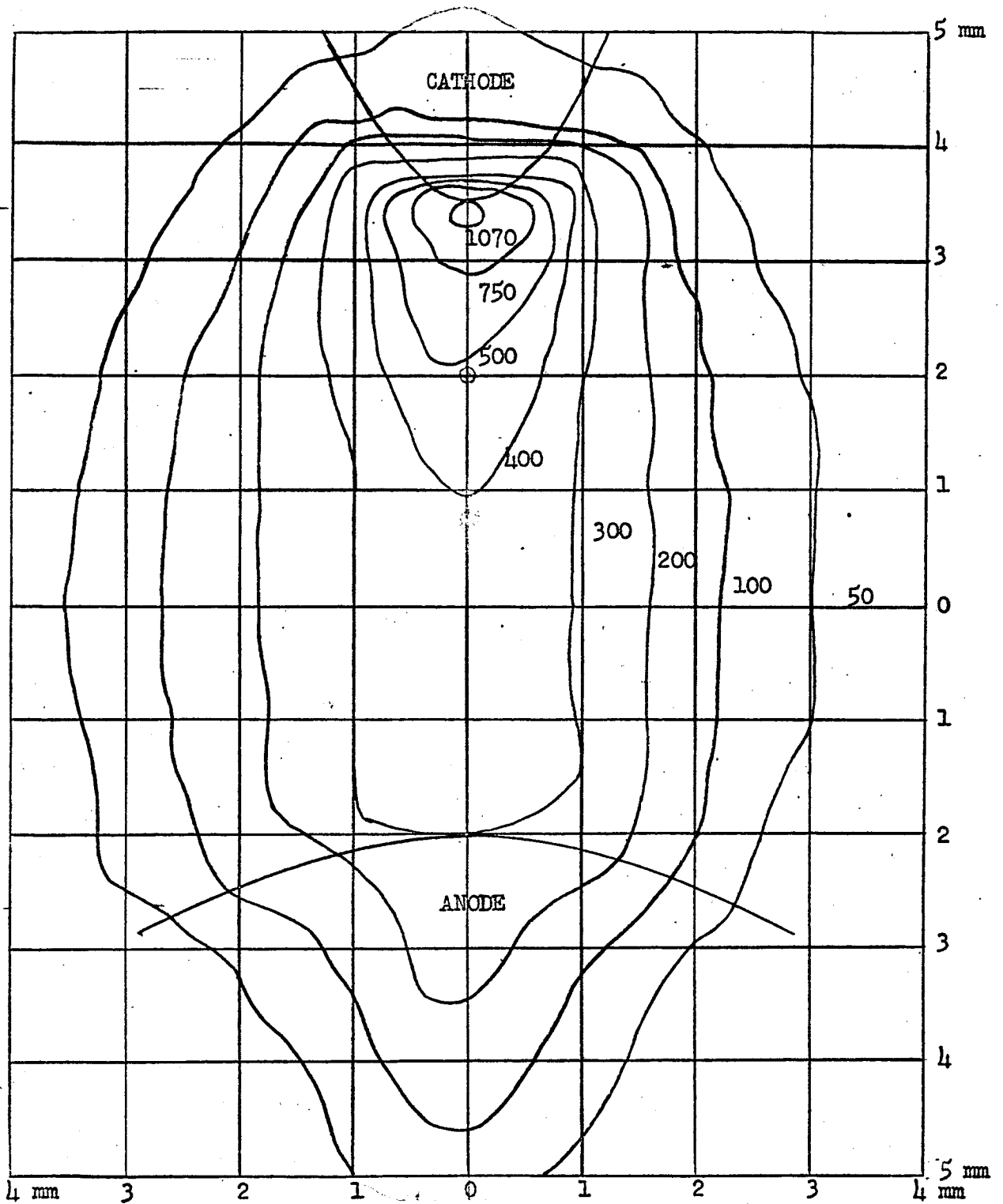


Figure 3 - 4



ISO - BRIGHTNESS CONTOUR LINES FOR A SAHX-2500F
MERCURY-XENON LAMP ARC
(candles/mm²)

Figure 4 - 10 Actual Data Plot Sample

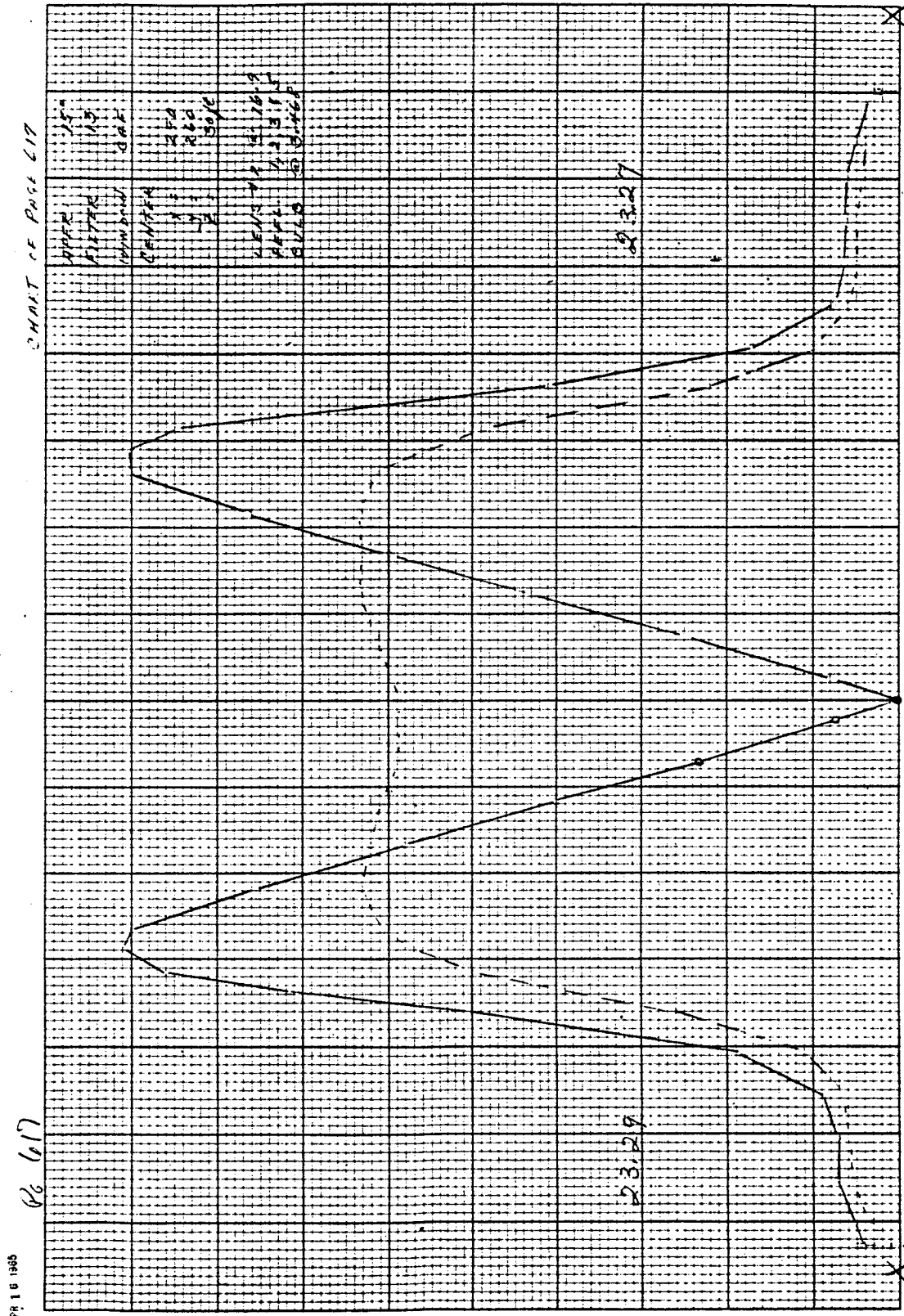


Figure 5 - 14 Spectral Beam Pattern and Deviation—One Lens Plate

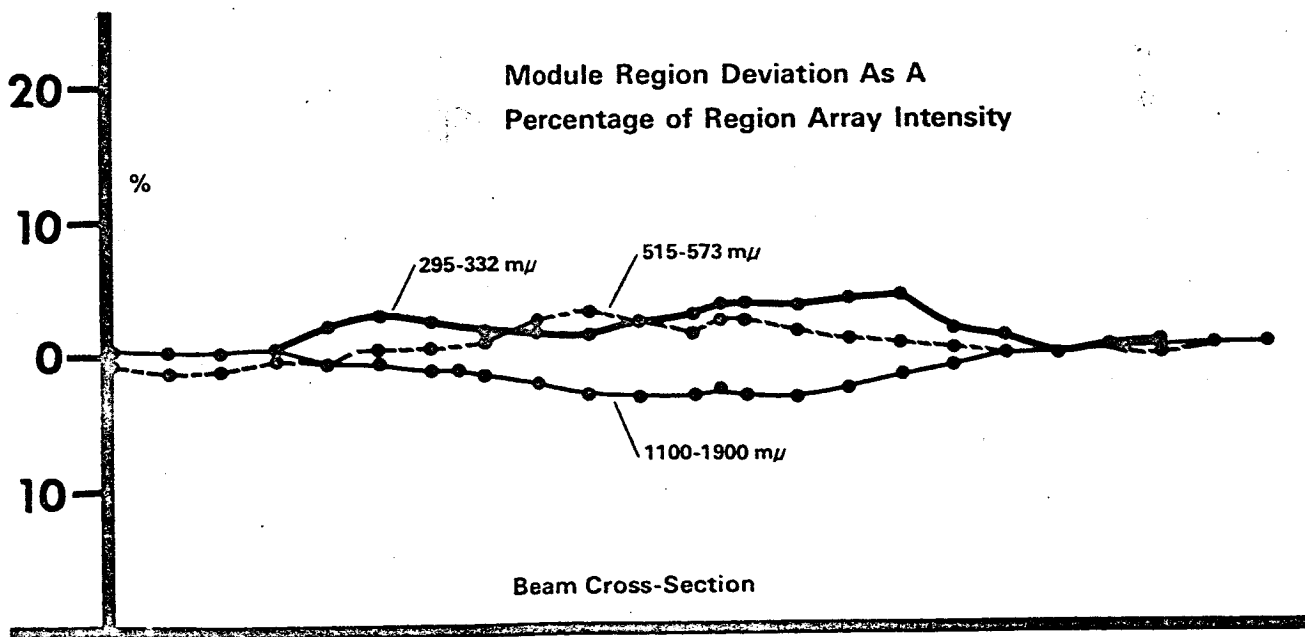
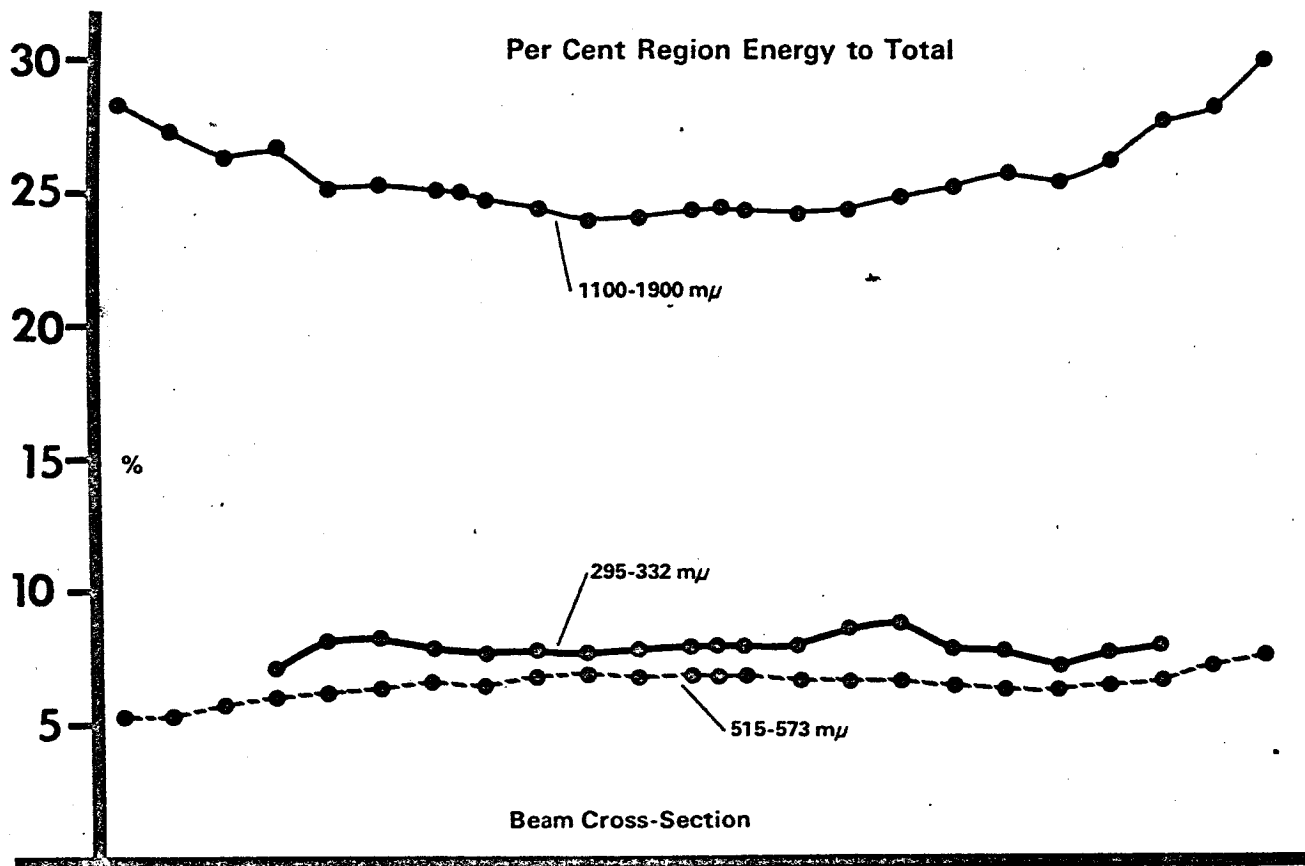


Figure 5 - 12 Spectral Beam Pattern and Deviation—Two Lens Plates

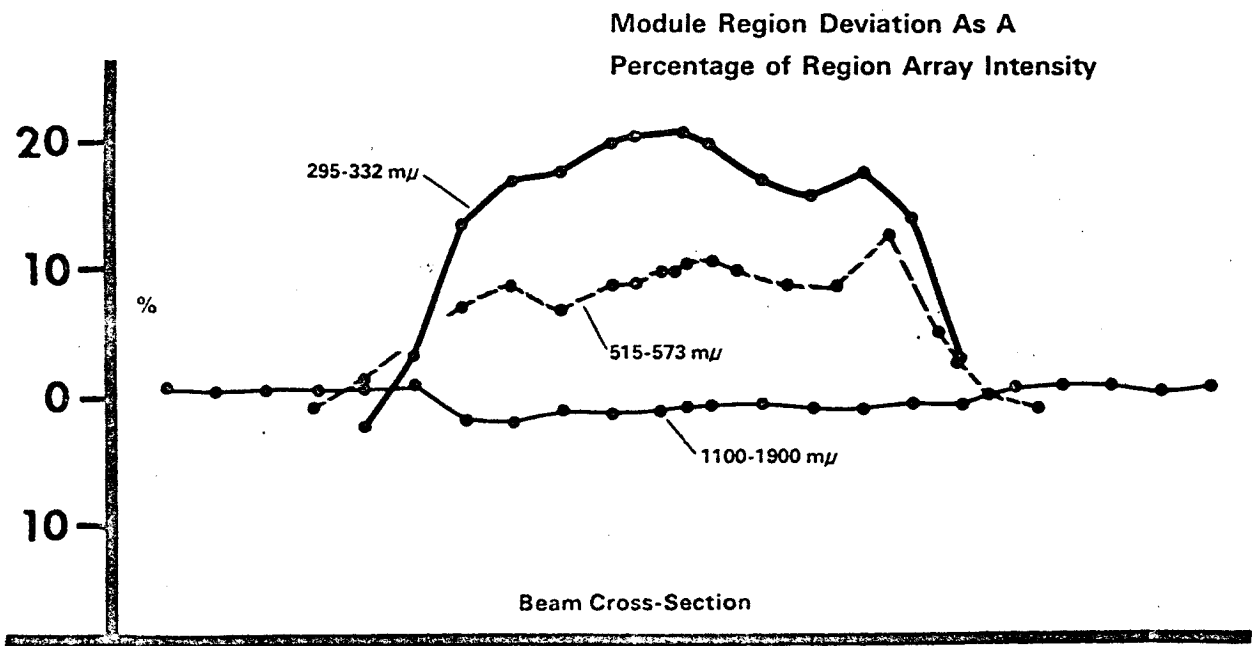
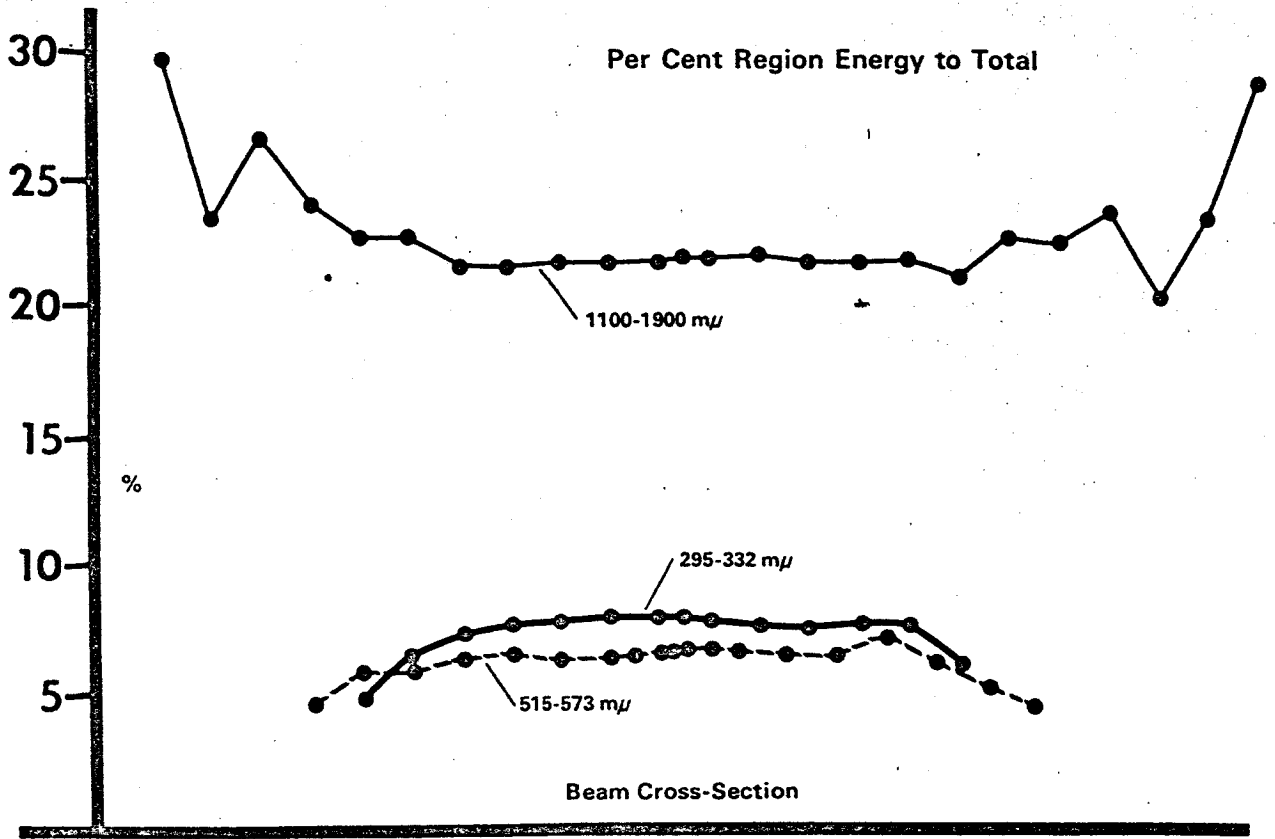


Figure 5 - 6 Spectral Beam Pattern and Deviation—Reflectors Only

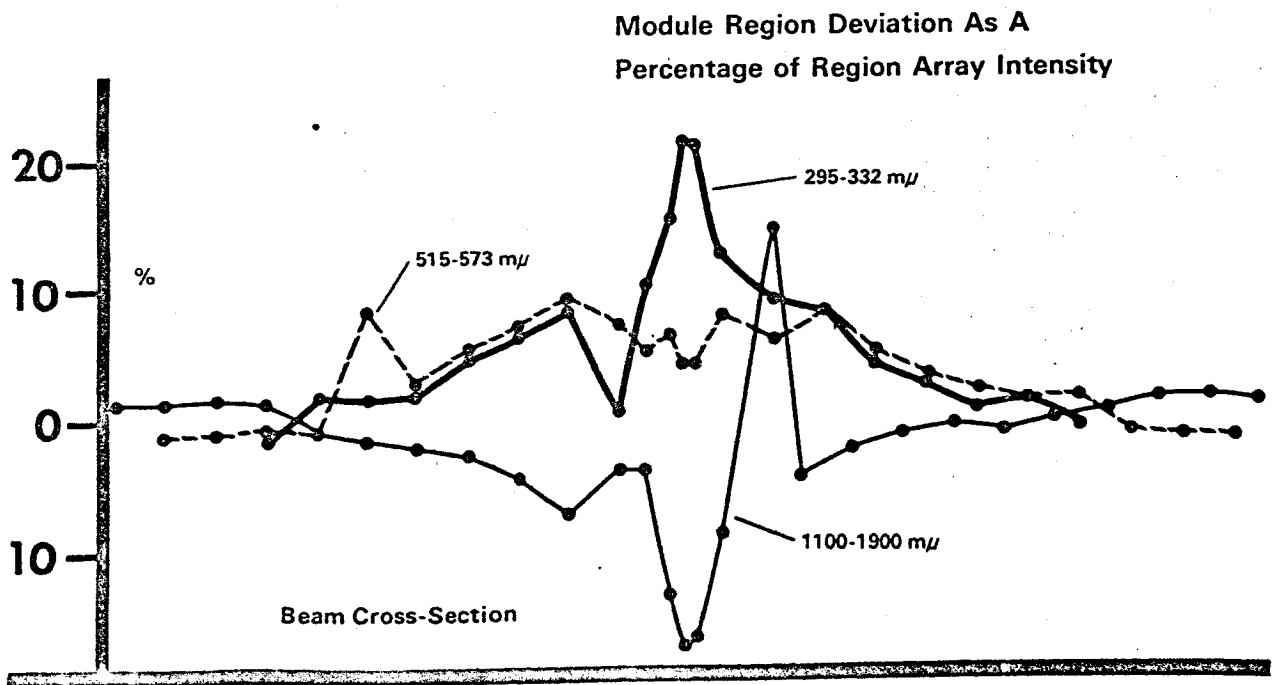
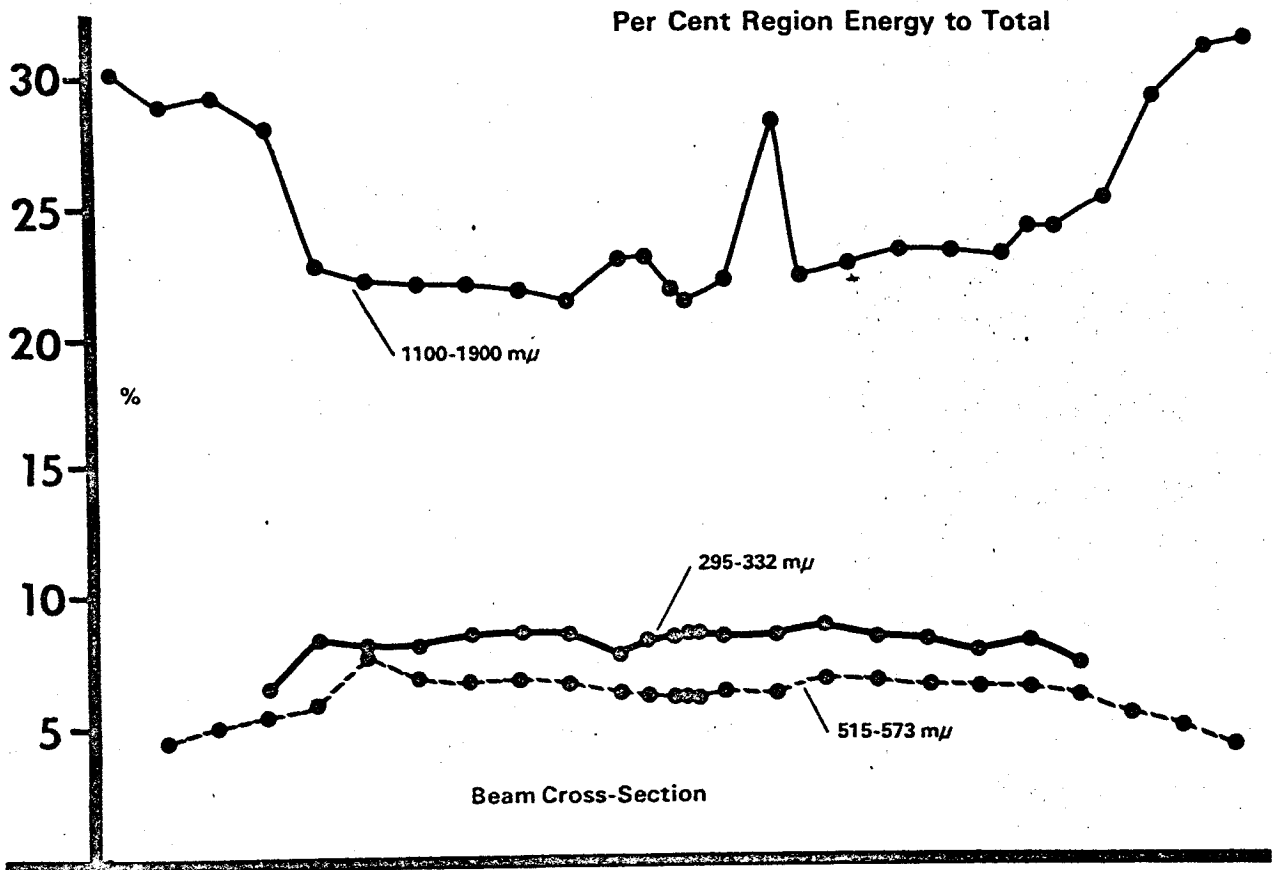


Figure 5 - 7 Beam Intensity Pattern—One Lens Plate

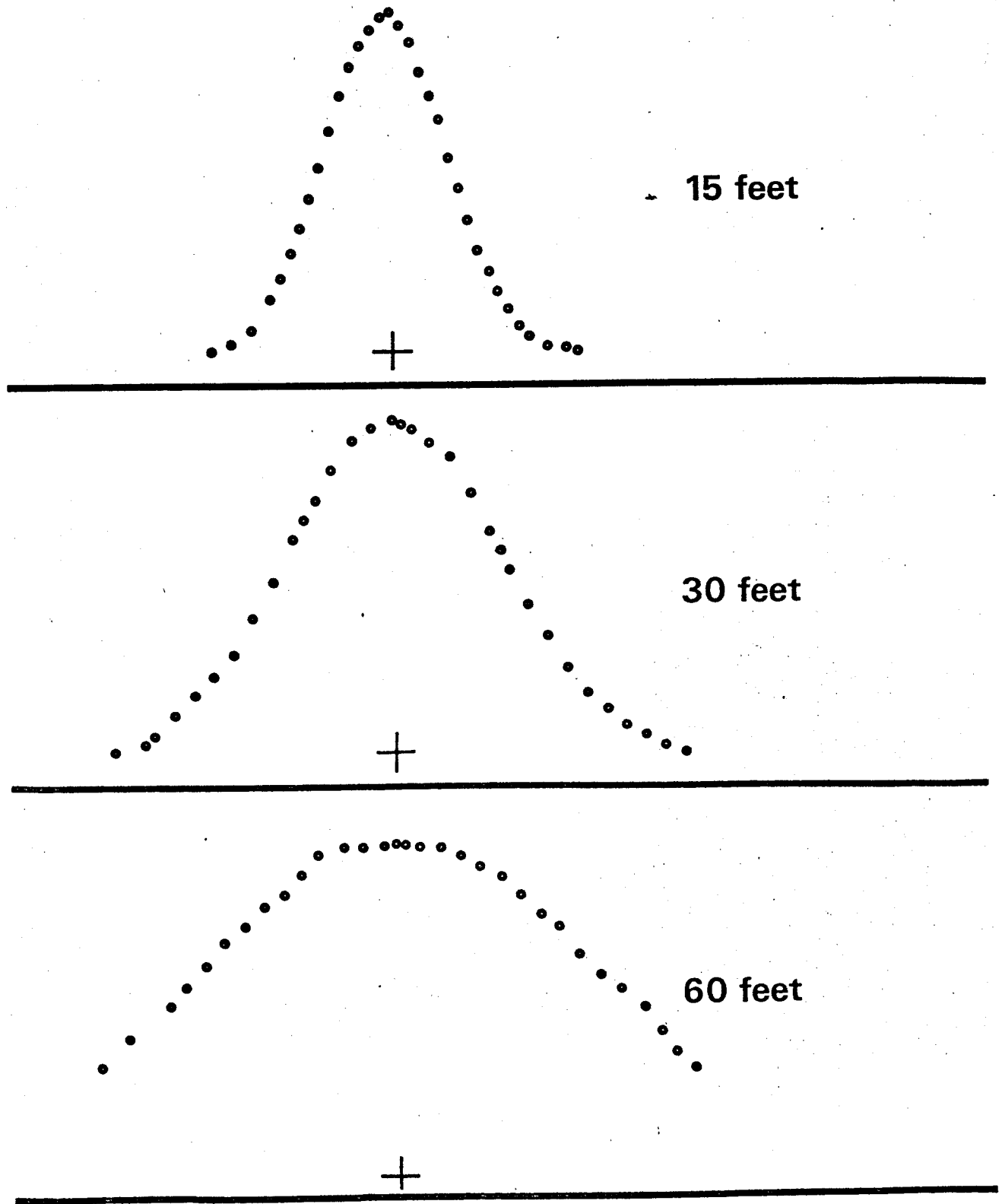


Figure 5 - 9 Beam Intensity Pattern—Two Lens Plates

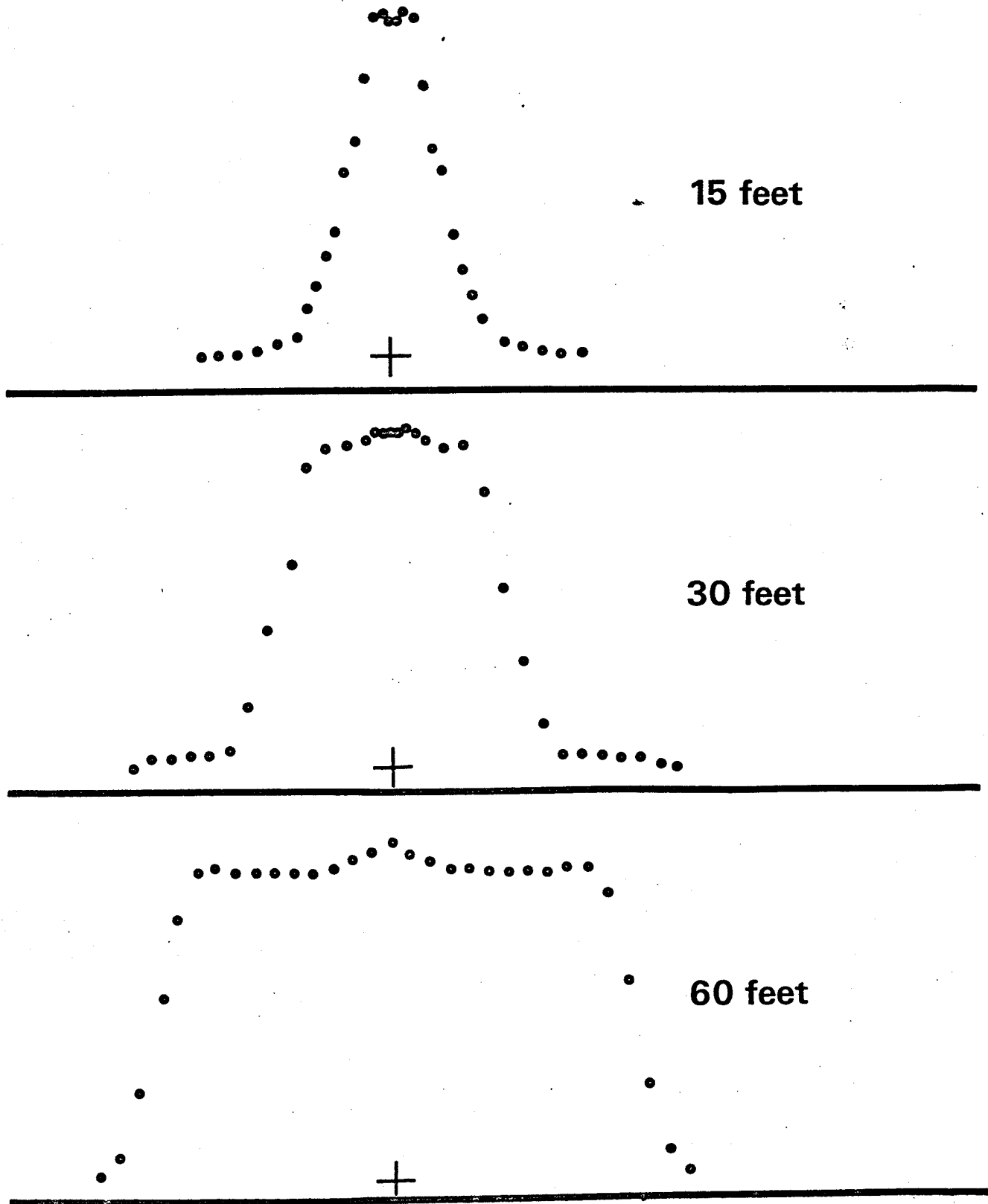


Figure 5 - 4 Beam Intensity Pattern—Reflectors Only

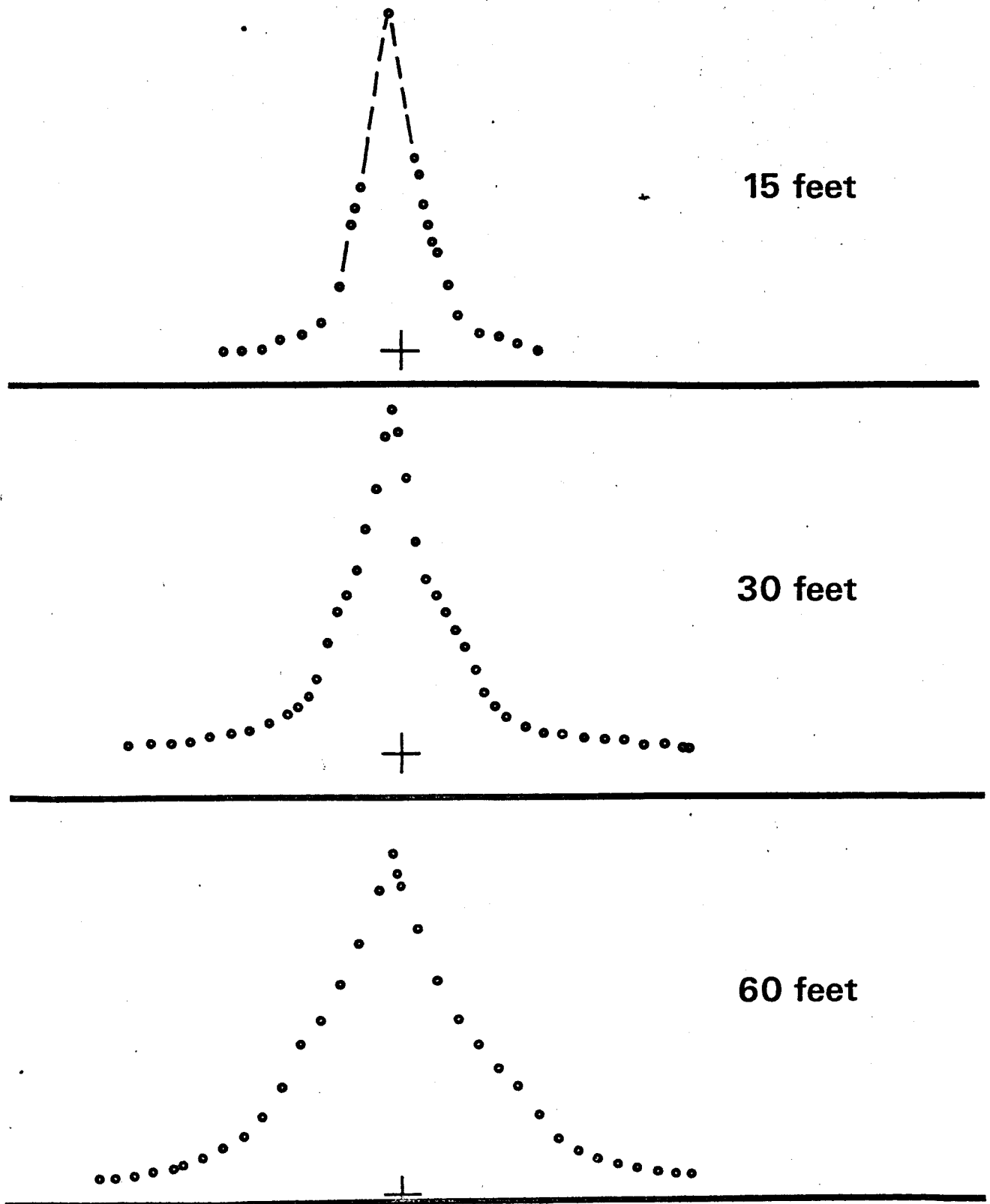
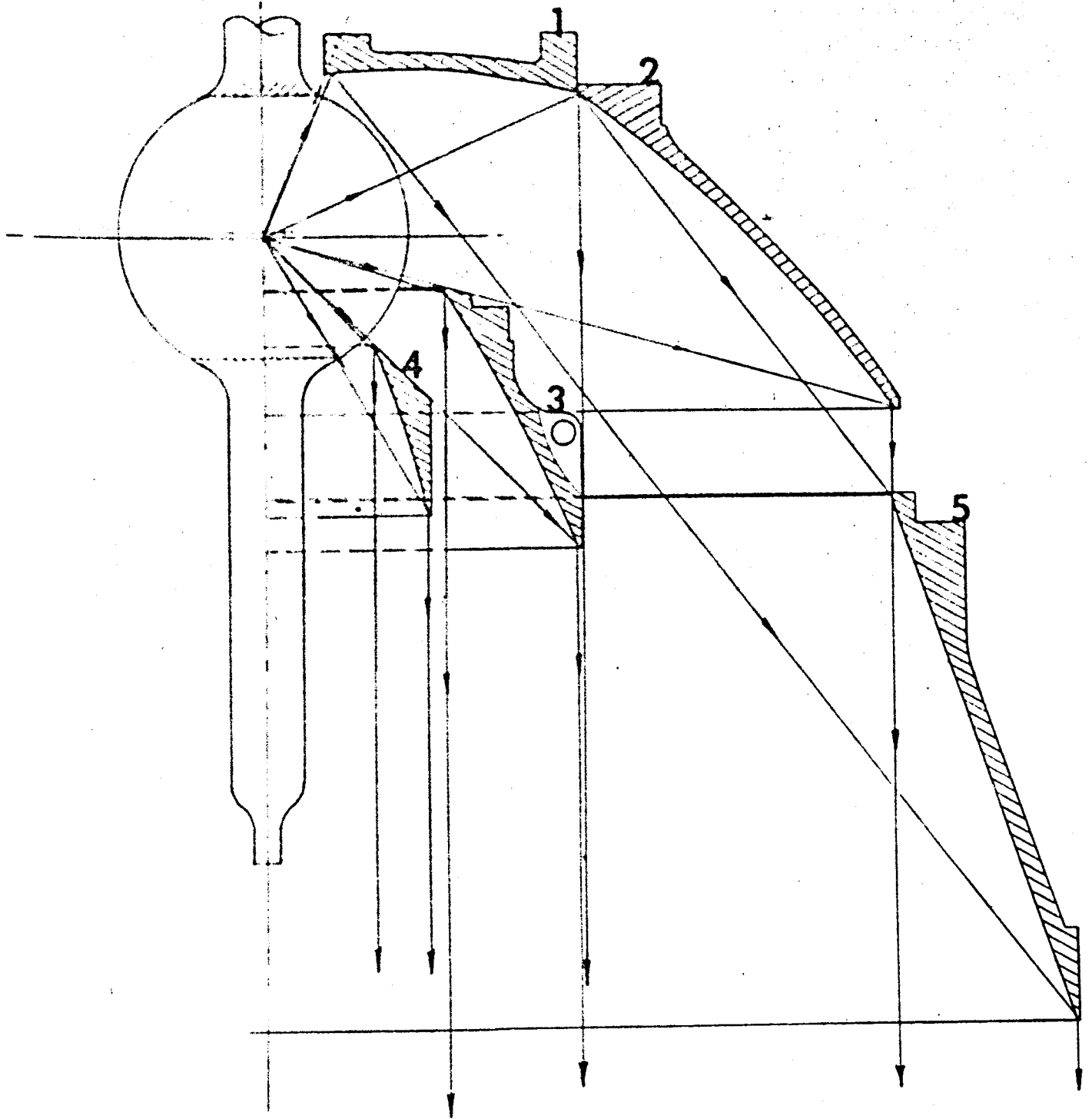
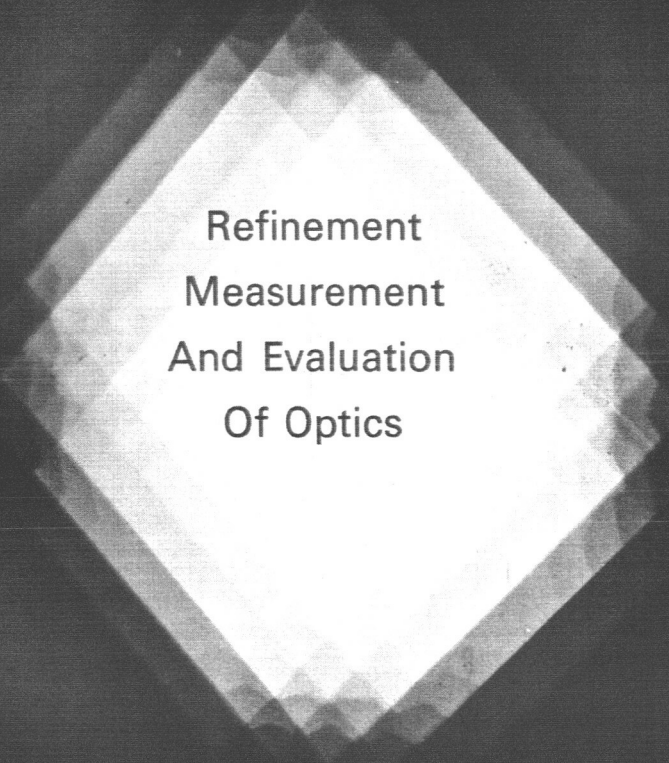


Figure 3 - 22

Module Schematic





Refinement
Measurement
And Evaluation
Of Optics



SOLAR MODULE

for

Lewis Research Center, NASA

Figure 3 - 1

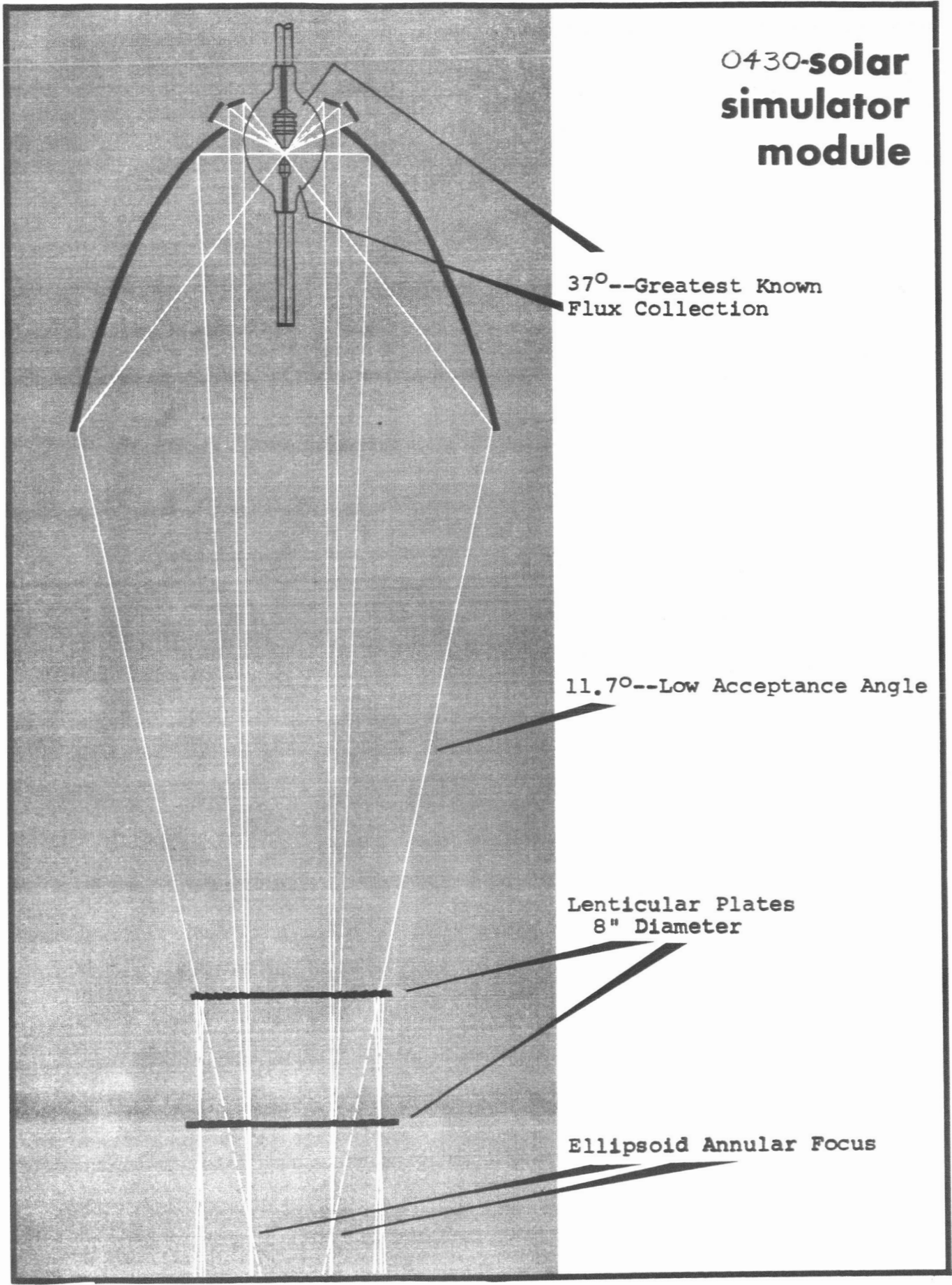


Figure 3 - 18 Prototype Module—Two Lens Plates

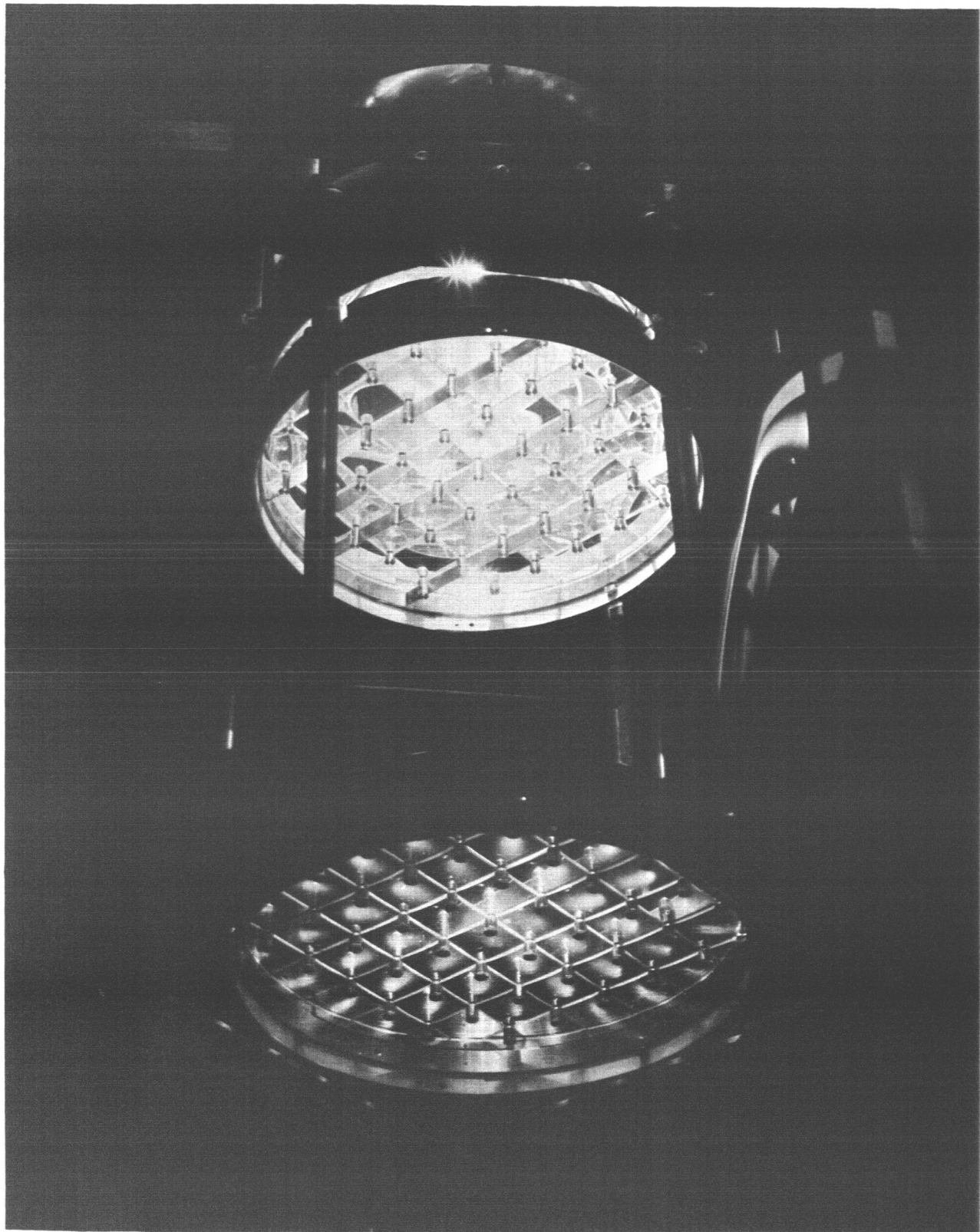


Figure 4 - 7 Control Console and X-Y Plotter

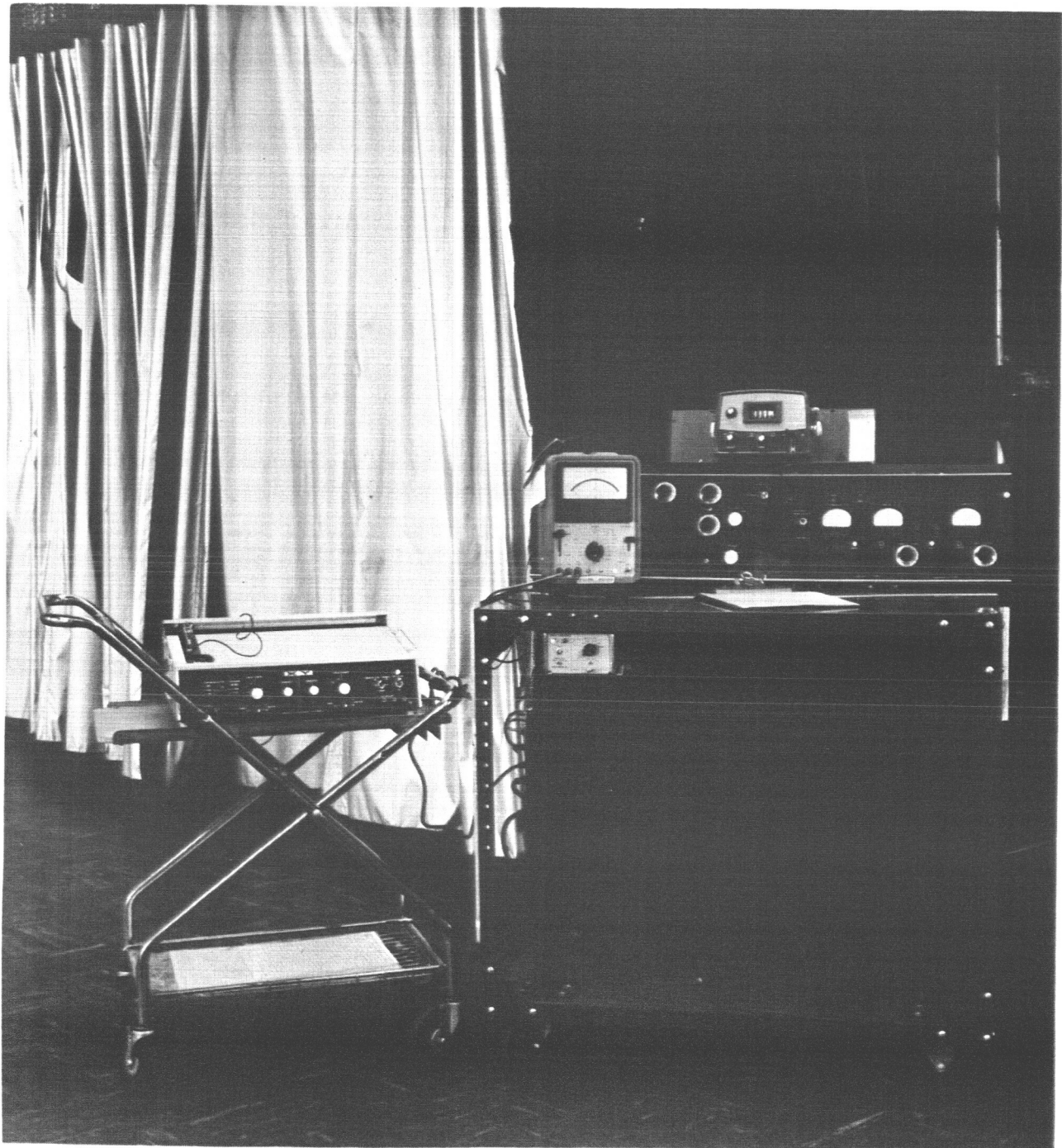


Figure 4 - 5 Radiometer Mounted on Cart

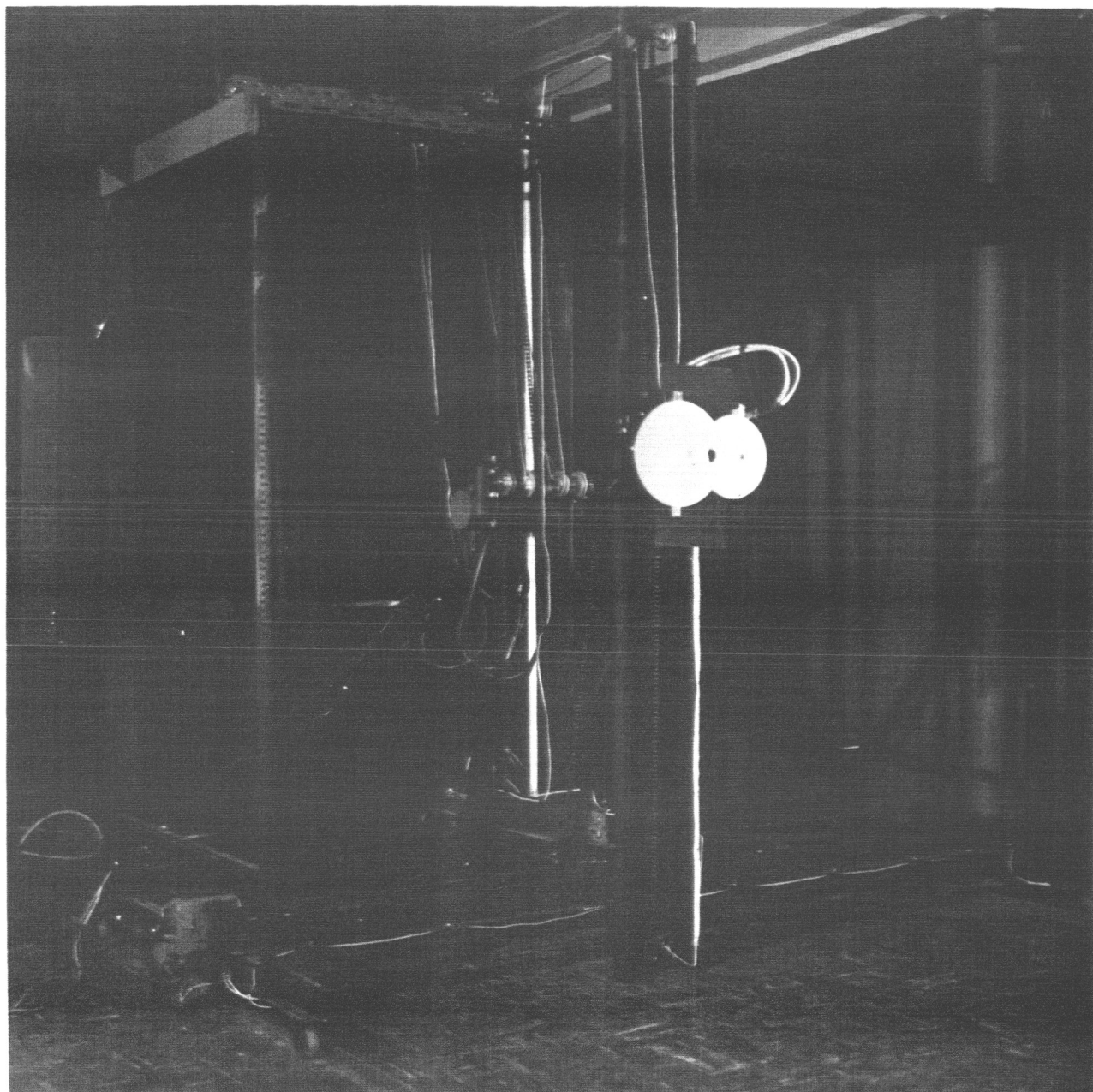


Figure 4 - 9 Operation of Console During Beam Measurement

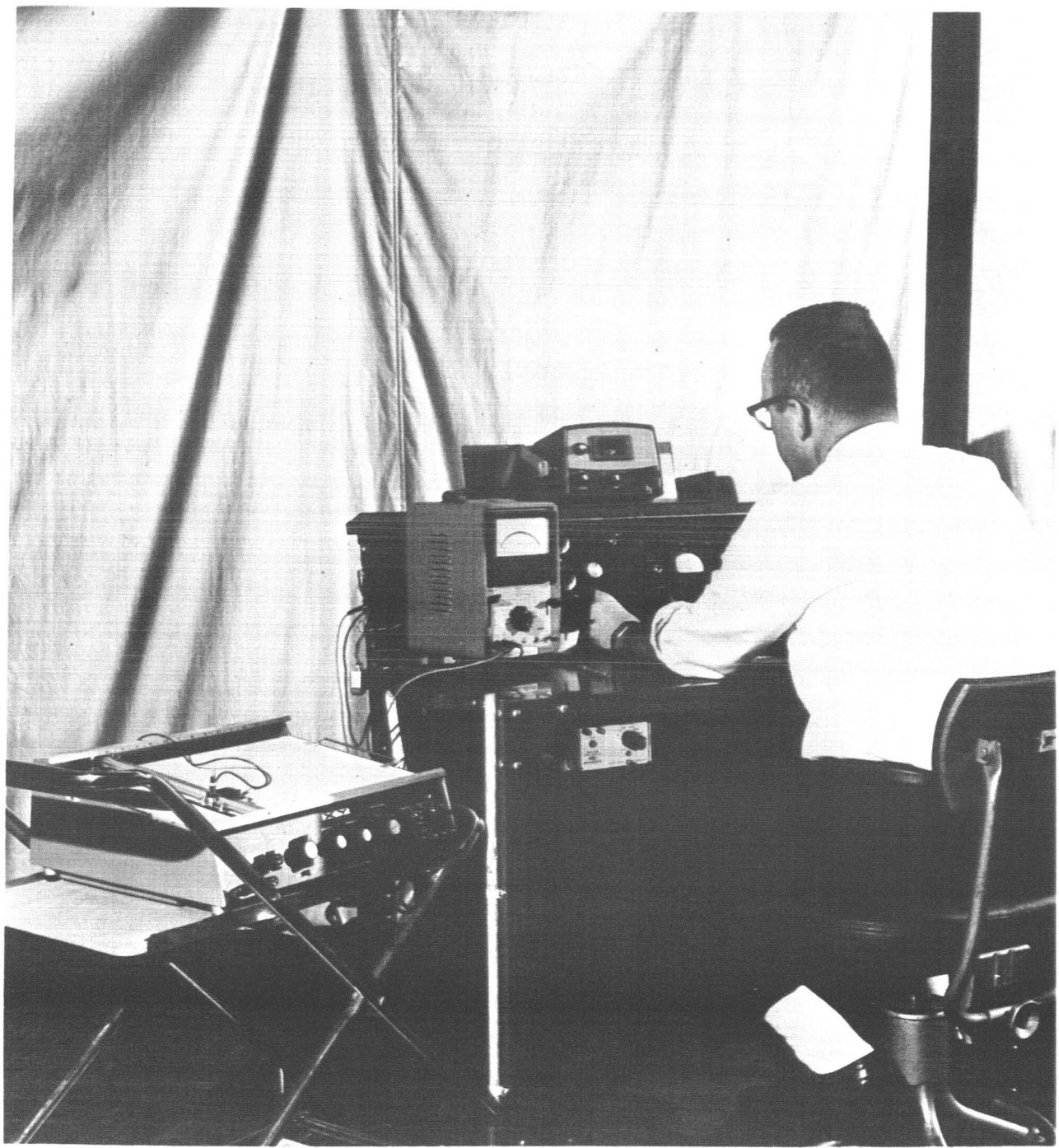


Figure 5 - 1 Prototype Module—Reflectors Only

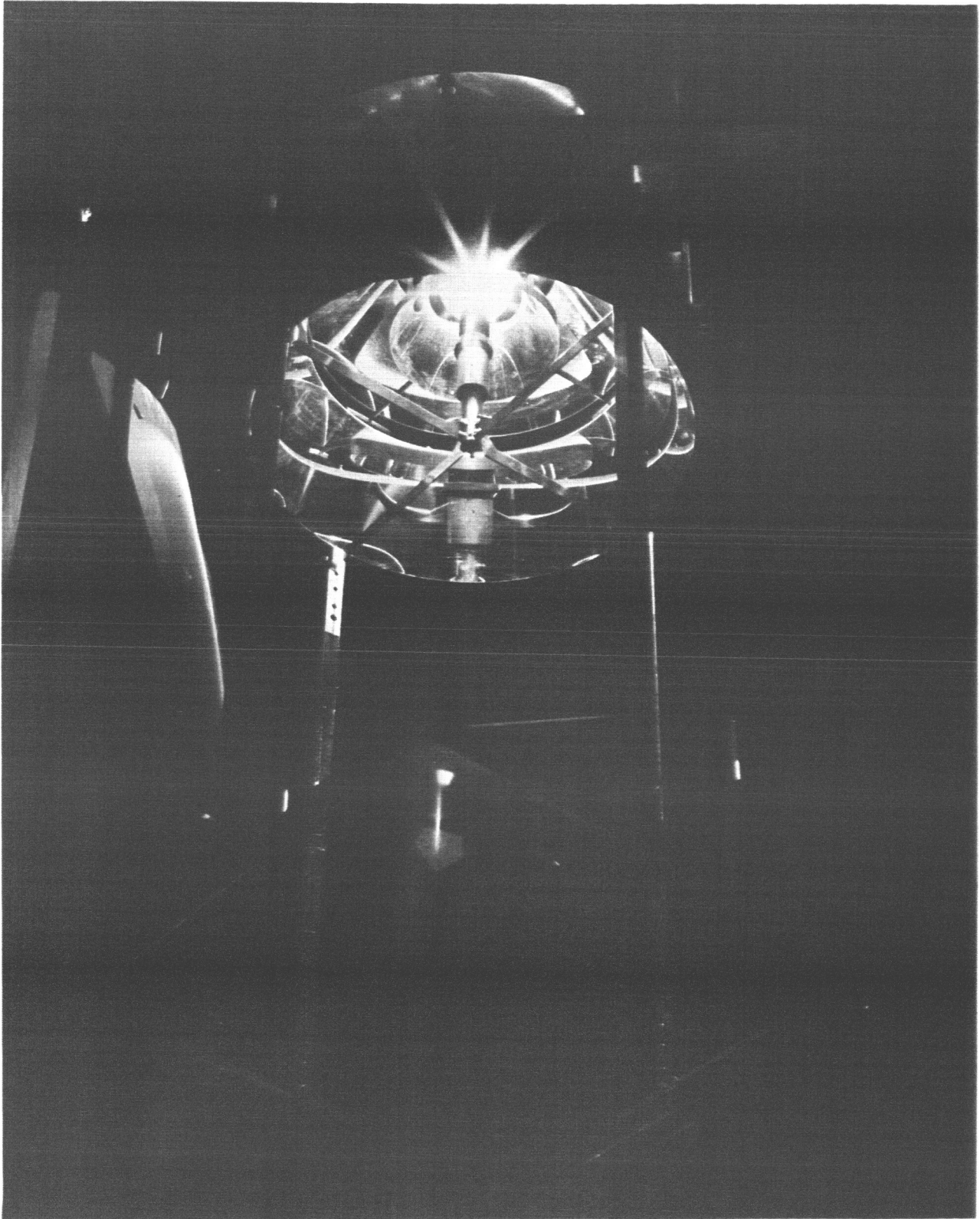


Figure 5 - 8 Beam Pattern at 60 Feet with Two Lens Plates

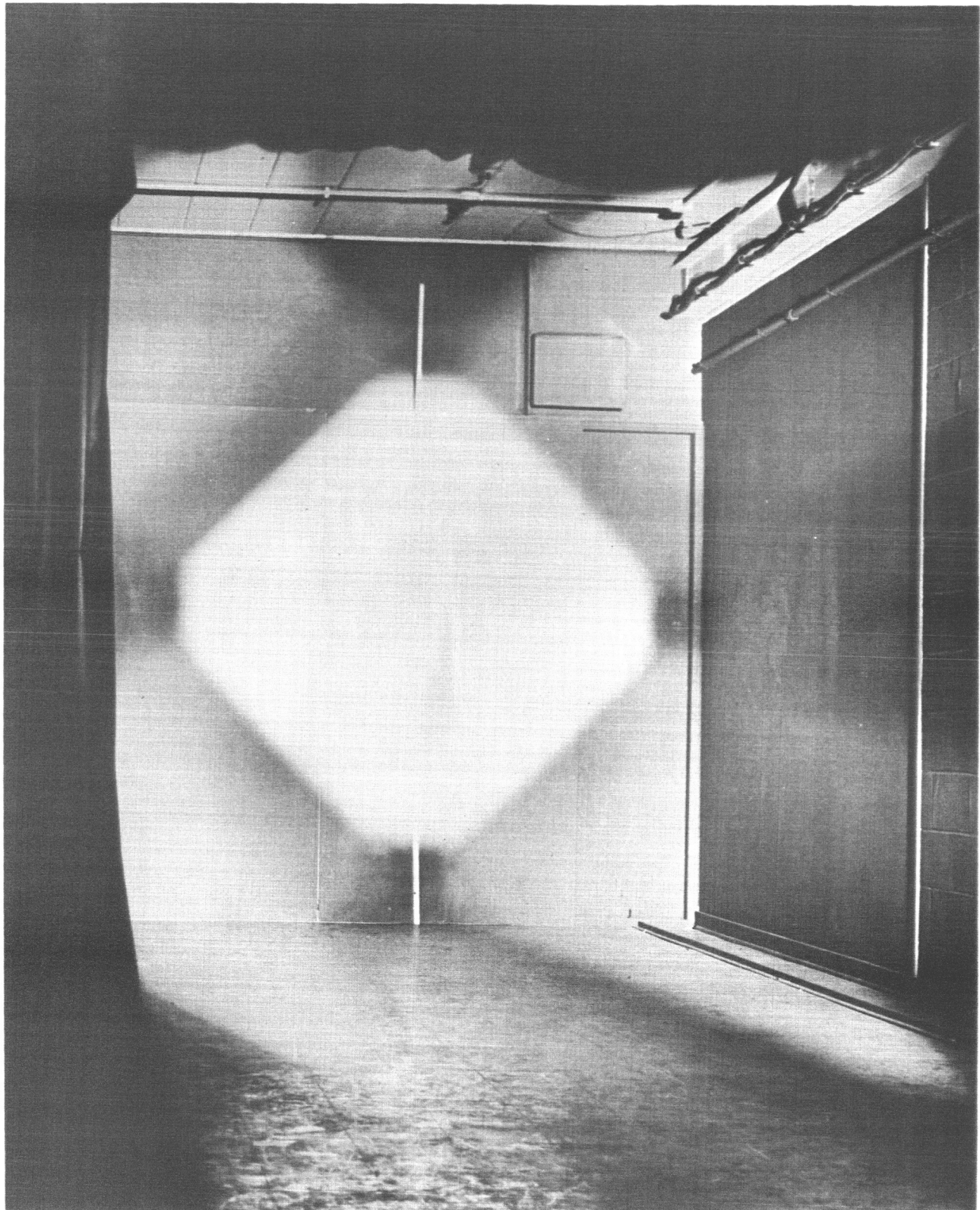


Figure 5 - 10 Beam Pattern for Two Lens Plates Focused at 15 Feet

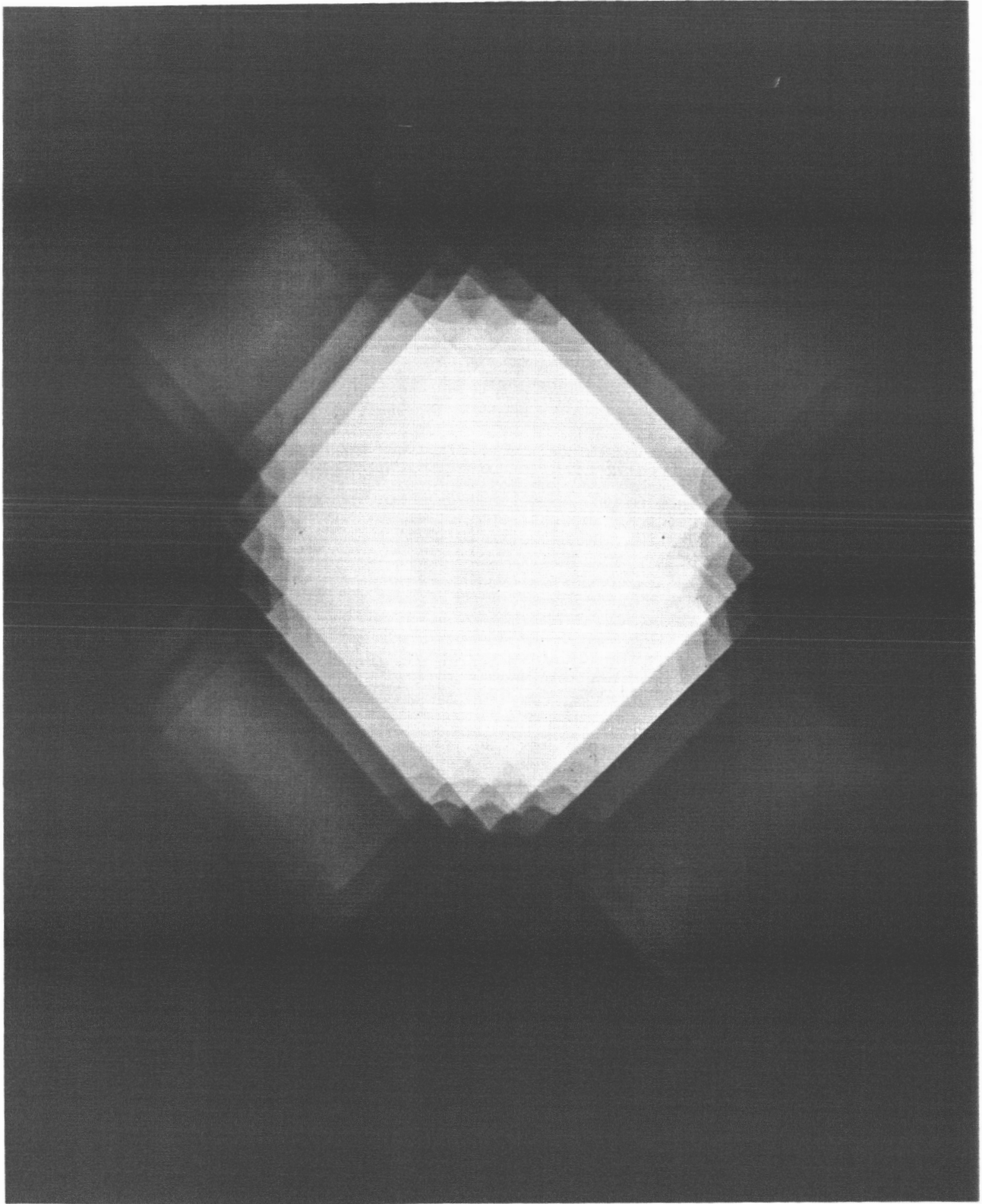


Figure 5 - 11 Beam Pattern at 60 Feet for Two Lens Plates Focused at 15 Feet

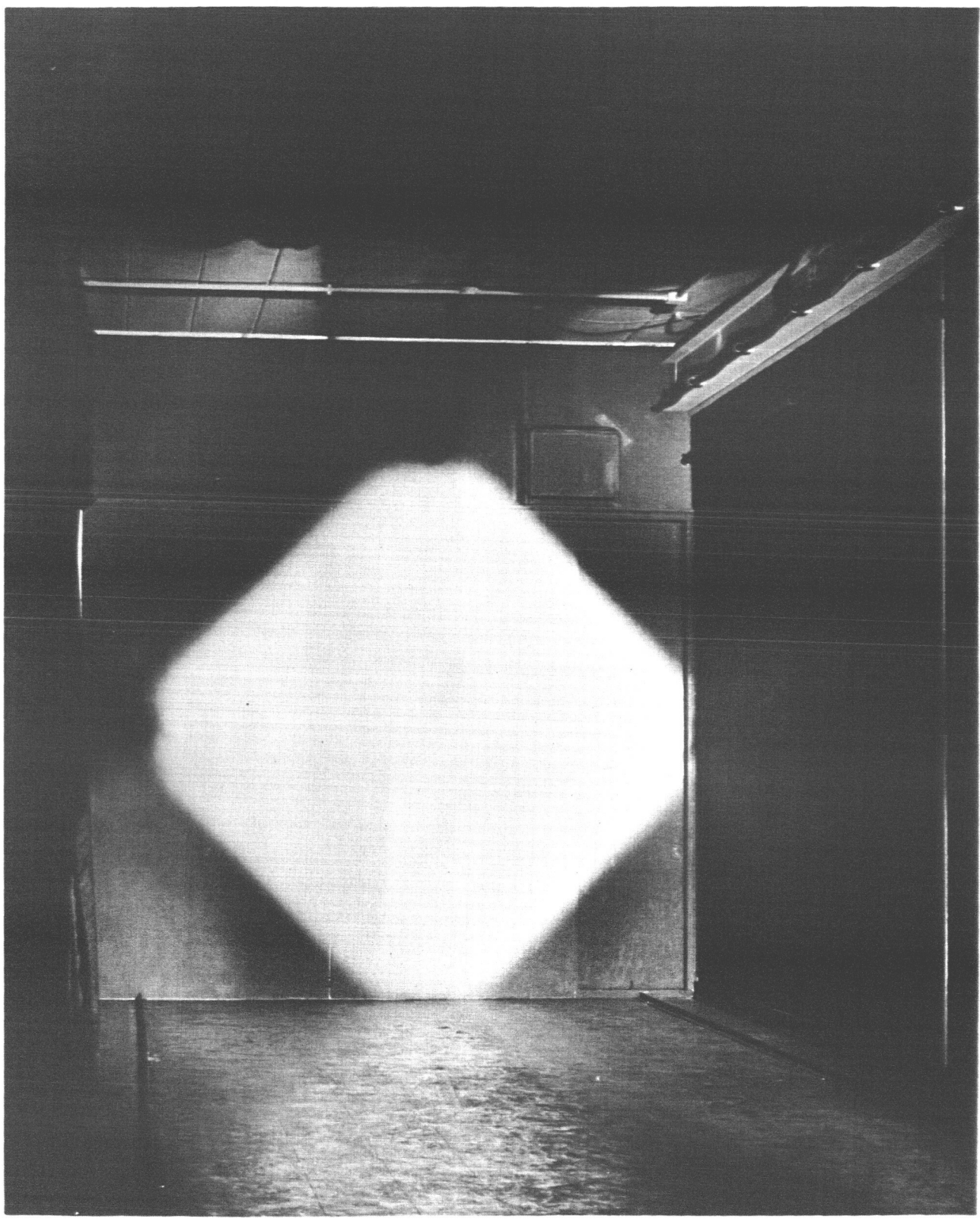
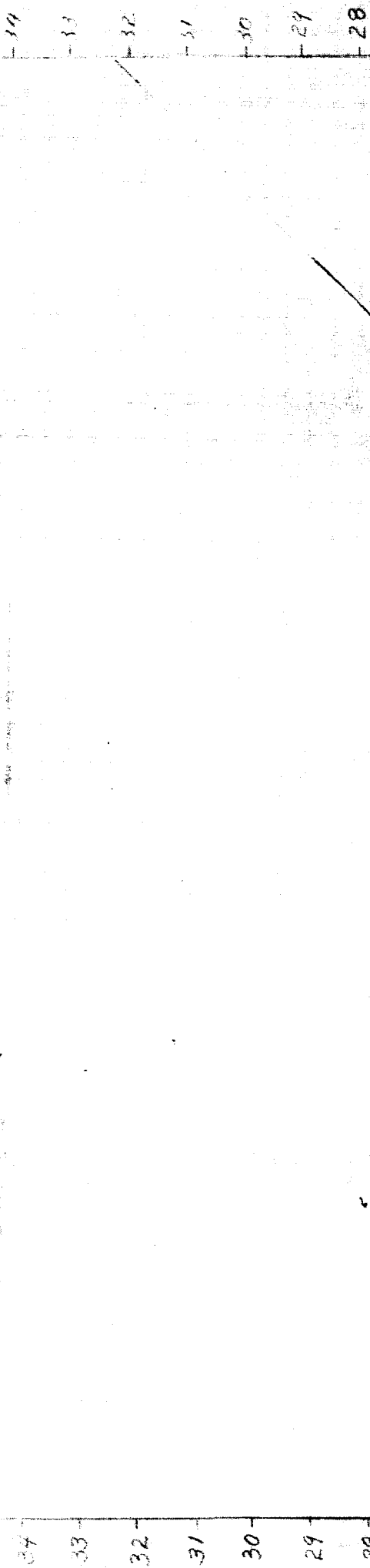


FIG 4-3

MARK III RADIONMETER 146977-0
AIR & THERM CALIBRATION CURVES 11/25/64

4-3-1



27
26
25
24
23
22
21
20
19
18
17
16

BOTH CURVES ARE STRAIGHT
TO THIS VELOCITY →

VELOCITY INCREASED
WITHOUT GURTH INNOV. →

4.3.2

27
26
25
24
23
22
21
20
19
18
17
16

14
13
12
11
10
9
8
7
6
5
4
3
2
1

0.111 $\mu\text{g}/\mu\text{g} \cdot \text{sec}^{-2}$

1.4R SPANIC / WITH
GUMMITE 10000

0.0844 $\text{mV}/\mu\text{g} \cdot \text{sec}^{-2}$

43-3

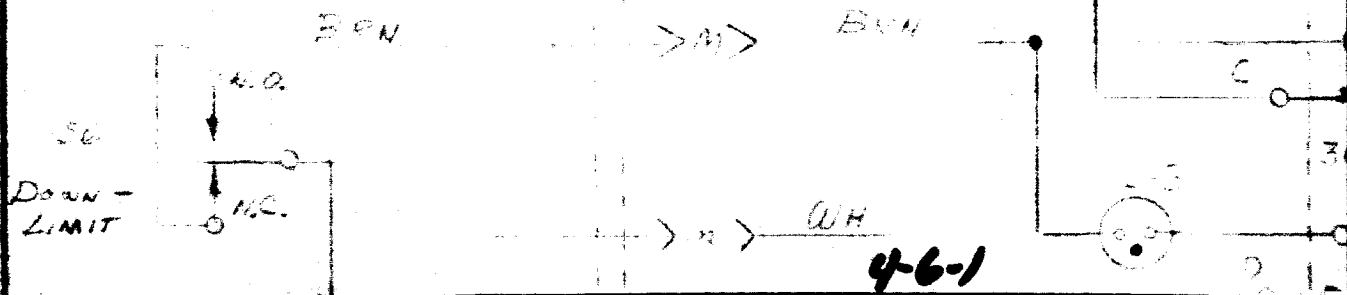
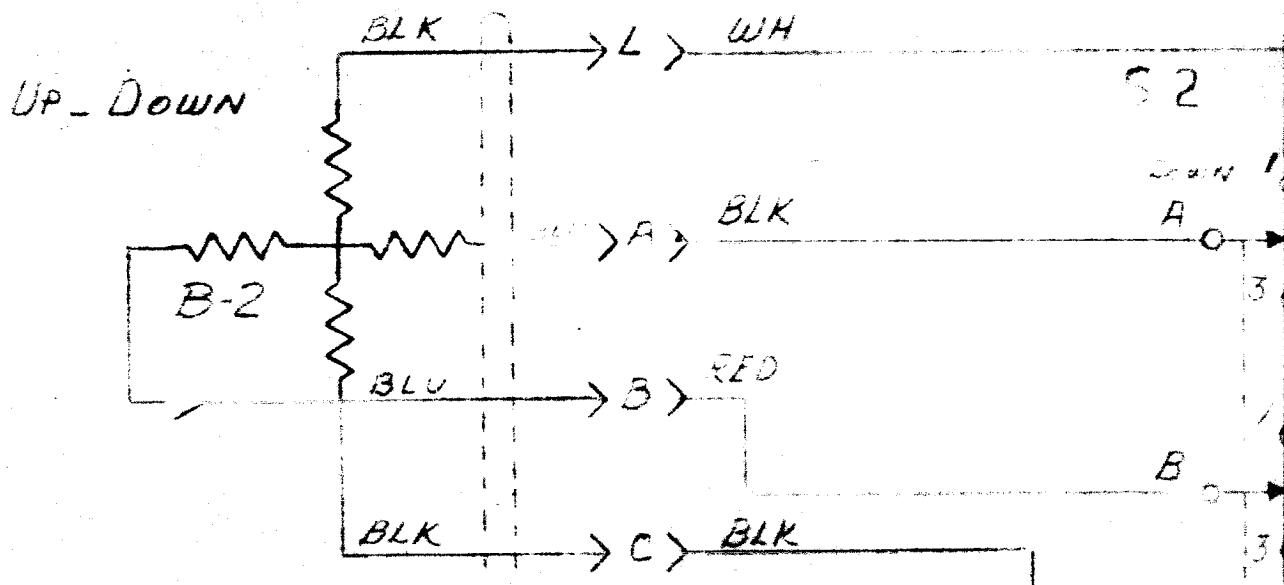
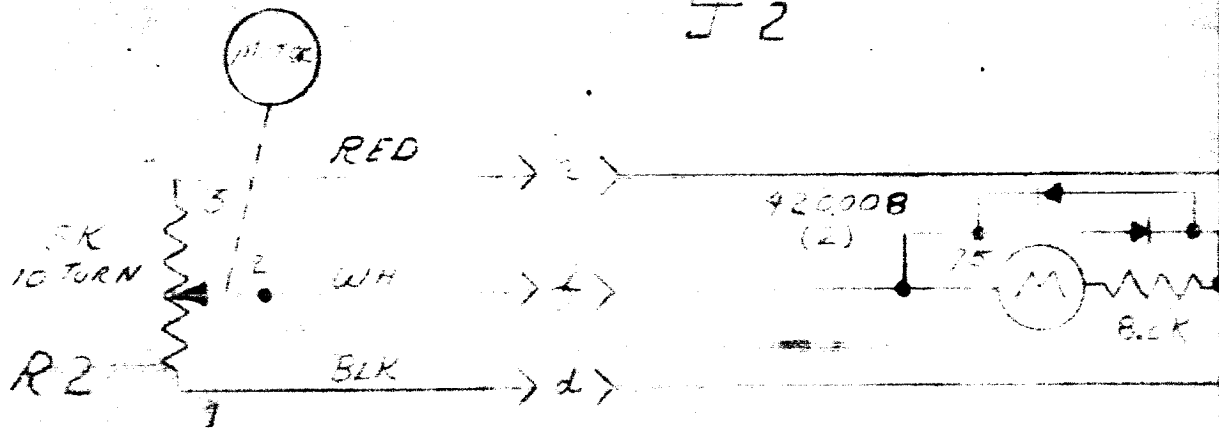
60 80 100 120 140 160 180 200 220 240 260 280 300

$\mu\text{g}/\text{g} \cdot \text{sec}^{-2}$

A

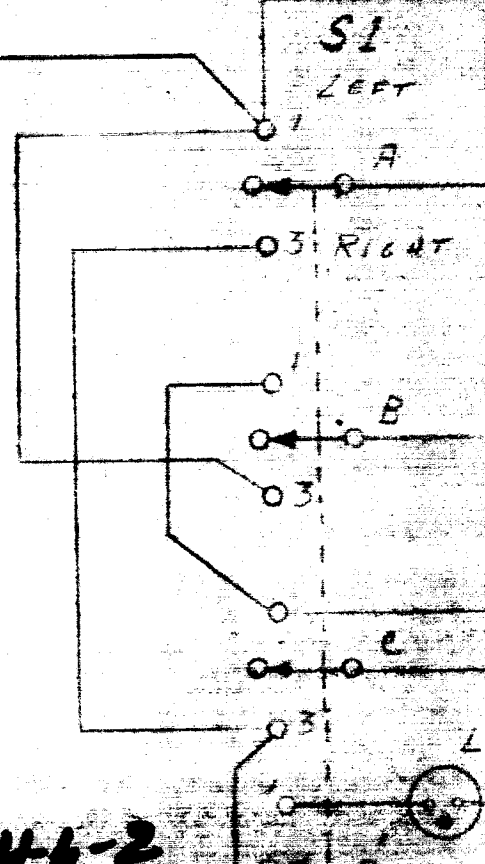
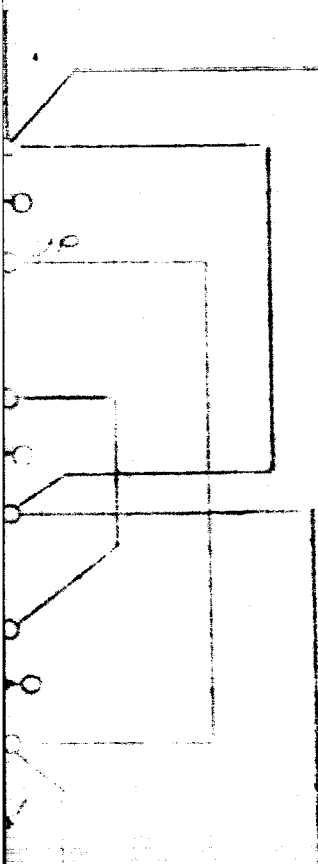
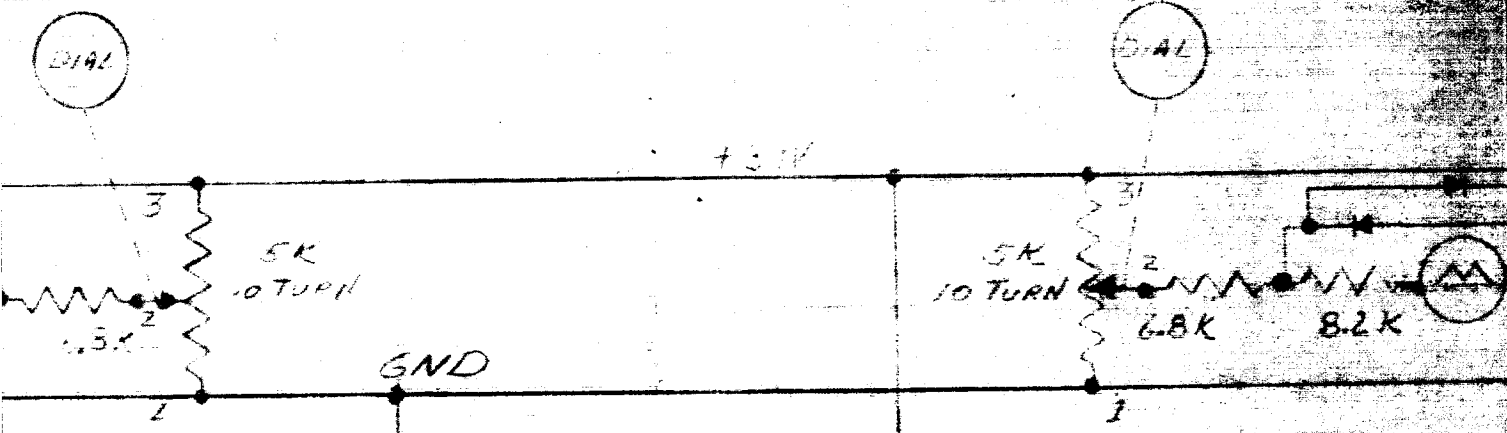
B

UP - DOWN
J2



C

D



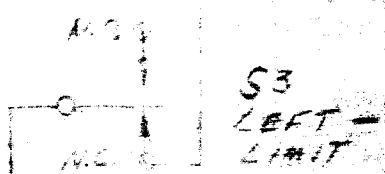
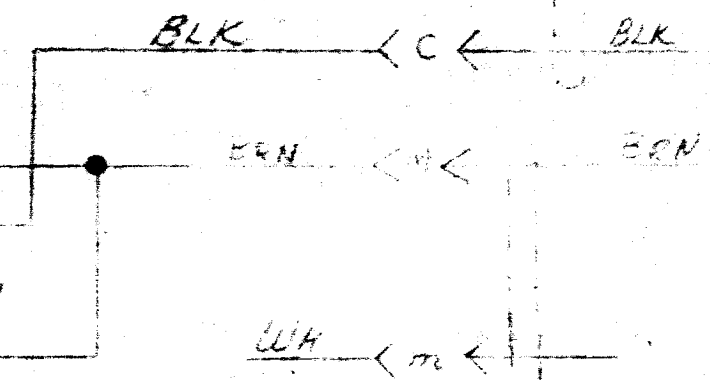
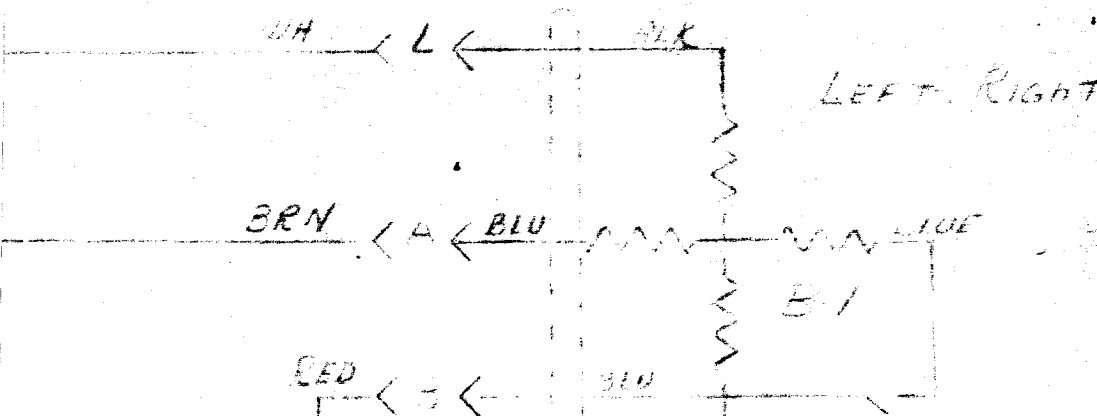
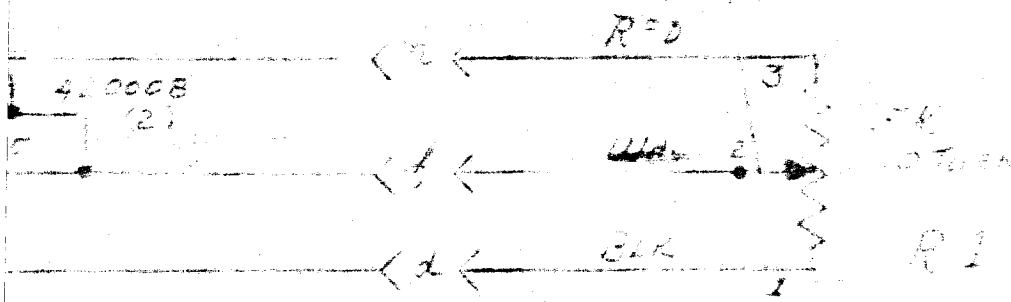
46-2

E

F

LEFT RIGHT

J1



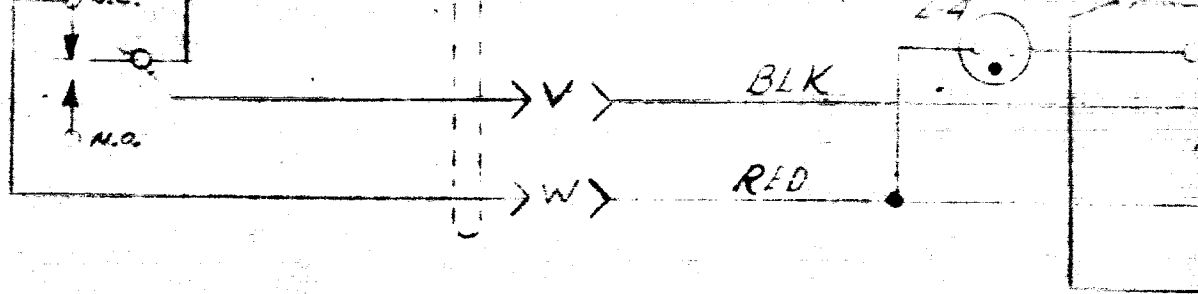
4-6-3

1

2

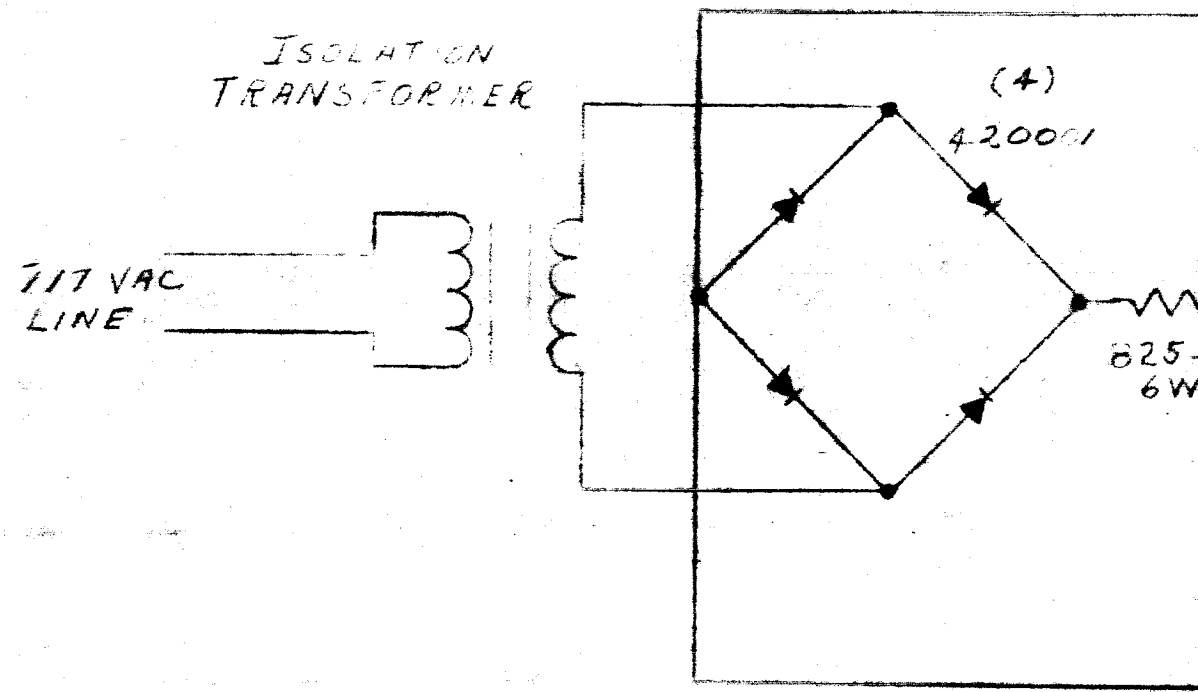
3

SS
UP +
LIMIT

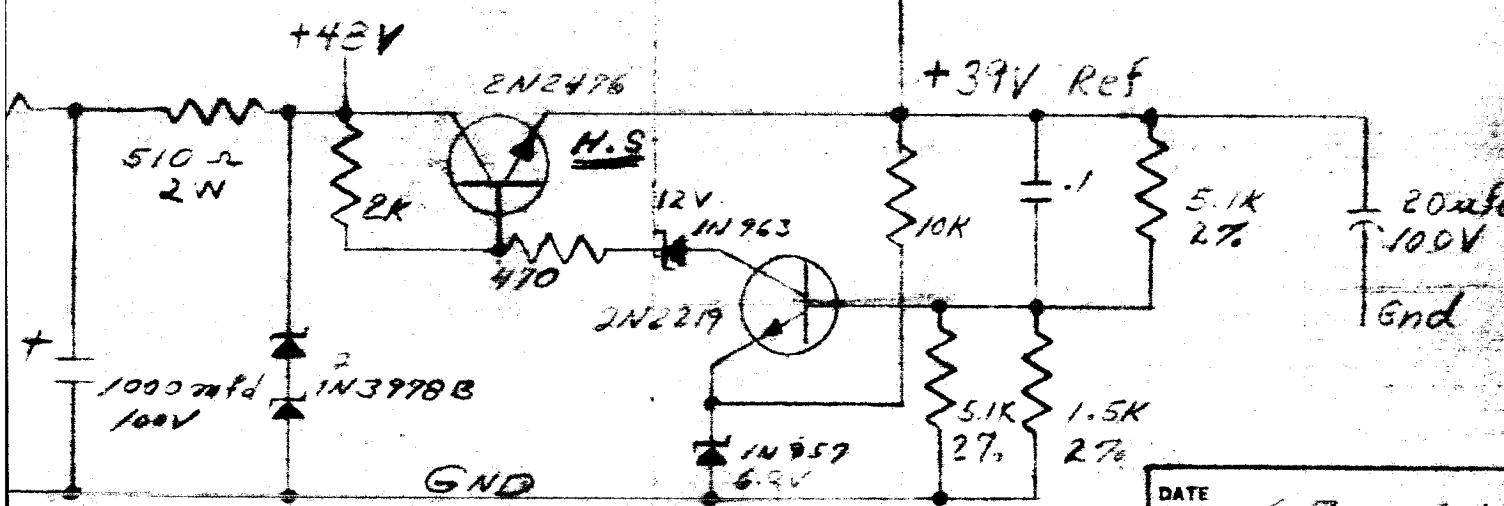
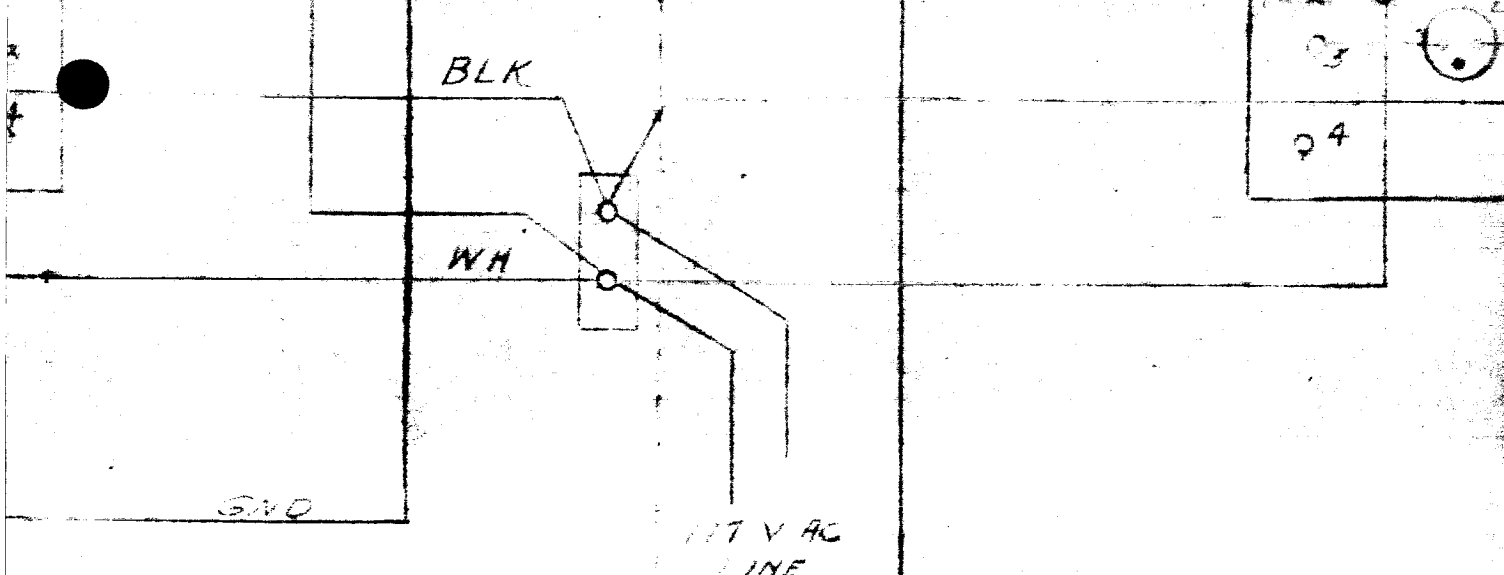


ISOLATION
TRANSFORMER

717 VAC
LINE



4-64



| | |
|------------|----------|
| DATE DRAWN | 6 Feb 64 |
| DRAWN BY | |
| CHK. BY | |
| APP. BY | |
| SCALE | |

4-6-5

BLK



RED

S4
RIGHT
LIMIT

TITLE

SCHEMATIC
CONTROL,
SOLAR - SIMULATOR

LINEAR ALPHA, INC.
EVANSTON, ILLINOIS

USED ON

Figure 4-6

DWG.
NO.

C 100604

SHEET

1 of 2

E

F

4-6-6

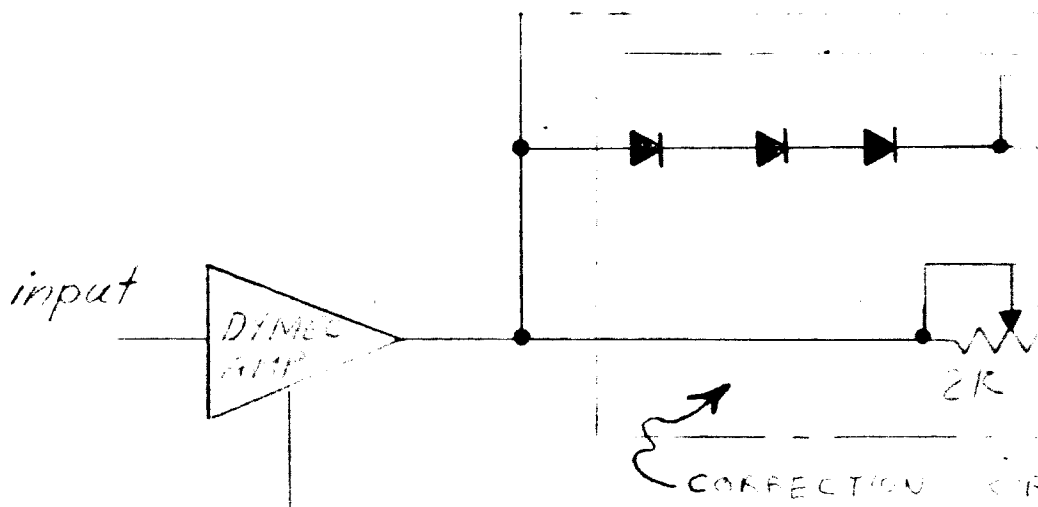
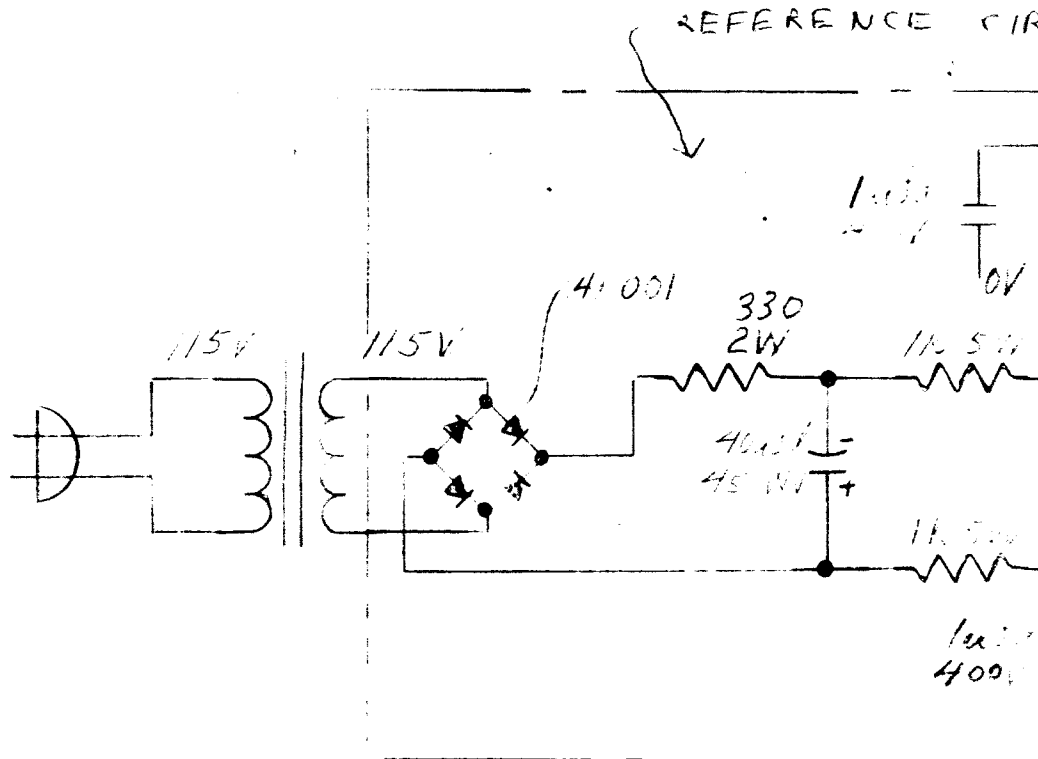
A

B

1

2

3

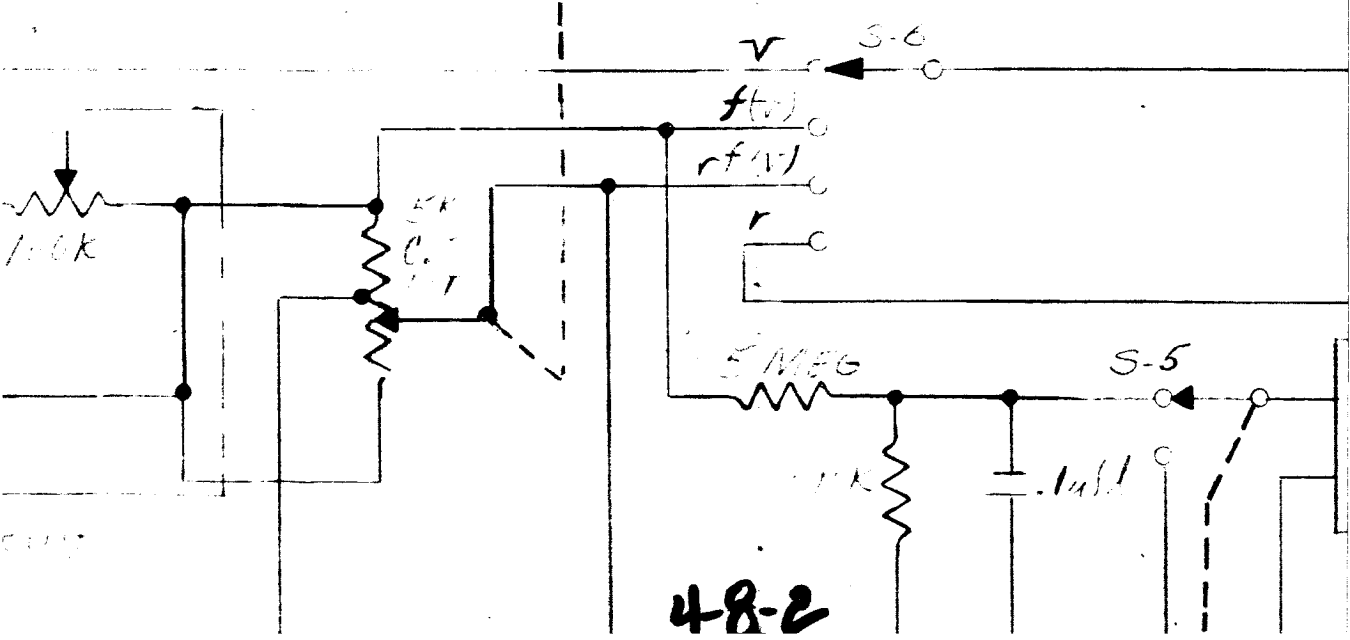
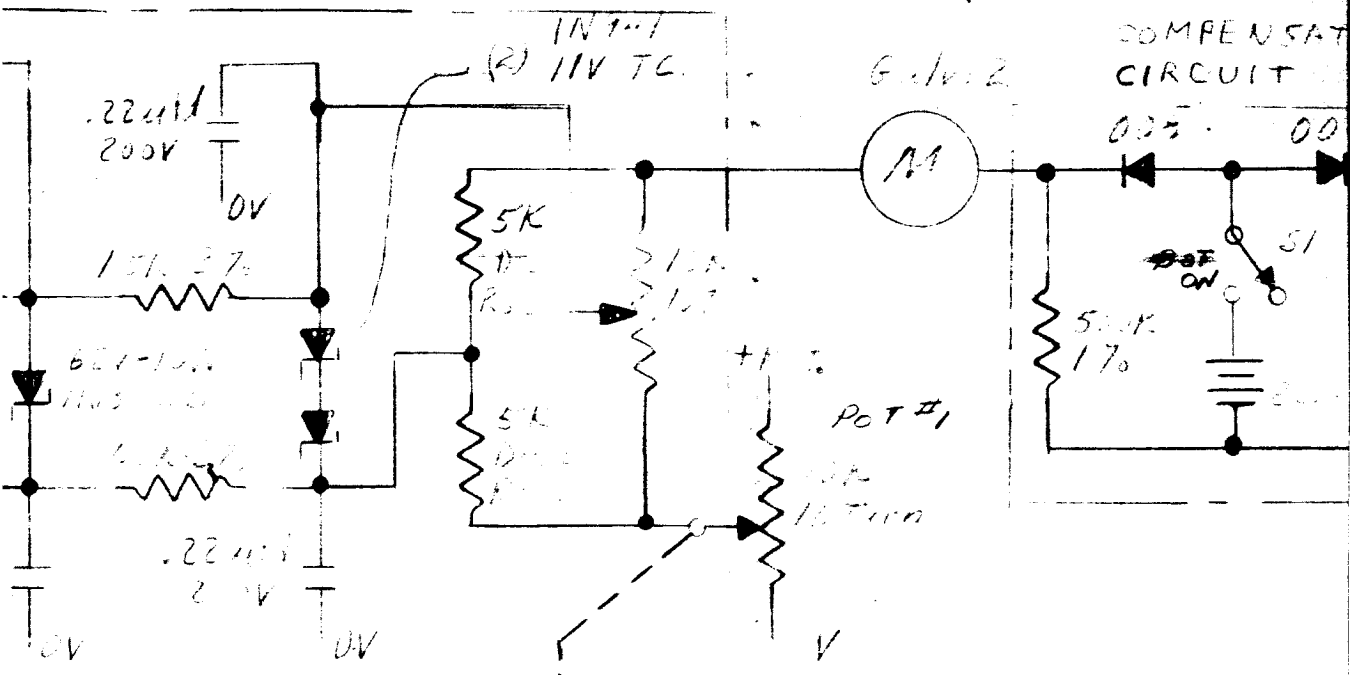


4-8-1

C

D

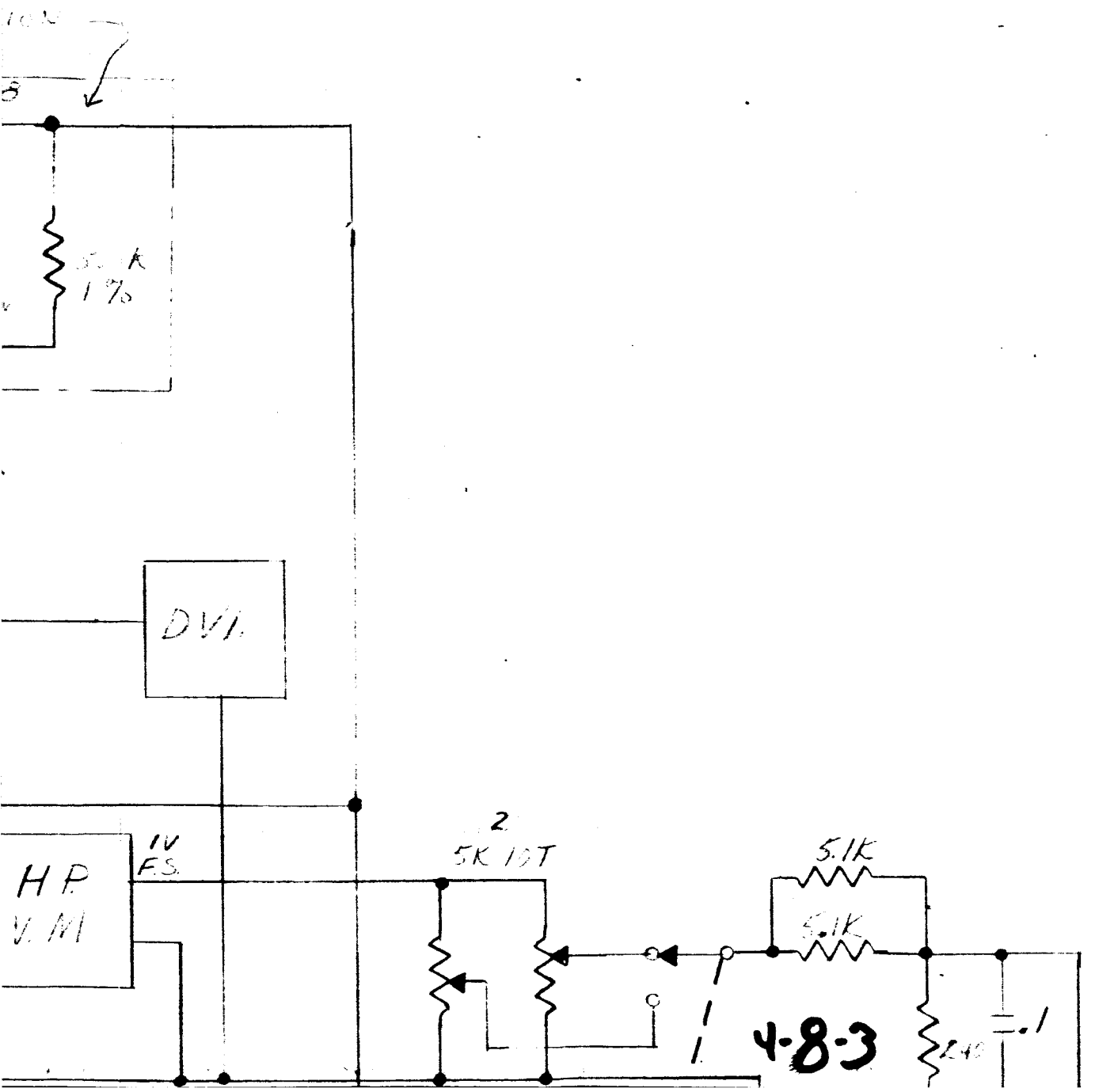
CURT



48-2

E

F



1

2

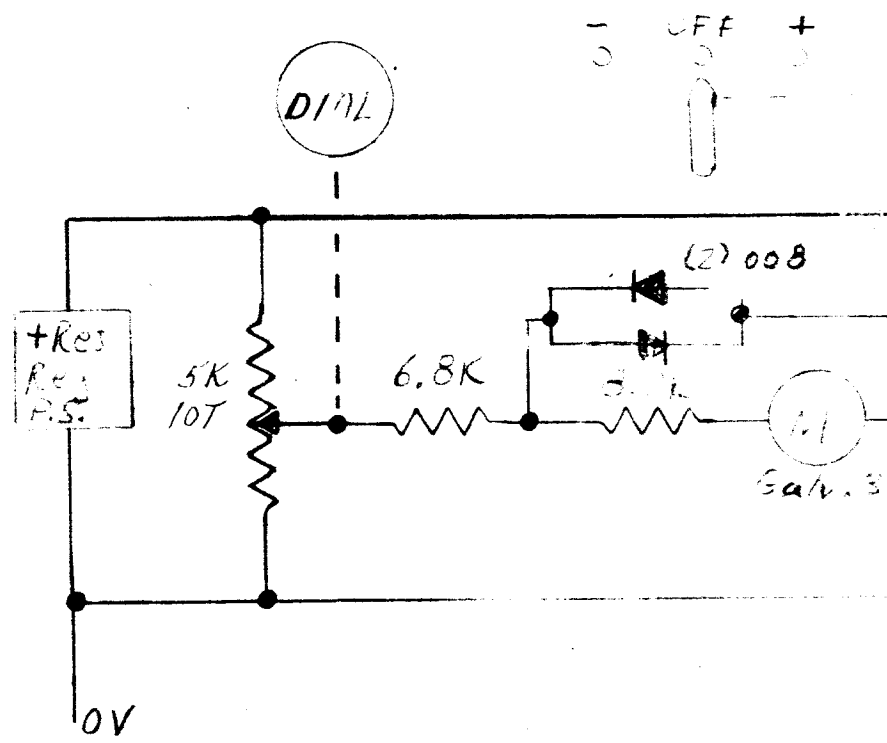
3

4

5

6

7



A 4-8-4

B

10V

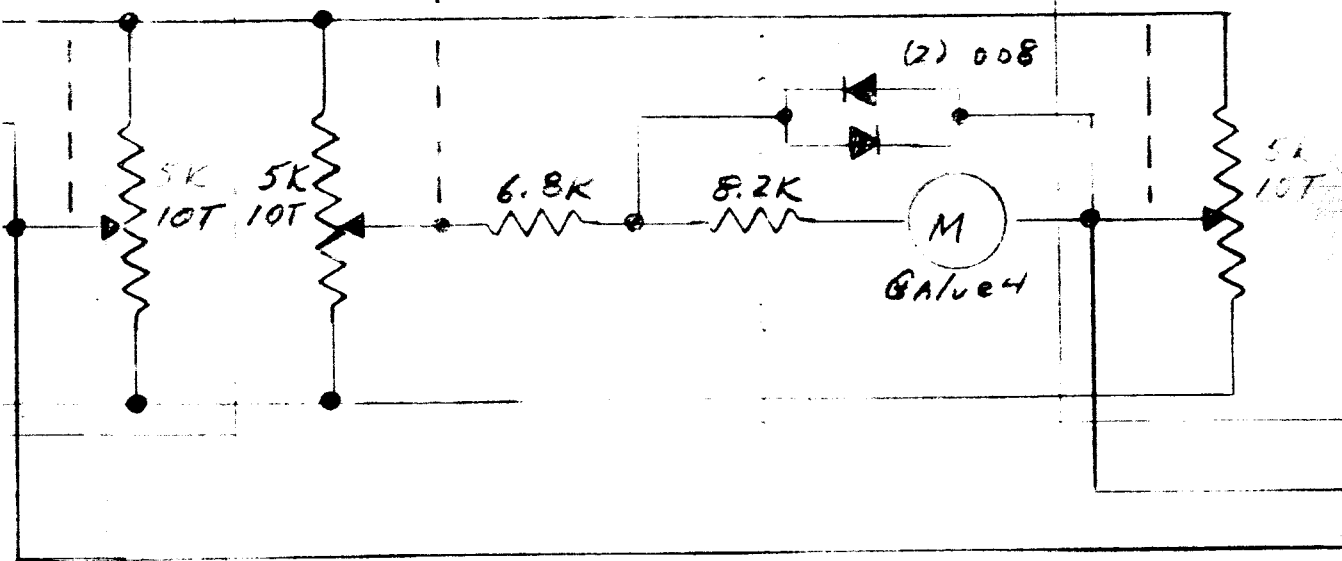
LOCATED ON THE CART

0 0 0

MOTOR

DIAL

MOTOR



| | |
|--|---------------|
| UNLESS SPECIFIED DIMENSIONS IN INCHES ANGULAR TOL. $\pm \frac{1}{2}^\circ$ DECIMAL TOL. .XX $\pm .02$.XXX $\pm .008$ HOLES $\pm .002$ | DATE DRAWN |
| | DRAWN BY |
| | CH'K BY |
| | APP. BY |
| SCALE | |

C

D

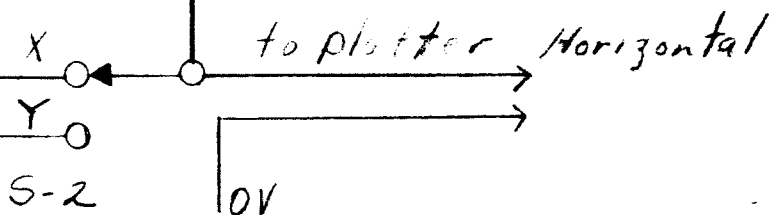
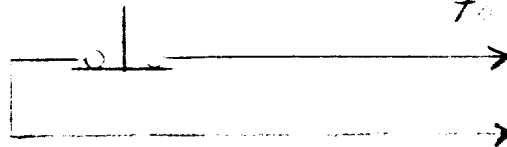
4-8-5

LOCATED ON
THE CART

To Plotter
Vertical

Push to Plot

to Plotter



| | | | |
|--------|--|--|------------|
| Feb 65 | TITLE Solar Simulator Direct Computing Plotter | LINEAR ALPHA, INC. EVANSTON, ILLINOIS | |
| ? K | | | |
| | USED ON Figure 4-8 | DWG. NO. | C 100603 A |
| | | SHEET | 1 OF 1 |

E

F

4-8-6